

Role of Hydrological Process Representation on Erosion, Deposition, and Sediment

Yield Estimate

by

Tan Zi

Department of Civil and Environmental Engineering
Duke University

Date: _____

Approved:

John D. Albertson, co-chair

Mukesh Kumar, co-chair

Amilcare Porporato

Gabriel Katul

Tomasz Hueckel

Stefano Orlandini

Dissertation submitted in partial fulfillment of
the requirements for the degree of Doctor
of Philosophy in the Department of
Civil and Environmental Engineering in the Graduate School
of Duke University

2016

ABSTRACT

Role of Hydrological Process Representation on Erosion, Deposition, and Sediment

Yield Estimate

by

Tan Zi

Department of Civil and Environmental Engineering
Duke University

Date: _____

Approved:

John D. Albertson, co-chair

Mukesh Kumar, co-chair

Amilcare Porporato

Gabriel Katul

Tomasz Hueckel

Stefano Orlandini

An abstract of a dissertation submitted in partial fulfillment of the requirements for the
degree of Doctor of Philosophy in the
Department of Civil and Environmental Engineering in the Graduate School
of Duke University

2016

Copyright by
Tan Zi
2016

Abstract

Soil erosion by water is a major driven force causing land degradation. Laboratory experiments, on-site field study, and suspended sediments measurements were major fundamental approaches to study the mechanisms of soil water erosion and to quantify the erosive losses during rain events. The experimental research faces the challenge to extent the result to a wider spatial scale. Soil water erosion modeling provides possible solutions for scaling problems in erosion research, and is of principal importance to better understanding the governing processes of water erosion. However, soil water erosion models were considered to have limited value in practice. Uncertainties in hydrological simulations are among the reasons that hindering the development of water erosion model. Hydrological models gained substantial improvement recently and several water erosion models took advantages of the improvement of hydrological models. It is crucial to know the impact of changes in hydrological processes modeling on soil erosion simulation.

This dissertation work first described the development of an erosion modeling tool (GEOtopSed) that takes advantage of the comprehensive hydrological model (GEOtop). The newly created tool was then tested and evaluated at an experimental watershed. The GEOtopSed model showed its ability to estimate multi-year soil erosion rate with varied hydrological conditions. To investigate the impact of different

hydrological representations on soil erosion simulation, a 11-year simulation experiment was conducted for six models with varied configurations. The results were compared at varied temporal and spatial scales to highlight the roles of hydrological feedbacks on erosion. Models with simplified hydrological representations showed agreement with GEOTopSed model on long temporal scale (longer than annual). This result led to an investigation for erosion simulation at different rainfall regimes to check whether models with different hydrological representations have agreement on the soil water erosion responses to the changing climate. Multi-year ensemble simulations with different extreme precipitation scenarios were conducted at seven climate regions. The differences in erosion simulation results showed the influences of hydrological feedbacks which cannot be seen by purely rainfall driven method.

To my beloved wife Jing Tao,
for being a constant source of love and support;
and
to my little sweetheart Yizhen Zi,
for your cute giggles.

Contents

Abstract	iv
List of Tables.....	x
List of Figures	xii
Acknowledgements	xvi
1 Introduction.....	1
1.1 Motivation	1
1.2 Hydrological processes and soil water erosion.....	3
1.3 Hydrological processes representations in soil erosion and sediment transport models.....	6
1.4 Long Term Soil Water Erosion Model Applications	9
1.5 Chapter overviews	11
2 Simulating the spatio-temporal dynamics of soil erosion, deposition, and yield using a coupled sediment dynamics and 3D distributed hydrologic model.....	13
2.1 Introduction.....	13
2.2 Process Formulation, Model Implementation, and Verification.....	17
2.2.1 The GEOtop model: A short review	17
2.2.2 Process formulation of the sediment dynamics model.....	18
2.2.3 Model Implementation.....	22
2.2.4 Model verification at plot scale	23
2.3 Model Application at Watershed Scale	26
2.3.1 Site description	26

2.3.2	Input data	30
2.3.3	Model implementation in Dripsey catchment	31
2.3.4	Sensitivity analysis.....	32
2.3.5	Model Performance During Calibration and Validation Periods	38
2.3.5.1	Evaluation metrics.....	38
2.3.5.2	Calibration period	40
2.3.5.3	Validation period.....	42
2.4	Results and Analyses	46
2.4.1	Temporal variations in modeled estimates	46
2.4.2	Spatially distributed estimates of erosion and deposition	52
2.5	Summary and Conclusions	56
3	Inter-comparing erosion, deposition, and sediment yield estimates using process representations ranging from empirical to physics-based.....	61
3.1	Introduction.....	61
3.2	Method	69
3.2.1	Selected model representations.....	69
3.2.2	Site descriptions and model input data	73
3.2.3	Model calibration and validation.....	76
3.2.4	Model comparisons.....	78
3.3	Result.....	79
3.3.1	Temporal comparisons	79
3.3.2	Spatial distribution.....	97

3.4	Conclusion	106
4	The role of hydrologic feedback to the suspended sediment yield responses to different precipitation regimes: Implications on the evaluation of climate change impacts on erosion.....	108
4.1	Introduction.....	108
4.2	Data and Methodology	110
4.2.1	Physically based erosion model	110
4.2.2	Experiment design	111
4.2.3	Experiment sites for different climate regions	112
4.2.4	Weather generation.....	114
4.3	Results	118
4.4	Discussion.....	122
4.5	Conclusion	126
5	Conclusions and Future Work.....	128
5.1	Conclusions	128
5.2	Suggestions for Future Work.....	131
	References	133
	Biography.....	152

List of Tables

Table 2-1 Summary of plot experiment. The experiment data are from Ran et al. (2012). Numbers in the parenthesis are simulation results from GEOtopSed.....	25
Table 2-2 Ranges and numerical sensitivity index (NSI) of hydrologic parameters	34
Table 2-3 Ranges and numerical sensitivity index (NSI) of erosion and sediment dynamics parameters	35
Table 2-4 Performance of stream flow and total suspended sediment yield simulation in calibration and validation periods.....	44
Table 2-5 Performance of stream flow and suspended sediment simulations in wet and dry periods.....	45
Table 2-6 The mean and standard deviation of erosion and deposition areas.....	53
Table 3-1 Varied representations of detachment, deposition and transport processes in sediment models	66
Table 3-2 List of sediment models and representation schemes of detachment, deposition and transport processes in them. See Table 3-1 for representation details.....	66
Table 3-3 Selected model configurations*.....	72
Table 3-4 Performance of stream flow and total suspended sediment yield simulation in calibration and validation periods.....	78
Table 3-5 Fisher approximate unbiased estimator of SSY modeling at different temporal scales (values in parenthesis are Fisher estimator without data in 2010)	81
Table 3-6 Area portion statistics	99
Table 3-7 Agreement and disagreement percentage and Cohen’s Kappa coefficient(Cohen, 1960) between different models. R is short for RUSLE_TC, M is short for MUSLE_S_TC and MUSLE_G_TC, G is short for GEOtopSed, “+” stands for erosion, “-” stands for deposition.....	102
Table 3-8 Statistics of agreement and disagreement area between RUSLE_TC and GEOtopSed (dry year).....	105

Table 3-9 Statistics of agreement and disagreement area between MUSLE_S_TC and GEOtopSed (wet year).....	105
Table 3-10 Statistics of agreement and disagreement area between MUSLE_G_TC and GEOtopSed (dry year in parenthesis)	106
Table 4-1 Information of selected weather stations.....	114
Table 4-2 Mean soil loss (ton ha-1 yr-1) of unit plot for different scenarios with different methods(G: GEOtopSed, E: rainfall erosivity).....	120
Table 4-3 Coefficient of variation (CV) of soil loss of unit plot for different scenarios with different methods(G: GEOtopSed, E: rainfall erosivity).....	121
Table 4-4 Changes of average annual runoff, average soil moisture and erosion days per year between two scenarios.....	124

List of Figures

Figure 1-1 Demonstration of soil erosion processes on a hillslope. Source: (Hagen and Foster, 1990)	4
Figure 1-2 Comparison of different model types with respect to scale, input requirements and kind of output. Source: (de Vente and Poesen, 2005)	10
Figure 2-1 Modeled and observed records for rainfall scenarios 10 (left column), 14. (middle column), and 18 (right column). The first row are the time series of precipitation and surface runoff; the second row are time series of precipitation and suspended sediment concentration (SSC); and the third row are time series of plot-average soil moisture of three subsurface layers. In the top two rows, precipitation (P) is plotted on the secondary axis.	26
Figure 2-2 Location of Dripsey catchment in County Cork, Ireland. The location of the meteorological tower is where “Dripsey” is marked in yellow. The right top panel is the Google Earth image of Dripsey catchment. The lower panel shows the conceptualization of rills (discussed in section 2.3.3).....	28
Figure 2-3 Observed monthly variations in precipitation (P), discharge volume (Q) and suspended sediment losses (SSY) in the Dripsey catchment	29
Figure 2-4 Sensitivity of rill width ratio, w_{dx} (a) and soil cohesion, ζ (b) on suspended sediment yield (SSY) for a range of precipitation intensities.....	37
Figure 2-5 Model estimates of daily discharge and daily suspended sediment yield (SSY) during the calibration period. (a) plot of observed (with subscription ‘o’) and simulated (with subscription ‘s’) daily average stream flow rate; (b) scatter plot of observed and simulated daily average stream flow rate; (c) plot of observed and simulated daily total SSY; (d) scatter plot of observed and simulated daily total SSY. Black solid line in panel (b) and (d) is the 1:1 line. Blue dashed line is the best-fit line.	41
Figure 2-6 Model estimates of discharge and suspended sediment yield (SSY) during the validation period. (a) plot of observed and simulated daily average stream flow rate. The wet and dry periods were identified by letter ‘W’ and ‘D’ ; (b) scatter plot of daily average stream flow rate; (c) plot of observed and simulated daily total SSY; (d) scatter plot of daily total SSY. Black solid line in panel (b) and (d) is the 1:1 line. Blue dashed line is the best-fit line.....	43

Figure 2-7 Scatter plot of daily observed SSY and EI30, color coded with daily simulated catchment-average soil moisture; the inset figure is a zoom-in of daily observed SSY between 0-1 ton/d and EI30 between 0 – 1.2×10^4 MJ*mm*ha ⁻¹ *h ⁻¹ ; (b) Scatter plot of daily observed SSY from 2002 to 2003 and daily simulated catchment average soil moisture.....	47
Figure 2-8 The hourly rainfall, observed discharge and SSY of two selected events (a,d); the simulated spatial distribution of soil loss area for two selected events (b,e), area with soil losses were black; the changes of saturated ratio of the simulated first layer soil moisture of the whole catchment (e,f); the plots for first event were on the top.	48
Figure 2-9 (a) The integrated model is able to capture occurrence of runoff events after a dry periods. The red box identifies the periods used in panel b, c, and d; (b) Observed and simulated flow rate; (c) Observed and simulated soil moisture (top 25 cm) (d)observed and simulated daily SSY	51
Figure 2-10 (a) Spatial map of soil erosion and deposition for each land pixel (unit:ton/ha/yr) for the entire two year simulation period; (b) Scatter plot between erosive loss(E_s) and slope-length factor for each land pixel; (c) Color chart of the logarithm of simulated erosive loss (log(ton)) for a range of slope (on x-axis) and specific flow accumulation area (on y-axis). Also included on the two axes are the bar plots of total erosive losses per unit area for different Slope and specific catchment area classes; (d) Color chart of the logarithm of simulated deposition (log(ton)). Also included on the two axes are the bar plots of total deposition per unit area for different Slope and specific catchment area classes. Note: grey cells in (c) and (d) are used to identify joint classes with no data.	54
Figure 3-1 Three major processes for erosion and sediment transport	62
Figure 3-2 Location of Dripsey catchment in County Cork, Ireland. The yellow square is the location of flux tower.	74
Figure 3-3 (a) Multi-year(2002-2012) monthly average rainfall Dripsey; (b) Daily rainfall probability plot.....	75
Figure 3-4 Scatter plot for SSY comparison with different model representations and temporal scales (from left to right: daily, monthly, seasonal, and yearly). Points with red color were points of case one in later discussion.....	83

Figure 3-5 The scatter plot of Q and E for two models (left) and zoom-in scatter plot (right)	85
Figure 3-6 (a) Scatter plot of overland flow simulated by curve number method and GEOTopSed; (b) scatter plot of rainfall erosivity versus overland flow simulated by GEOTopSed; (c) rainfall erosivity versus overland flow simulated by curve number method;.....	86
Figure 3-7 Comparison simulations with and without soil moisture feedbacks on soil cohesion.....	87
Figure 3-8 Scatter plots of overland flow simulated by GEOTopSed versus the differences of SSY. The points were color coded with normalized watershed average antecedent soil moisture (θ). The points with black edges indicate underestimation of Q by other model configurations w.r.t. GEOTopSed.....	88
Figure 3-9 (a) Zoomed-in scatter plots of Δ SSY versus Q_G for $Q_G < 6$. (b) the scatter plots of Δ SSY versus ΔQ when $Q_G < 6$ and $\Delta Q < 0$. All plots were color coded with normalized watershed average antecedent soil moisture (θ)......	89
Figure 3-10 (a) scatter plots of SSY by GEOTopSed and RUSLE-TC, color coded with precipitation, only average antecedent soil moisture ($\theta > 0.95$) were showed. (b) the scatter plot for Δ SSY and P, color coded with (P- Q_G). Circles with black edge represent $P < 12.5$ mm, pentagrams with pink edge were points showed in (a)......	90
Figure 3-11(a) Time series of P and Q for case one; (b) time series of normalized soil moisture and Δ SSY.	92
Figure 3-12 Rainfall (a), surface flow (b), soil moisture (c) and SSY (d) generated by GEOTopSed model in 2010.....	95
Figure 3-13 (a) P,Q and SSY time series, (b) the sensitivity analysis on soil cohesion, (c) changes of the soil moisture during the selected period, (d) changes of the soil cohesion during the selected period	96
Figure 3-14 Spatial distribution of annual aggregated erosion, deposition area of different models. Grey color identifies the erosional area and red color shows the depositional area.	98
Figure 3-15 Comparison of erosion/deposition locations between different models.....	103

Figure 3-16 PDFs of drainage area (DA) for agreed erosional and depositional area of different model pairs.	106
Figure 4-1 Selected weather stations in this study. The bars are monthly rainfall for each station and the blue line is the monthly average temperature. Different colors for states identifies different climate regions proposed by National Climate Data Center(Karl and Koss, 1984).....	113
Figure 4-2 (a) Observed and simulated monthly precipitation (base scenario) for three different weather stations, (b) Observed and simulated precipitation probability density functions for three different weather stations.....	116
Figure 4-3 Fitted and observed temperature and relative humidity time series for four stations.....	117
Figure 4-4 Absolute soil loss (left) and relative change of soil losses (right) based on Scenario 2 (a,c Erosivity method, b,d GEOTopSed) for different sites and different scenarios	119
Figure 4-5 Rainfall PDFs of scenario 1 and scenario 9 for three different sites	122
Figure 4-6 Probability densities of the first layer soil moisture for three locations.....	123
Figure 4-7 The buffer effect of soil on hydrological driving force	125

Acknowledgements

I would like to sincerely thank my advisor Professor John D. Albertson and co-advisor Professor Mukesh Kumar, for their invaluable guidance, patience during my study at Duke University. Professor Albertson provided me the opportunity to come to Duke for my graduate study and led me into the research area of hydrology and erosion. His vision for science and ability to pinpoint key points of research always inspire me to think more deeply and solve more challenging questions. Professor Kumar patiently guided me in every aspect of scientific research during my thesis work. His constructive suggestions, motivational encouragement, and our in-depth discussions all tremendously helped me in pursuit of my doctorate degree. Words cannot express my appreciation enough.

I also would like to take this opportunity to thank Professor Amilcare Porporato, Professor Gabriel Katul, Professor Tomasz Hueckel, and Professor Stefano Orlandini for serving on my committee. All your input, help, and support mean a lot to me. I feel really lucky to have the opportunity to work with such extraordinary scientists like you.

Special thanks are given to the Department of Civil and Environmental Engineering of Duke University. The spiritual and financial supports from the department are crucial for me to stay in Ph.D. program and have the chance to finish. Current and former directors of graduate students, Professor John E. Dolbow, Professor

J. Jeffrey Peirce, and Professor Tomasz Hueckel, and our supportive departmental staffs, Ruby Nell Carpenter, Rebecca Dupre, I thank you deeply from my heart.

During my longtime Ph.D. student life in Durham, many faculties, friends, officemates, co-workers provided me help and support for me to overcome setbacks. The precious memories we created together will always be cherished.

Most importantly, my wife Jing Tao is always by my side since we first met. Her belief and comfort lighted up my struggling life. Our daughter, Yizhen Zi, is the best present during my Ph.D. study. Her giggling, crawling, walking, and even some silly stuff she did can always energize me and give me courage to face any challenges. This work would not have been possible without the love and support that my family gave me over all these years.

1 Introduction

1.1 Motivation

Soil erosion by water is a major driven force causing land degradation. Bakker et al. (2004; 2005) suggested 10cm of soil loss would result in 4% yield reduction and Tenberg et al. (1998) found bare soil's production 'half-life' is 10-16 times less than mulch covered soil due to erosion. Globally, 42.8% of the world's land are affected by water erosion(Reich *et al.*, 1999). According to the United States Department of Agriculture's National Resource Conservation Service (NRCS, 2010), in 2007, 99 million acres of land (28% of all cropland) were eroding above soil loss tolerance rates in the US (1-5 tons/acre per year). There were 0.96 billion tons of soil loss due to water erosion in US in 2007.

Laboratory experiments, on-site field study, and suspended sediments measurements were major fundamental approaches to study the mechanisms of soil water erosion and to quantify the erosive losses during rain events. It is challenging to extrapolate the results from laboratory experiments and plot scale observations to a watershed or regional scale (Boardman, 2006). Suspended sediments concentration observation at outlet of a watershed could not be disaggregated into distributed soil loss within the whole watershed (Walling, 1983). Suspended sediment yield is difficult to be used to estimate erosion due to the variability of sediment delivery ratio associating with different temporal and spatial scales (Boardman, 2006).

Given all the challenges that experimental studies face, soil water erosion modeling provides possible solutions for scaling problems in erosion research, and is of principal importance to better understanding the governing processes of water erosion (de Vente and Poesen, 2005). Soil water erosion models are trying to predict the soil losses from land surface with hydrological forces acting on. The relation between soil losses and the driven forces can be described either by empirical regression functions (Wischmeier and Smith, 1960) or by description of the physical processes such as raindrop impact, flow shear stress, and settling of suspended sediments (Bagnold, 1966). Dozens of soil water erosion models were developed following the aforementioned two paths (Williams, 1975; Wischmeier and Smith, 1978; Knisel, 1980; Laflen *et al.*, 1991; Renard *et al.*, 1991; DeRoo *et al.*, 1996; Morgan *et al.*, 1998; Arnold and Fohrer, 2005; Heppner *et al.*, 2006; Kim *et al.*, 2013).

However, water erosion models were “of limited value in the real as opposed to the academic world” (Boardman, 2006). The reasons hindering the practical usage of erosion models include difficulties of acquiring data, the uncertainties from hydrological simulations, and the inherent uncertainties of erosion model itself. Thanks to the improvements that hydrological models gained in recent years, it is possible to investigate the uncertainties of soil erosion modeling caused from hydrological simulations by integrating erosion module into a comprehensive hydrological model. Heppner *et al.* (2006) and Kim and Lee (2013) made progresses towards this direction.

Given the necessity and possibility, the broad goal of this work is to investigate:

1) what is the performance of a comprehensive hydrological model with an erosion module? 2) how is aforementioned model configuration different with other erosion models with relatively simple hydrological representations? 3) what are the implications of the model applications for long term erosion predictions, such as climate change impacts, when taking account for the impact of hydrological processes on soil erosion processes? Future research directions towards soil erosion field and modeling studies are proposed by this work based on the investigation results of the three questions.

1.2 Hydrological processes and soil water erosion

Soil water erosion processes can be divided into raindrop detachment, detachment and deposition in inter-rill area/rills, and sediments transport in overland flow, rills, and channels (Figure 1-1). To accurately describe/predict soil water erosion processes, properly quantify the forces acting on the land surface and describe the land surface characteristics are crucial. The impact from raindrops and shear stress of the overland flow are two major forces causing soil detachment. The sediment transport and deposition processes are closely related to the hydrological state of surface flow. Thus the soil erosion processes are closely related to hydrological processes.

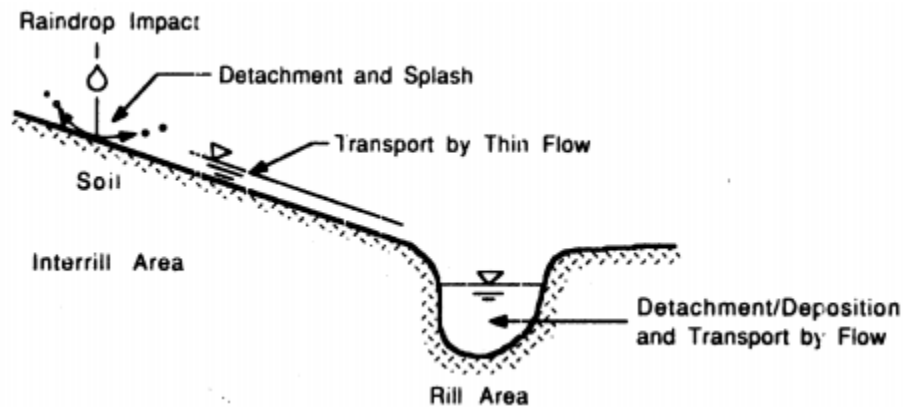


Figure 1-1 Demonstration of soil erosion processes on a hillslope. Source: (Hagen and Foster, 1990)

Various experimental studies show the impacts on soil erosion processes from varied hydrological states and processes. Rainfall, evapotranspiration, interception, infiltration, soil storage, and groundwater are all controlling variables of water erosion processes (Cook, 1937). Spatial and temporal variability of rainfall would influence runoff (Singh, 1997), soil moisture (Liu and Namkhai, 2000), and erosion rate (Kinnell, 2005; Bookhagen and Strecker, 2012). Changes of evapotranspiration losses can result in increase of water available for stream flow and meanwhile increase in soil loss (Croft and Monninger, 1953). Canopy interception can change the kinetic energy of rainfall drops (Vis, 1986), as well as redistribute rainfall (Cao *et al.*, 2008), thus impact the splash detachment processes (Noble and Morgan, 1983; Brandt, 1988; Calder, 2001). Infiltration was found to highly correlated to total soil loss (Miller and Baharuddin, 1986). Soil moisture was found not only correlated to infiltration (Philip, 1957) and runoff generation processes (Henninger *et al.*, 1976; Meyles *et al.*, 2003; Penna *et al.*, 2011), but

also soil physical characteristics such as aggregation stability (Haynes and Swift, 1990), thermodynamics (Edlefsen and Anderson, 1943), albedo (Idso *et al.*, 1975), and etc. Therefore it is a key component influencing erosion processes on both forces and object, which is also found highly correlated to soil loss by a number of studies (Luk, 1985; Fitzjohn *et al.*, 1998; Poesen *et al.*, 1999; Wei *et al.*, 2007; Ziadat and Taimeh, 2013). Surface runoff as one of the direct driving forces of soil detachment and sediment transport, is investigated at varied hydrologic regimes for the erosion study. Changes in connectivity of bare, runoff-generating areas, changes in runoff characteristics, and changes in capacity of the runoff to detach, entrain and transport sediment led to a nonlinear trajectory of erosion rates over the transition from grassland to shrubland (Turnbull *et al.*, 2010). A bimodal dominant discharge for suspended sediment transport was found in semi-arid areas, with one peak in the range of low flows and high flow for the other. Effective discharge was found to be significantly different across experimental basin (Ma *et al.*, 2010). Study showed that surface erosion was correlate to groundwater level when the level is shallow (Rockwell, 2002).

In general, it is evident that hydrological processes can impact soil erosion directly and indirectly. To better understanding the mechanics of soil erosion and sediment transport and to improve the performance of water erosion models, a comprehensive perspective towards hydrological processes is required, according to aforementioned experimental studies.

1.3 Hydrological processes representations in soil erosion and sediment transport models

The effort of quantitatively estimating soil losses caused by water erosion started in 1940s (Musgrave, 1947; Smith and Whitt, 1948). The Universal Soil Loss Equation (USLE) developed by Wischmeier and Smith (1960) and its descendants RUSLE (Renard *et al.*, 1991), MUSLE (Williams, 1975) are the most used empirical water erosion model frames. These soil water erosion models use rainfall or runoff erosivity, soil erodibility, and other regression factors to predict the total amount of soil loss in the area of interest. Rainfall or runoff erosivity is the major driving force that causes soil water erosion. The soil loss was found correlated to rainfall erosivity (R_r), which is related to rainfall kinetic energy (E) and maximum rainfall intensity (I_{30}) (Wischmeier and Smith, 1958; Wischmeier, 1959):

$$R_r = E \cdot I_{30} . \quad (1.1)$$

Equation (1.1) was then adopted in USLE, RUSLE based models. The rainfall erosivity simplifies the representation of hydrological processes that causing soil water erosion. Only rainfall records are needed for erosivity calculation. The impact of hydrological processes of flow generation, flow propagation, and other related processes on soil erosion were estimated with regression factors. No explicit representations were required for erosion estimation using rainfall erosivity method.

The runoff erosivity (R_q) is similar to rainfall erosivity, but the peak flow rate (q_{peak}) and surface runoff volume (Q) are used to estimate the runoff erosivity:

$$R_q = 11.8(Q \cdot q_{peak})^{0.56} . \quad (1.2)$$

Models adopted runoff erosivity method are required to convert precipitation to runoff volume and rate, thus certain levels of hydrological representations are necessary.

Different means were seen for runoff erosivity based erosion models to estimate the runoff volume and rate. One of the most popular methods to estimate the volume of surface runoff for a given rainfall event is the Soil Conservation Service Curve Number (SCS-CN) method (SCS, 1972). Curve number method is a method with simple parameters that computes flow volume for a storm:

$$Q = \frac{(P - I_a)^2}{P - I_a + S} \quad (1.3)$$

where P is rainfall, I_a is initial absorption, and S includes all other loss. Curve number was used to account for the variation in runoff generation processes caused by different land surface conditions. The appropriateness of using this empirical based approximation of runoff generation process in erosion model was questioned by some researchers (Garen and Moore, 2005).

Physically based soil erosion models were aimed to quantify soil loss with more detailed recognition of erosion processes. Rainfall detachment, rill/inter-rill erosion, and sediment transport processes were described in several physically based models (Smith

et al., 1995; DeRoo *et al.*, 1996; Morgan *et al.*, 1998). All physically based water erosion models were taking advantage of more detailed representations for hydrological processes in order to simulate the mass and momentum balance of suspended sediment. The runoff generation processes is a crucial part for physically based water erosion models. Some of the erosion models were integrated into physically based hydrological model(Wicks and Bathurst, 1996; Morgan *et al.*, 1998; Heppner *et al.*, 2006; Kim *et al.*, 2013), the others contains a relatively detailed description of the runoff generation processes themselves(Laflen *et al.*, 1991; DeRoo *et al.*, 1996; Arnold and Fohrer, 2005) or use outputs from hydrological models for erosion calculation(Morgan *et al.*, 1999). Among all those models, Heppner *et al.* (2006) made significant headway in this direction by coupling sediment processes within an integrated hydrologic model, InHM (VanderKwaak and Loague, 2001). It is to be noted that InHM solves subsurface flow using the variably saturated 3D-Richards equation, while surface flow is simulated using diffusion wave approximation of St. Venant equation. Another notable effort in this direction was by Kim *et al.*, (2013), who coupled sediment processes within a hydrologic and hydrodynamic model tRIBS-OFM. The model uses a gravity-dominated formulation (Cabral *et al.*, 1992) to simulate vadose zone flow and a quasi-3D Boussinesq's equation under the Dupuit-Forchheimer assumptions to simulate groundwater flow (Ivanov *et al.*, 2004). These two models not only have the state of art representations of infiltration and runoff generation processes, but also make effort in

the direction of investigating the dynamic role of antecedent conditions and subsurface heterogeneity on erosion.

The one of the major recent developments of water erosion models is the description of hydrological processes. With more comprehensive representation of hydrological processes, the water erosion models are able to simulate erosion at event scale with the estimation of raindrop impact and flow shear stress based on rainfall rate, flow volume, and flow rate. How would these developments influences water erosion modeling needs to be investigated.

1.4 Long Term Soil Water Erosion Model Applications

Models with different detail levels are aimed to solve erosion problem for varied temporal and space scales (Figure 1-2). de Vente and Poesen (2005) reviewed some of the most used erosion models, and concluded that the physically based erosion models with detailed representations of hydrological processes are mainly applied at hillslopes and events scales. While the empirical erosion models, which are aimed for average erosion states for larger temporal and spatial scales, such as basins and multi-years. One of the obstacles that hinders physically based model to be utilized at larger temporal and spatial scales is the demanding for computation power. However, the limitation on hardware is going to be reduced as the technology develops. Another limitation for some of the physically based models is that they did not include enough details of subsurface water movement and water loss caused by evapotranspiration. As a result,

the antecedent condition is treated as a calibration factor (Knisel, 1980; Laflen *et al.*, 1991). This limits the long term applications of these models.

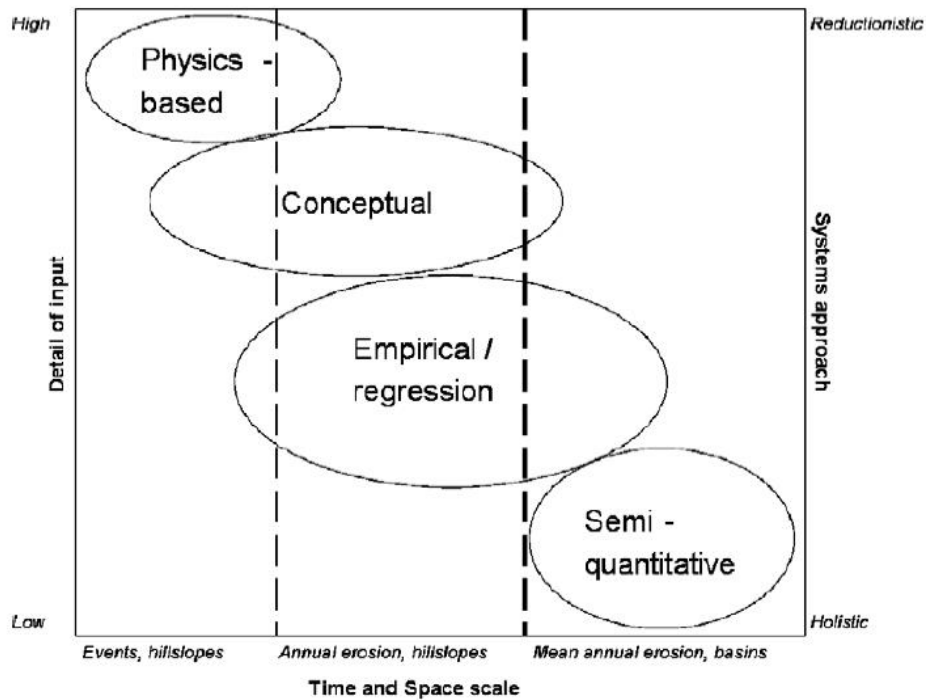


Figure 1-2 Comparison of different model types with respect to scale, input requirements and kind of output. Source: (de Vente and Poesen, 2005)

Empirical models, on the other hand, are designed for long term application (Wischmeier and Smith, 1978; Renard *et al.*, 1991). The concept of rainfall erosive is to reflect the average soil loss rate to the rainfall energy and intensity (Wischmeier and Smith, 1958). Both USLE and RUSLE are recommended to be used for long term average soil loss estimation. Without explicit representations of hydrological processes, empirical models were not able to capture transient variations of erosion processes, which are highly related to antecedent conditions. Thus empirical models have limit application

for events scale. Even though empirical models were designed for estimating long term average soil loss rate, the simplified hydrological processes in models make them incapable to capture the changes of soil loss rate if the hydrological feedbacks changes at long term scale.

With recent effort of physically based erosion model developments (Heppner *et al.*, 2006; Kim and Lee, 2013), it is possible for physically based models simulating erosion beyond events scale. These newly developed models enhanced the representations of hydrological processes thus extended their ability for tracking antecedent conditions by simulations of soil moisture dynamics, energy balances, and surface-subsurface water interactions. This allows us to investigate the role of hydrological feedbacks on long term soil water erosion.

1.5 Chapter overviews

Following these guidelines, this dissertation work first created an erosion modeling tool (GEOtopSed) that takes advantage of the comprehensive hydrological model (GEOtop). The newly created tool was tested at an experimental watershed. The performance of the model is evaluated, especially the role of antecedent condition on soil erosion simulation (Chapter 2). After the newly developed tool showed its ability to estimate multi-year soil erosion rate with varied hydrological conditions, the tool was used to compare with erosion models with different hydrological representations. A 11-year simulation was conducted for each of the selected models. The results were

compared at varied temporal and spatial scales to highlight the roles of hydrological feedbacks on erosion (Chapter 3). The differences in model hydrological representations led to an investigation for erosion simulation at different rainfall regimes. Multi-year ensemble simulations with different extreme precipitation scenarios were conducted at seven selected locations. The impacts of hydrological feedbacks on soil erosion were investigated by comparing the simulation results to purely changes caused by rainfall patterns. The differences in erosion simulation results showed the influences of hydrological feedbacks which cannot be seen by erosivity method (Chapter 4). In Chapter 5, the major results and limitations of this work were summarized and future work suggestions were proposed.

2 Simulating the spatio-temporal dynamics of soil erosion, deposition, and yield using a coupled sediment dynamics and 3D distributed hydrologic model

This chapter is a modified version of the journal article currently under review in *Environmental Modeling and Software* with the reference:

Tan Zi, Mukesh Kumar, Gerard Kiely, Ciaran Lewis, John Albertson, Simulating the spatio-temporal dynamics of soil erosion, deposition, and yield using a coupled sediment dynamics and 3D distributed hydrologic model (in review after major revision), *Environmental Modeling and Software*.

2.1 Introduction

Soil erosion by rainfall and overland flow is a widespread threat to soil fertility and water quality. Accurate estimation of soil loss and its spatial distribution is often needed for pollutant risk analyses, reservoir management, agriculture productivity forecasts, and soil and water conservation. In this regard, several distributed models have been developed to obtain erosion estimates (DeRoo et al., 1996; Wicks and Bathurst, 1996; Morgan et al., 1998; Hessel, 2005; Jain et al., 2005; de Vente et al., 2008). Notably, majority of distributed erosion-deposition models e.g., WEPP, EUROSEM etc., consider simplistic representations of vertical and lateral subsurface water flow, and often do not account for the lateral subsurface water movement, or the coupled dynamic interactions between vadose zone and the groundwater table, or the evolution of soil

moisture and groundwater with evapotranspiration. Given that the detachment, transport, and deposition of soil are dominantly influenced by the velocity and volume of overland flow (Julien and Simons, 1985), which in turn may be influenced by antecedent soil moisture conditions (Legates et al., 2011; Penna et al., 2011; Jost et al., 2012; Chen et al., 2014; Hueso-González et al., 2015), subsurface heterogeneity (Lewis et al., 2012; Ghimire et al., 2013; Orchard et al., 2013; Zimmermann et al., 2013; Niu et al., 2014; Tao and Barros, 2014), and groundwater distribution (Kumar et al., 2009; Miguez-Macho and Fan, 2012; Rosenberg et al., 2013; Safeeq et al., 2014; von Freyberg et al., 2015), it is important to consider the coupled impacts of antecedent hydrologic states (soil moisture and groundwater distribution) and subsurface hydrogeologic properties on sediment generation and yield. Failing to do so may limit the applicability of these models to a few events (Hessel et al., 2006; Mati et al., 2006; Ramsankaran et al., 2013) or to regimes where the dynamic role of antecedent conditions and subsurface heterogeneity on erosion are not large enough. Heppner et al. (2006) made significant headway in this direction by coupling sediment processes within an integrated hydrologic model, InHM (VanderKwaak and Loague, 2001). The study specifically evaluated the rainfall splash erosion component of the model on a 6 m by 2.4 m plot. Heppner et al. (2007) used the same model to perform sediment-transport simulations for six events in a 0.1 km² rangeland catchment. It is to be noted that InHM solves subsurface flow using the variably saturated 3D-Richards equation, while surface flow is

simulated using diffusion wave approximation of St. Venant equation. Equations corresponding to these coupled processes are spatially discretized using a control volume finite element strategy on each unstructured grid. A global implicit solver is used to perform the simulation. Another notable effort in this direction was by Kim et al., (2013), who coupled sediment processes within a hydrologic and hydrodynamic model tRIBS-OFM and validated their model against analytical solutions. Similar to InHM, tRIBS-OFM is also an unstructured grid based model. The model uses a gravity-dominated formulation (Cabral et al., 1992) to simulate vadose zone flow and a quasi-3D Boussinesq's equation under the Dupuit-Forchheimer assumptions to simulate groundwater flow (Ivanov et al., 2004). The model was used to evaluate sediment yield simulations for 10 events in a 0.036 km² Lucky Hills watershed located in southeastern Arizona, USA. Development of these physically-based integrated models of hydrology and sediment dynamics has opened new opportunities, especially in regards to understanding the impact of the hydrologic state on spatio-temporal distribution of erosion, deposition and yield. Notably, the aforementioned two models are not open-source.

Here, we develop an open-source, spatially-explicit, structured-grid based, sediment erosion/deposition module for a 3D surface-subsurface hydrologic model, GEOtop (Rigon et al., 2006; Endrizzi et al., 2014), and evaluate its applicability in explaining the sediment yield dynamics. Similar to InHM (Heppner et al., 2007), the

GEOtop model also solves subsurface flow using the variably saturated 3D-Richards equation, while surface flow is simulated using kinematic wave approximation of St. Venant equation. The sediment dynamics model developed here takes advantage of the GEOtop simulated distributed hydrological states such as moisture content, surface flow depth, and flow velocity. The model accounts for the influence of spatial heterogeneities in land surface characteristics, subsurface hydrogeology, and antecedent conditions in the generation of overland flow, and hence on the erosion and deposition of sediment in the catchment. The model developed here was applied on a much larger catchment (area = 15 km²) and for a longer period (simulation duration = 2 years) than in Heppner et al. (2007) and Kim et al. (2013), allowing validation of the coupled model for extended wet and dry periods. The coupled model is then used synergistically with the observed data to answer four pointed questions: a) Is the performance of the GEOtopSed model for simulating SSY, dependent on the flow regime and the model's ability to capture streamflow response? b) Does the daily suspended sediment yield (SSY) from the watershed vary monotonically with precipitation amount and energy? If not, does the hydrologic response of the watershed has a role to play in the departure from monotonic relation? c) Does the simulated source/sink area of sediments vary spatially from one event to other? If yes, is the variation driven by hydrologic state, specifically the surface soil saturation state? and d) To what extent does the linear relation between erosion and the slope-length factor (product of specific catchment area and slope), which is often

used in USLE-based model representations (e.g. USLE (Wischmeier and Smith, 1978), RUSLE (Renard et al., 1991), RUSLE2 (Foster et al., 2005)), hold for GeoTopSed simulated states and fluxes?

2.2 *Process Formulation, Model Implementation, and Verification*

2.2.1 The GEOtop model: A short review

The open-source GEOtop model (Rigon et al., 2006) is process based and simulates core hydrological processes such as unsaturated flow, saturated flow, overland flow, stream flow generation/routing, and surface energy balances. Overland flow modeling is performed using the kinematic wave approximation of St. Venant equation while subsurface flow and soil moisture simulations are performed by solving a variably-saturated representation of 3D Richards equation. By solving the Richards equation, GEOtop model can simulate the surface runoff generation processes due to both infiltration excess and saturation excess, and can also redistribute the sub-surface water both laterally and vertically, as determined by the head gradient. The model has been extensively tested and validated in Bertoldi (2004). The water and energy balance calculations in GEOtop were recently refined to account for soil freezing and thawing effects (Endrizzi et al., 2014). In summary, with detailed water and energy balance modules, GEOtop can provide accurate simulations of evapotranspiration and soil

moisture dynamics (Bertoldi et al., 2014; Della Chiesa et al., 2014), given adequate watershed data. By simulating coupled hydrologic states (e.g. surface flow depth, soil moisture and groundwater) on each grid of the model domain, the model is well suited to study the influence of watershed properties and subsurface states on spatially-distributed runoff, an important control on erosion, at multiple scales. Furthermore, as an open source software (<http://www.geotop.org/wordpress/>), the GEOtop model provides a complete hydrological model framework with ease for extensions. One such example is the incorporation of landslide occurrence prediction within the GEOtop framework by Simoni et al. (2008).

2.2.2 Process formulation of the sediment dynamics model

The sediment dynamics model developed here takes advantage of the GEOtop simulated distributed hydrological states such as moisture content, surface flow depth, and flow velocity. Here we only highlight the aspects of the model that are most relevant to the sediment erosion, deposition and transport modeling. Readers may refer to GEOtop model papers (Rigon et al., 2006; Endrizzi et al., 2014) to learn more about the individual process representations.

GEOtop simulates soil moisture in each subsurface layer by solving the 3D Richards equation:

$$(C(H)\phi + S_w S_s) \frac{\partial H}{\partial t} + \nabla \cdot (-K \nabla H) + S_w = 0 \quad (2.1)$$

where $d\theta[-]$ is the rate of change of moisture content within a control volume, K [m s^{-1}] is the hydraulic conductivity, H [m] is the sum of pressure and potential head, and S_w is the source/sink mass flux [s^{-1}], S_s is the specific storage coefficient [m^{-1}], ϕ is porosity [-], and $C(H)$ is the specific moisture capacity function.

Surface overland flow is routed along the flow direction using kinematic wave approximation of the Saint-Venant equation represented as:

$$\frac{\partial h}{\partial t} + \frac{\partial q}{\partial x} = q_L \quad (2.2)$$

where h is depth of overland flow [m], x is a local coordinate system oriented along the flow direction [m]; q is flow rate per unit width [$\text{m}^2 \text{s}^{-1}$], and q_L is vertical inflow or outflow rate (to the surface water) per unit area [m s^{-1}]. The flow direction is defined along the line of steepest downslope head gradient between the grid and its eight neighbors. The overland flow equation is coupled to the continuity equation of sediment transport at each time step using:

$$\frac{\partial hC}{\partial t} + \frac{\partial qC}{\partial x} = E_x \quad (2.3)$$

where C is sediment concentration in the overland flow within each cell [kg m^{-3}], and E_x is the exchange rate of sediment per unit surface area [$\text{kg m}^{-2} \text{s}^{-1}$] at the interface of soil and water. E_x is composed of three major mechanisms: rainfall splash detachment (D_R), flow detachment (D_F) and deposition (D_P), as:

$$E_x = D_R + D_F - D_P . \quad (2.4)$$

D_R [$\text{kg m}^{-2} \text{s}^{-1}$] is approximated by DeRoo et al. (1996):

$$D_R = (0.1033 \frac{Ke}{\zeta} e^{-1.48h} + 3.58) \cdot I \quad (2.5)$$

where ζ is soil cohesion [kPa], Ke is rainfall kinetic energy [$\text{J m}^{-2} \text{mm}^{-1}$], and I is the precipitation intensity [mm h^{-1}]. D_F and D_P [$\text{kg m}^{-2} \text{s}^{-1}$] are related to transport capacity (T_C) based on the erosion-deposition theory proposed by Smith et al. (1995a):

$$D_F = (T_C - C) \cdot y \cdot v_s \quad (2.6)$$

$$D_P = (T_C - C) \cdot v_s \quad (2.7)$$

where y is an efficiency coefficient that is a function of soil cohesion (DeRoo et al., 1996), and v_s is settling velocity of the particles [m s^{-1}]. The dependence of soil cohesion on soil moisture (Bullock et al., 1988) and root tensile strength (Wu et al., 1979) is captured using:

$$\zeta_s = \left(\frac{\theta}{\theta_s}\right)^2 \zeta_{ss} \quad (2.8)$$

$$\zeta_{add} = 1.2 * R_S \quad (2.9)$$

$$\zeta = \zeta_{add} + \zeta_s \quad (2.10)$$

where ζ_s , ζ_{ss} , ζ_{add} are bare soil cohesion, saturated bare soil cohesion and additional cohesion by roots respectively, θ and θ_s are the soil moisture and saturated soil moisture contents respectively, and R_s is the root total tensile strength [kPa]. The transport capacity is based on the experiments conducted by Govers (1990):

$$T_C = a(\omega - \omega_{cr})^b * \rho \quad (2.11)$$

where ω is the unit stream power [m s^{-1}] (Yang, 1972), ω_{cr} is the critical power that initiates flow detachment of soil particles [m s^{-1}], ρ is the density of soil particles [kg m^{-3}], and a and b are empirical parameters related to soil particle size.

The sediment mass balance in each stream channel reach was calculated using:

$$\frac{\partial h_c C_c}{\partial t} + \frac{\partial q_c C_c}{\partial x} = I_n \quad (2.12)$$

where q_c is the discharge per unit width in channel [m s^{-1}], h_c is the water depth of channel [m], C_c is sediment concentration in channel [kg m^{-3}], and I_n is the sediment exchange rate per unit area between adjacent land cells and the channel cell [$\text{kg m}^{-2} \text{s}^{-1}$]. The suspended sediment yield (SSY) [kg] at the outlet of the catchment was the integration of suspended sediments over the period of interest:

$$SSY = \int Q_{ol} C_{ol} dt \quad (2.13)$$

where Q_{ol} is the discharge rate at outlet [$\text{m}^3 \text{s}^{-1}$], C_{ol} is the sediment concentration at the outlet cell [kg m^{-3}] and dt is an hourly integration time step. The period of integration in the ensuing analyses varied from hourly to annual scale and has been appropriately identified at relevant locations.

2.2.3 Model Implementation

The GEOtop model first solves the finite difference discretization of 3D Richards equation (equation (2.1)) using Bi-conjugate gradient stabilized method (Vorst, 1992). An absolute numerical tolerance of 10^{-4} mm is used for ensure water balance. This requires performing simulations at an adaptive time-step with time intervals generally ranging from minutes to hours. After solving the 3D Richards equation, H in the top layer is used to calculate the head gradient for estimation of infiltration/exfiltration flux in equations (2.1) and (2.2), at a user defined interval (hourly in this study). Finite difference discretization of the surface flow, channel routing, and sediment transport equations (equations (2.2), (2.3), and (2.12)) are then solved altogether using a forward explicit Euler method. To ensure stability, Courant-Friedrichs-Lewy (CFL) condition is used. The Courant number is set to 0.25. If the CFL condition is not satisfied, the time step is reduced by 75% adaptively until it gets satisfied. Although the integrated model simulations are performed using an adaptive time-stepping scheme, the model outputs are printed at constant intervals.

2.2.4 Model verification at plot scale

GEOtopSed was first evaluated on a soil flume setup discussed in Ran et al. (2012). The setup included a rainfall simulator, a tilted soil flume, an overland flow collector, and a set of soil water content monitor devices. The rainfall simulator was used to generate rain events of varying intensity, duration, moving direction, rainfall position, and no-rainfall interval. The size of the soil flume was 5 m long by 1 m wide. In the flume, a 30 cm thick soil layer with a fixed slope of 25°, and containing 13% clay, 58% silt, and 29% sand was set on top of a 5 cm thick sand layer. Surface runoff and sediment were collected at the end of the soil flume in a metal container placed slightly below the soil surface. All other boundaries of the soil flume were impermeable. Readers are referred to Ran et al. (2012) to learn more about the experimental setup. The model simulations were performed on a grid discretization with a resolution of 1m x 1m x 10cm in x, y and z directions. The model results were output at 3 minutes interval in this experiment.

Out of 33 rainfall scenario experiments discussed in Ran et al. (2012), here we summarize the results for three scenarios (No.10, No.14, and No.18) with markedly different rainfall intensities (Table 2-1). For scenario 10 (Figure 2-1) which included rain events of highest rainfall intensity (> 80 mm/h) and shortest duration among the three selected scenarios, the model was able to capture the observed timing of both flow and SSC peaks. Observed flow peaks were also captured accurately. Further analyses of

simulation results suggest that a smaller runoff peak for the first event, even though the duration and intensity of all the precipitation events were almost identical, was because of drier antecedent soil moisture conditions in the top soil layer. Once the moisture deficit of top layer is fulfilled, additional precipitation contributes to infiltration-excess runoff even while the lower soil layers are not yet saturated. Since the second event occurred only 0.25 hours after the first one, the top soil layer was still near saturation resulting in a larger runoff peak than the first event. For later events, several model cells were fully saturated i.e. all vertical layers were saturated, indicating that both infiltration-excess and saturation-excess processes played a role in generation of runoff peaks for these events. The model was also able to capture the relatively smaller runoff peak magnitude in scenarios 14 and 18 due to the reduced intensity of events. Overall, the timing of simulated SSC peaks also matched the peak in observed records. For scenario 10, the model was able to capture the magnitude and the decreasing trend in SSC for events 2 to 5. The first simulated SSC peak was however underestimated. Analyses of simulated states suggest that the decreasing trend in SSC may be explained based on the combined effects of increase in flow volume which reduces SSC, reduction in sediment generation with small decrease in peak flow, and an increase in soil cohesion with increasing soil moisture which impedes sediment generation. For scenario 14, the model was again able to capture the decreasing trend in SSC for the four events. In scenario 18, the SSC was measured only for two events as the first precipitation pulse

did not generate any response. The model captured the magnitude of runoff peak corresponding to the third event, but underestimated for the second event. It is to be noted that the runoff generated for the second event is negligible and SSC estimates are very sensitive at these magnitudes.

Table 2-1 Summary of plot experiment. The experiment data are from Ran et al. (2012). Numbers in the parenthesis are simulation results from GEOTopSed.

Scenario No.	Event	Rainfall intensity (mm/h)	Rainfall amount (mm)	Rainfall duration (h)	No-rainfall interval (h)	Time of runoff peak (h)	Runoff peak (ml/s)	SSC (kg/ m ³)
10	US001	3.99	1.00	0.2	0	0.12(0.15)	30.2(31)	57.08(25.6)
	US002	4.42	1.10	0.25	0.25	0.09(0.15)	38.8(41)	30.05(32.6)
	US003	5.05	1.26	0.25	0.5	0.20(0.25)	40(40)	19.53(32.7)
	US004	6.08	1.52	0.25	1	0.12(0.15)	38.9(35)	14.30(24.2)
	US005	3.80	0.95	0.25	3	0.18(0.15)	40.8(36)	10.63(20.3)
14	UM001	9.15	9.57	0.5	0	0.24(0.4)	13.6(17)	69.35(89.4)
	UM002	9.28	9.64	0.5	0.5	0.27(0.3)	21.95(21)	36.76(33.4)
	UM003	9.47	9.73	0.5	1	0.21(0.3)	22.4(23)	24.20(18.3)
	UM004	1.09	0.54	0.5	3	0.27(0.5)	21.45(20)	16.78(18.7)
18	UW001	9.63	9.63	1	0	0.00(0)	0(0)	0.00(0)
	UW002	3.45	3.45	1	1	0.27(0.65)	0.233(1)	4.77(0.001)
	UW003	4.35	4.35	1	3	0.33(0.65)	7.5(11)	6.71(6.38)

In summary, the GEOTopSed model generally captured both the trend and the quantity of runoff and suspended sediment concentration (SSC). It is to be noted that an accurate simulation of runoff and consequently of SSC was possible because of comprehensive representation of surface and subsurface hydrological processes in the model.

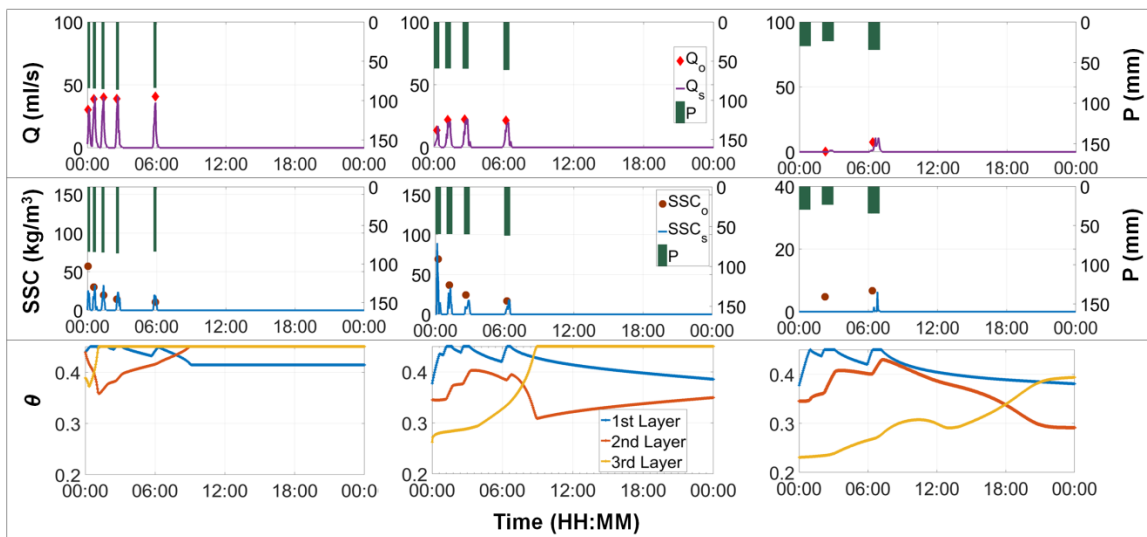


Figure 2-1 Modeled and observed records for rainfall scenarios 10 (left column), 14 (middle column), and 18 (right column). The first row are the time series of precipitation and surface runoff; the second row are time series of precipitation and suspended sediment concentration (SSC); and the third row are time series of plot-average soil moisture of three subsurface layers. In the top two rows, precipitation (P) is plotted on the secondary axis.

2.3 Model Application at Watershed Scale

2.3.1 Site description

The coupled model was applied at a small experimental catchment, in Dripsey, Ireland (Figure 2-2). Given that groundwater and antecedent soil moisture have been

found to play an important role on runoff generation (Lewis et al., 2013) and nutrient transport (Warner et al., 2009) in the catchment, the site serves as a good test case for validating the integrated model at catchment scale. The Dripsey catchment is located approximately 25 km northeast of Cork, and has an area of 15 km². The elevation of this catchment ranges from 60 to 210 m. It is a beef and dairy producing agricultural catchment and is almost 100% covered by perennial ryegrass. The catchment slopes gently, with around 85% of the area having less than 3% grade. Gleys and podzols are the two major soil types. The experimental field site is managed by the Hydromet team of the University College Cork (UCC). There is a meteorological flux tower at the top of the catchment (elevation 192 m) where radiation, wind speed, air temperature, surface temperature, relative humidity, and soil moisture (at five depths) have been measured at 30 minutes interval since 1998 (Albertson and Kiely, 2001). All the meteorological data from the site are archived in the FLUXNET repository (<http://fluxnet.ornl.gov>). At the catchment outlet (elevation 60 m), stream flow was monitored continuously at 30 minutes interval for a period of over two years (2002-2003). Flow-weighted water samples at the catchment outlet were collected using an ISCO 6712 auto-sampler with intake set at approximately 0.25 m above the streambed (Lewis, 2003; Lewis, 2011).

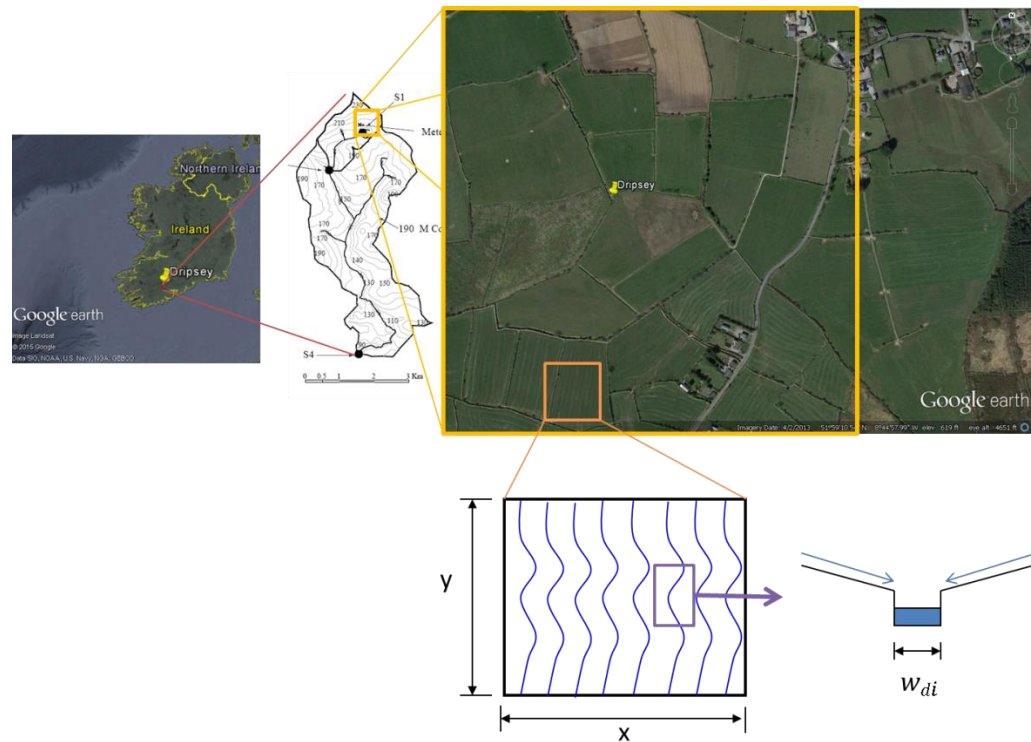


Figure 2-2 Location of Dripsey catchment in County Cork, Ireland. The location of the meteorological tower is where “Dripsey” is marked in yellow. The right top panel is the Google Earth image of Dripsey catchment. The lower panel shows the conceptualization of rills (discussed in section 2.3.3).

The climate in the study region is temperate maritime, and is characterized by high humidity and a lack of temperature extremes during the year. The minimum daily temperature for years 2002 and 2003 was -0.2°C . The mean annual precipitation locally is approximately 1400 mm. The annual precipitation in the Dripsey catchment for year 2002 and 2003 was 1823 mm and 1178 mm, respectively. Winter and spring were the wetter seasons while summer was generally dry (Figure 2-3). No precipitation was recorded during the period with temperature below 0°C during the two years.

Suspended sediment losses over the catchment were estimated from measured data of stream flow volume and suspended sediment concentration. The monthly variations in suspended sediment yield are shown in Figure 2-3. Notably, the runoff ratio in January, 2003 is larger than one. This indicates that antecedent groundwater recharge participated in delayed streamflow response in this month. Marked variations in runoff ratio through the year underscores the need for appropriate partitioning of the water budget across different stores of the hydrologic continuum.

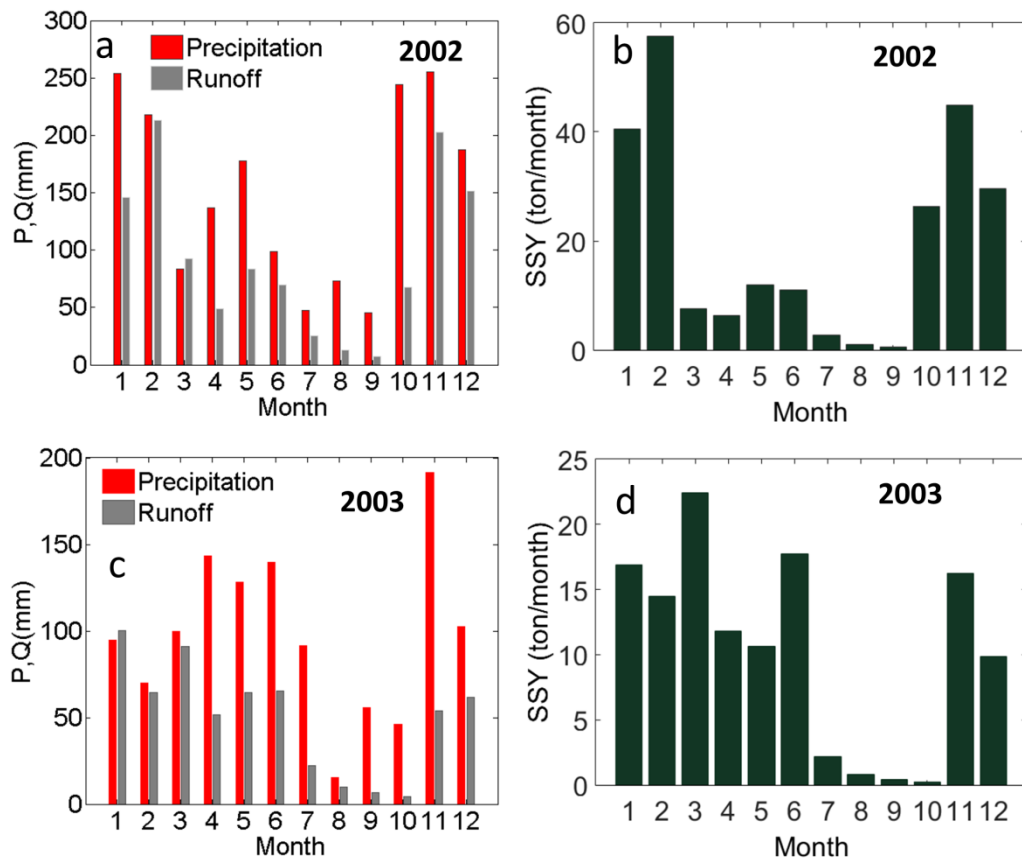


Figure 2-3 Observed monthly variations in precipitation (P), discharge volume (Q) and suspended sediment losses (SSY) in the Dripsey catchment

2.3.2 Input data

GEOtop requires a digital elevation model (DEM), land use/land cover (LULC) map, and soil type map to simulate the hydrological processes for a catchment. The soil type map and soil parameters were obtained from Irish Forestry soils (IFS) database and in situ soil samples (Lewis, 2011). LULC parameters were derived based on classifications using the Corine land cover 2000 database and land use data observed in the catchment. The stream channel was delineated using DEM processing in GIS. The derived extent of stream was validated against the regional channel map. Geomorphic properties of the channel were defined based on the DEM data. All thematic maps were resampled at 50 m × 50 m spatial resolution. Meteorological data such as precipitation, temperature, incoming shortwave radiation, air pressure, relative humidity, wind speed and direction in half-hourly time steps were collected at the HYDROMET flux tower at Dripsey. Because of the small size of the catchment (area = 15km²) and absence of any other precipitation data fine enough to resolve the heterogeneities within the watershed, the rainfall was assumed to be uniform within the catchment. The assumption is reasonable given the mild topographic relief and a uniform land cover within the catchment. The stream flow and suspended sediment concentration data, collected by the water level recorder and water ISCO 6712 auto-sampler at the outlet of catchment, were used to both calibrate and validate the model.

2.3.3 Model implementation in Dripsey catchment

The integrated model simulations were performed at 50 m × 50 m spatial resolution. Simulation results were output at hourly temporal resolution. While overland flow (from either saturation excess or infiltration excess) is generated over the entire land surface cell in the original GTOPO model, a rill width ratio (w_{dx}) parameter was introduced in the sediment dynamics model to account for the flow organization within each cell. The assumption here is that the generated overland flow is transferred into small rills (Figure 2-2) in which overland flow gets concentrated and the potential of rill erosion is high. The rill width ratio (w_{dx}) was calculated using the following equation:

$$w_{dx} = \frac{\sum_i w_{di}}{x_w} \quad (2.14)$$

where i is the rill index within a cell, w_{di} is the width of i^{th} rill [m], and x_w is the width of the cell [m]. In other words, w_{dx} is the fraction of a grid cell covered by overland flow, when overland flow is active. The soil erosion calculations were accordingly modified to account for erosion under a redistributed overland flow regime. Rain splash detachment occurred in the entire cell while the flow detachment only occurred within the rills. While rill characteristics can be observed, the absence of relevant data for the site leads us to consider rill characteristics as a calibration parameter. This is an important area for future research attention.

The model accounts for erosion, deposition, and transport of suspended sediment on the hillslopes. However, considering that the bank and bed erosion and deposition in first order river channels are not significant (Golubev, 1982), these processes were not included in sediment dynamics calculations in the channel. All the sediment entering the channels was assumed to directly reach the outlet of the watershed. It is to be acknowledged that this assumption may cause bias in suspended sediment yield estimates, especially from large basins wherein river beds and banks can be a significant source and/or sink of sediment.

2.3.4 Sensitivity analysis

A global multivariate sensitivity analyses was first conducted to evaluate the role of physics-based parameters that may impact soil erosion and deposition. The methodology is based on a Monte Carlo framework, and can be used to analyze the influence of a parameter while also considering the influence of all other parameters at the same time (Franks et al., 1997). The parameters chosen for the sensitivity analysis included hydrologic properties that may influence runoff generation (Table 2-2) and land properties that may influence soil erodibility (Table 2-3). Ranges of some of the soil parameter such as saturated conductivity for different layers (K), soil residual water content (θ_r), wilting point (θ_w), field capacity (θ_{fc}), saturated water content (θ_s), and soil median particle size (D_{50}) were assigned based on the sand-silt-clay fraction of in situ soil samples (Lewis, 2011). The LAI range was assigned based on the land cover of the

catchment. Other parameters (Table 2-2, Table 2-3), such as Chezy's roughness coefficient (C_m), rill width ratio (w_{dx}), and root area ratio (R_a) were assigned a conservative range large enough to encompass the range of parameters used in previous studies. Model simulations were conducted using a single rainfall event for 10,000 random sets of parameters, which were sampled from uniform distributions across the specified parameter ranges. Based on the rank of Nash-Sutcliffe coefficients (NSE) for each parameter set, the 10,000 parameter sets were divided into ten performance classes, each with 1000 parameter sets. The classes were ranked by NSE from low to high, i.e. Class 1 consisted of parameter sets with lowest NSE while Class 10 comprised of parameter sets with highest NSE. A numerical sensitivity index (NSI) was used to quantify the sensitivity (Montaldo et al., 2003):

$$NSI = \frac{1}{n_c N x_{range}} \sum_{i=1}^{n_c} \sum_{j=1}^N x_d(i, j) \quad (2.15)$$

where x_d is the difference between the parameter values of two classes for the j th cumulative frequency and for i th pair of cumulative frequency curves, n_c is the total number of pairs of cumulative frequency classes (with 10 classes, $n_c = 45$), and N is the number of cumulative frequency values in each performance class ($N=1000$ in this case). x_{range} is the range of parameter values. NSI is an indicator of the distance between each class. A larger value of NSI for a parameter indicates higher sensitivity to it. It is to be noted that while generating the parameter sets, extra care was taken to ensure that the

considered values of dependent parameters were physically realistic. For example, only the parameter sets with soil residual water content (θ_r), wilting point (θ_w), field capacity (θ_{fc}) and saturated water content (θ_s) in increasing order were considered. It is also possible that only certain ranges of parameters may co-exist. However, because of the absence of any parameter-concurrency data for the region, the sensitivity analyses did not consider this.

Table 2-2 Ranges and numerical sensitivity index (NSI) of hydrologic parameters

Variable Name	Description	Range	NSI
LAI	Leaf area index	0.1-4	0.073
C_F	Canopy fraction	0-1	0.0009
C_m	Chezy's roughness coefficient	0.01-5	0.0325
w_{dx}	Rill width ratio	0.01-1	0.073
D_1 [mm]	Soil depth of first layer	25-300	0.0731
K_{h_L1} [mm s ⁻¹]	Horizontal saturated conductivity(1 st layer)	0.00036-0.12	0.0008
K_{v_L1} [mm s ⁻¹]	Vertical saturated conductivity(1 st layer)	0.00036-0.06	0.0322
θ_{r_L1}	Residual water content (1 st layer)	0.03-0.06	0.0033
θ_{w_L1}	Wilting point(1 st layer)	0.06-0.16	0.0040
θ_{fc_L1}	Field capacity(1 st layer)	0.3-0.5	0.0050
θ_{s_L1}	Saturated water content(1 st layer)	0.3-0.6	0.0045
K_{h_L2} [mm s ⁻¹]	Horizontal saturated conductivity(2 nd layer)	0.00036-0.12	0.0012
K_{v_L2} [mm s ⁻¹]	Vertical saturated conductivity(2 nd layer)	0.00036-0.06	0.0001
θ_{r_L2}	Residual water content (2 nd layer)	0.03-0.06	0.0035
θ_{w_L2}	Wilting point(2 nd layer)	0.06-0.16	0.0006

θ_{fc_L2}	Field capacity(2 nd layer)	0.3-0.5	0.0013
θ_{s_L2}	Saturated water content(2 nd layer)	0.3-0.6	0.0062
K_{h_L3} [mm s ⁻¹]	Horizontal saturated conductivity(3 rd layer)	0.00036-0.12	0.0076
K_{v_L3} [mm s ⁻¹]	Vertical saturated conductivity(3 rd layer)	0.00036-0.06	0.0119
θ_{r_L3}	Residual water content (3 rd layer)	0.03-0.06	0.0026
θ_{w_L3}	Wilting point(3 rd layer)	0.06-0.16	0.0006
θ_{fc_L3}	Field capacity(3 rd layer)	0.3-0.5	0.0048
θ_{s_L3}	Saturated water content(3 rd layer)	0.3-0.6	0.0005

Table 2-3 Ranges and numerical sensitivity index (NSI) of erosion and sediment dynamics parameters

Variable Name	Description	Range	NSI
C_m	Chezy's roughness coefficient	0.01-5	0.3569
R_s [MPa]	Root tensile strength	0.001-0.1	0.0236
R_a	Root area ratio	0.001-0.1	0.0033
w_{dx}	Rill width ratio	0.01-1	0.3569
D_{50} [μm]	Median particle size	5-200	0.3563
ζ [kPa]	Soil cohesion	0-30	0.0237

The sensitivity of hydrologic and land surface parameters is presented individually here. Among the 23 parameters selected for the hydrological sensitivity analysis, leaf area index (*LAI*), rill width ratio (w_{dx}), depth of the first soil layer (D_1), Chezy's roughness coefficient (C_m), and vertical hydraulic conductivity of the first soil layer (K_{h_L2}) were found to be among the five most sensitive parameters for runoff

generation (Table 2-2). Similarly, C_m , w_{dx} and D_{50} were observed to be the three most sensitive parameters for sediment yield simulations (Table 2-3). Root tensile strength (R_s) and soil cohesion (ζ) also were important players in sediment yield simulations, though to a lesser extent than the other three parameters identified above. Among the three most sensitive parameters for sediment yield, D_{50} can be estimated from soil texture and C_m can be related to land cover and land use. w_{dx} can be highly varied between different watersheds or land parcels depending on micro-topographic heterogeneity arising from natural causes or implementation of agricultural practices (e.g. tillage farming). The other two sensitive parameters for sediment yield simulations: root tensile strength (R_s) and soil cohesion (ζ), are correlated, as R_s proportionally affects ζ (see equations (2.7), (2.8), and (2.9)) and both the parameters have a tendency to reduce soil erosion.

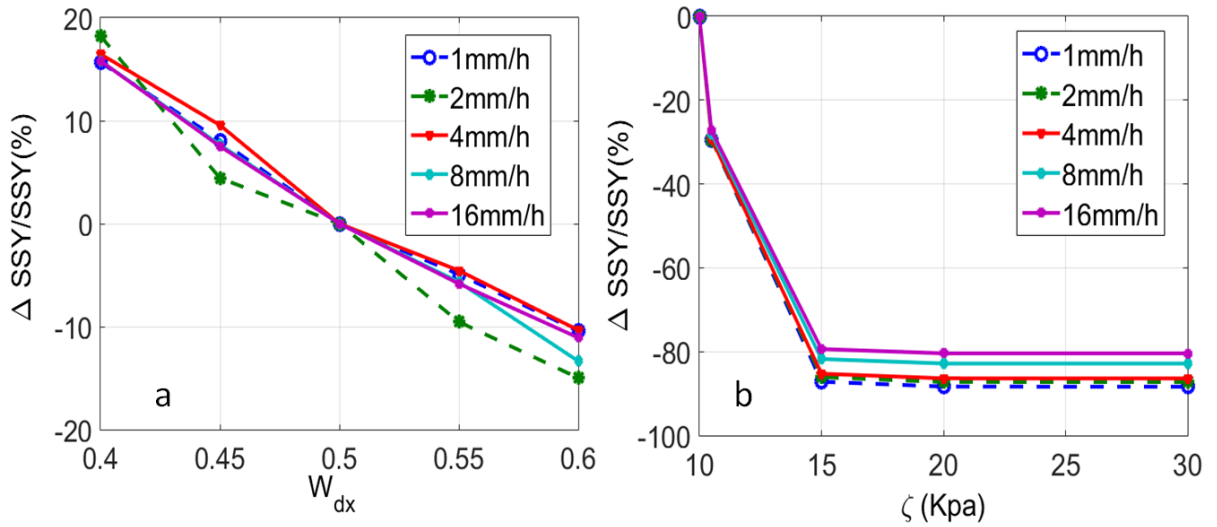


Figure 2-4 Sensitivity of rill width ratio, w_{dx} (a) and soil cohesion, ζ (b) on suspended sediment yield (SSY) for a range of precipitation intensities.

Having identified the most sensitive parameters, next a univariate sensitivity experiment was performed to investigate the role of two sensitive but independent parameters (w_{dx} and ζ) on erosion simulations. This involved forcing the model with a 32 mm precipitation event of 24 hours duration. As shown in Figure 2-4, increasing w_{dx} caused a reduction in suspended sediment losses. This is because for a wider rill, overland flow depth and velocity is smaller resulting in a smaller shear stress between water and soil surface to detach the soil particles. It is to be noted that the relative changes in w_{dx} (base value equals to 0.5) were larger than the relative changes in SSY. For example, 20% decrease in w_{dx} increased sediment yield by 15%. This was due to the offset effect of reduction in flow detachment area when the rills are narrower.

Five additional sensitivity experiments with varying rainfall intensities, but with identical precipitation amount, were conducted to evaluate potential controls of event

characteristics on the sensitivity of sediment yield to w_{dx} . Different rainfall intensities did not show significant impacts on sensitivity analysis, indicating that flow detachment rather than splash erosion, was the major driving force for water erosion in Dripsey catchment. This is possibly caused by the dense grassland vegetation cover within Dripsey catchment which protected the soil surface from detachment by raindrops. Similar sensitivity experiment for soil cohesion (ζ) showed that the sediment yield decreased with increase in ζ . The influence of soil cohesion on erosion was the largest when cohesion value was between 10 to 20 kPa. Notably, as the precipitation intensity increased, the sensitivity to soil cohesion decreased.

It is to be noted that sediment yield simulations could be influenced both by parameters that control rainfall-runoff processes and parameters that define the land surface and soil characteristics. This makes calibration of a physically based integrated erosion-deposition models much more challenging than integrated hydrologic models.

2.3.5 Model Performance During Calibration and Validation Periods

2.3.5.1 Evaluation metrics

Performance of the model was evaluated using four metrics: Relative bias (RB), Nash–Sutcliffe efficiency (NSE), index of agreement (IOA), and Root mean square error ($RMSE$). RB evaluates the relative distances between observed (O) and simulated (S) data with respect to the observed mean (\bar{O}) using:

$$RB = 100 \frac{\sum_{i=1}^n (S_i - O_i)}{n\bar{O}} \quad (2.16)$$

where n is the length of data series. NSE (Nash and Sutcliffe, 1970) is a dimensionless goodness-of-fit indicator that ranges from negative infinity to one. A NSE value of 1 indicates a perfect fit between observed and simulated data.

$$NSE = 1 - \frac{\sum_{i=1}^n (O_i - S_i)^2}{\sum_{i=1}^n (O_i - \bar{O})^2} \quad (2.17)$$

In the context of watershed hydrologic modeling, Moriasi et al. (2007) summarized that the model performance could be considered as “Good” if the RB is less than 15% for streamflow and 30% for sediment, and NSE is larger than 0.65 for monthly time step simulations. For finer time step, the equivalent “goodness” threshold of NSE is lower, e.g. NSE value of 0.65 for monthly time step may yield a NSE value of 0.4 for daily time step (Fernandez et al., 2005). IOA (Willmott, 1981) is used to detect the differences in the observed and simulated means and variances, especially during the intense rainfall events as the metric is sensitive to extreme values. IOA ranges from 0 to 1. A value of 1 indicates a perfect match, and 0 indicates no agreement at all. Krause et al. (2005) concluded that IOA of 0.65 could indicate a good model performance, although IOA is not sensitive to systematical under- or over- estimation:

$$IOA = 1 - \frac{\sum_{i=1}^n (O_i - S_i)^2}{\sum_{i=1}^n (|S_i - \bar{O}| + |O_i - \bar{O}|)^2} \quad (2.18)$$

RMSE quantifies prediction error as:

$$RMSE = \sqrt{\frac{\sum_{i=1}^n (O_i - S_i)^2}{N}} \quad (2.19)$$

A *RMSE* value of zero indicates perfect fit. If the value is less than half of the standard deviation of the observations, the model performance may be considered as good (Singh et al., 2005).

2.3.5.2 Calibration period

The calibration was carried out using hourly flow data and suspended sediment concentration data from Jan 1st, 2002 to Mar 14th, 2002 (73 days, 10% of the observed data). The GEOTop model spin-up was performed using the meteorological data of Dec, 2001. The calibration process mainly focused on the most sensitive parameters, as identified in the global sensitivity analyses. C_m , D_1 , and w_{dx} were the three major parameters calibrated for the flow simulation. ζ and D_{50} were mainly calibrated for erosion simulation. The initial values of the calibration parameters were set to the median of the ranges in Table 2-2 and Table 2-3. The model calibration was based on both mass balance and goodness of fit of hydrograph and sedigraph. The goal was to at least limit the relative bias (*RB*) of total discharge volume and total SSY to less than 15% and to have *NSE* of daily average flow rate and daily total SSY to be larger than 0.4.

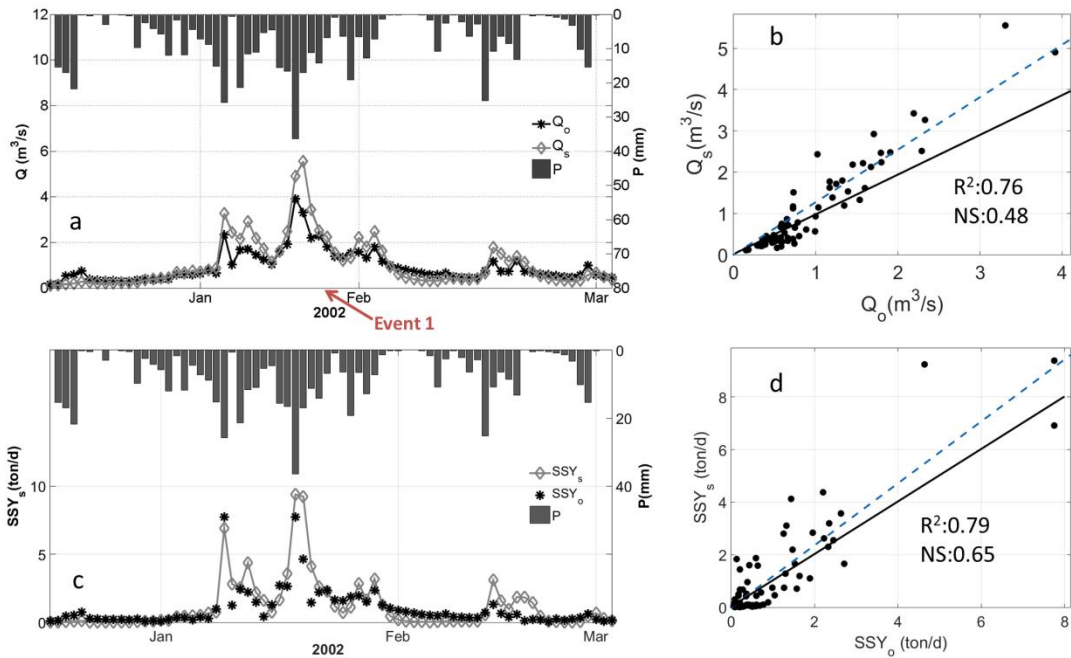


Figure 2-5 Model estimates of daily discharge and daily suspended sediment yield (SSY) during the calibration period. (a) plot of observed (with subscription 'o') and simulated (with subscription 's') daily average stream flow rate; (b) scatter plot of observed and simulated daily average stream flow rate; (c) plot of observed and simulated daily total SSY; (d) scatter plot of observed and simulated daily total SSY. Black solid line in panel (b) and (d) is the 1:1 line. Blue dashed line is the best-fit line.

The observed and simulated stream flow series in calibration period are shown in Figure 2-5a and Figure 2-5b. Observed and simulated total discharge volumes per unit area over the calibration period were 411 mm and 472 mm, respectively ($RB \sim 15\%$). The R^2 and Nash-Sutcliff coefficient (NSE) were 0.76 and 0.48, respectively. The index of agreement (IOA) was 0.92 and the root mean square error ($RMSE$) was 3.03mm/day. The NSE , IOA , and RB values indicate a “good” model performance based on the threshold proposed by Moriasi et al. (2007) and Krause et al. (2005). The $RMSE$ was 71% of the standard deviation of observed streamflow, which means that the model performance

was not good (Singh et al., 2005). Large *RMSE* value is because of the model's tendency to overestimate high flow and underestimate low flow (Figure 2-5b).

In regards to the estimates of suspended sediment yield (*SSY*), the model also showed good agreement with the observations. The observed and modeled total suspended sediment losses were 72.76 and 79.94 tons, respectively, for the calibration period. The *RB* was 9.87%. R^2 and *NSE* were 0.79 and 0.65, respectively (Figure 2-5c, Figure 2-5d). The *RMSE* was 0.83 ton/day (56% of the standard deviation of observed *SSY*) and *IOA* was 0.93. The model performance based on the *NSE*, *IOA*, and *RB* values can be termed as "very good". The *SSY* during the peak flow were overestimated, just like the overestimation of high flows by the hydrologic model.

2.3.5.3 Validation period

The model was validated using data from Mar 15th, 2002 to the end of 2003. Observed and simulated total discharge per unit area were 1303.8 mm and 1287.7 mm, respectively. The time series of cumulative observed and simulated discharge volume matched each other for most of the period, and the *RB* was only -1.2%. In general, the model reasonably simulated both the timing and magnitude of stream flow during the validation period (*RMSE*: 1.47mm/day or 56% of the standard deviation of observed discharge; *NSE*: 0.5; and *IOA*: 0.9). However, the model simulation overestimated high flows and underestimated low flows, much like it performed during the calibration period.

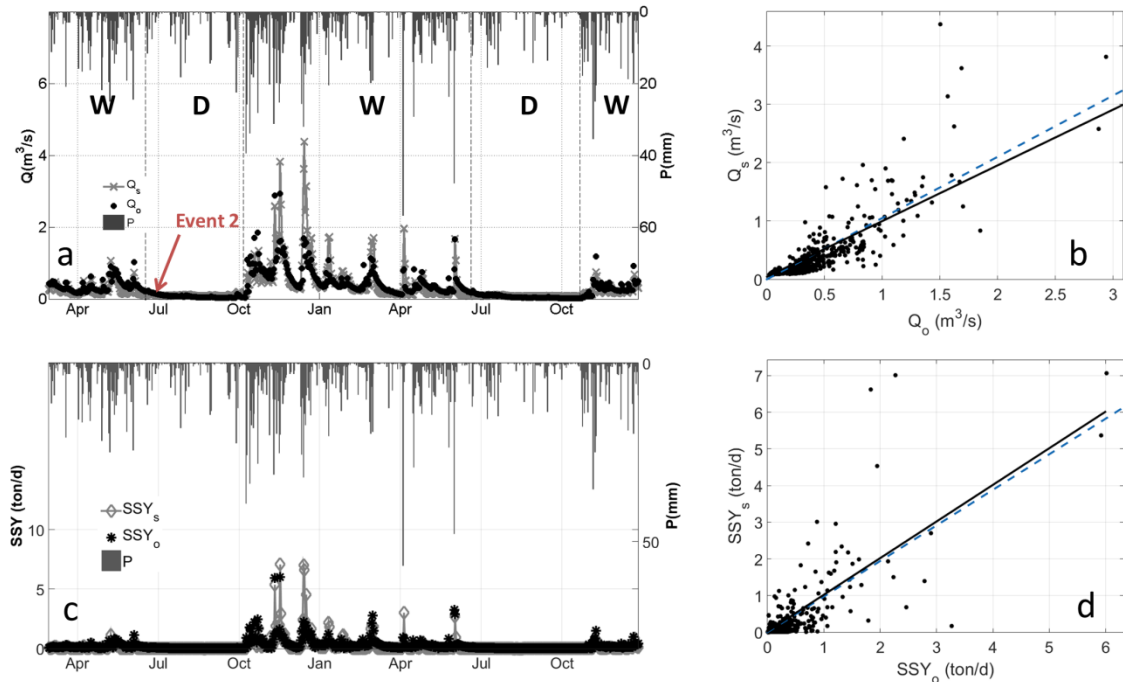


Figure 2-6 Model estimates of discharge and suspended sediment yield (SSY) during the validation period. (a) plot of observed and simulated daily average stream flow rate. The wet and dry periods were identified by letter 'W' and 'D' ; (b) scatter plot of daily average stream flow rate; (c) plot of observed and simulated daily total SSY; (d) scatter plot of daily total SSY. Black solid line in panel (b) and (d) is the 1:1 line. Blue dashed line is the best-fit line.

The performance of SSY simulation registered similar biases as that shown in streamflow simulation. The observed and simulated total annual suspended sediment losses were 170.66 and 132.48 tons, respectively. The total simulated SSY for validation period had a relative bias of -22.37%. The erosion model did not miss any erosion events during the validation period. Similar to the flow simulation results, SSY estimates were somewhat larger than observed during high flows and smaller during low flows. The *RMSE* was 0.41 ton/day (53% of the observed SSY) and the value of *IOA* was 0.86. *NSE*

was 0.32. Relatively poor *NSE* is because of the metric's sensitivity to overestimation of SSY peaks.

Table 2-4 Performance of stream flow and total suspended sediment yield simulation in calibration and validation periods

	Calibration		Validation	
	<i>Q</i>	<i>SSY</i>	<i>Q</i>	<i>SSY</i>
<i>NSE</i>	0.48	0.65	0.5	0.32
<i>IOA</i>	0.92	0.93	0.9	0.86
<i>RB</i>	15%	9.87%	-1.2%	-22.37%
<i>RMSE</i>	3.03	0.83	1.47	0.41

The model performances of flow and SSY simulation during calibration and validation periods are summarized in Table 2-4. The *NSE* and *IOA* values of modeled flow in calibration and validation periods were similar. The *RMSE* of simulated flow in validation period was smaller than in calibration period. The differences between observed and simulated flow rate were smaller during the low flows than high flows. This was partly because of the longer duration of low flow during the validation period. The model performance of suspended sediment simulation in validation period was not as good as in calibration period, even though the performances of flow simulation in both periods were similar. This was due to the bias in the flow simulation and power-law relationship between flow rate and water transport capacity, which exacerbated the SSY estimates.

Table 2-5 Performance of stream flow and suspended sediment simulations in wet and dry periods

	Q_w	Q_d	SSY_w	SSY_d
<i>NSE</i>	0.33	-0.75	0.25	-1.52
<i>IOA</i>	0.88	0.59	0.85	0.44
<i>RB</i>	4.55%	57.58%	-20.65%	-95.76%
<i>Bias</i>	-56.32	39.15	-34.44	-3.80

In order to investigate the performance of the integrated model during markedly different flow regimes, a 20-day moving average discharge threshold of 0.2 m³/s was used to divide the simulation series into wet and dry periods (see Figure 2-6a). The total duration of the dry period was 173 days, almost 27% of the two years. The total precipitation during the dry period was 326.6 mm, which is almost 11% of the total precipitation. Table 2-5 summaries the performances of the integrated model for both flow and SSY simulations during wet and dry periods. Both simulations showed better agreement with observed data during wet periods than in dry periods. In general, discharge volume was overestimated for dry periods and underestimated in wet periods, while the SSY was underestimated in both wet and dry periods. It is to be noted however that for large peaks, both flow rate and SSY was overestimated by the model. The negative *NSE* and *RB* indicate that the calibrated parameter set did not provide accurate enough estimates of flow and SSY during dry periods. This is in line with the findings of Jetten et al. (1999) that showed erosion-deposition models cannot

guarantee good performance, especially during dry periods, if the events used for calibration are not representative of the prevailing flow regime. It is to be noted that even though the suspended sediment simulation was not good enough during dry period, the bias of suspended sediment is only 9.94% of the total bias.

2.4 Results and Analyses

2.4.1 Temporal variations in modeled estimates

SSY from the catchment varied markedly from day to day and also non-monotonically with daily precipitation magnitude and intensity (Figure 2-7a). The R^2 between observed daily SSY and daily rainfall was only 0.14. The R^2 between observed daily SSY and the product of daily total rainfall kinetic energy and maximum 30-minute rainfall intensity (EI_{30}) was relatively better but still modest, and was equal to 0.53. It is to be noted here that the lagged correlation magnitude between observed daily SSY and daily rainfall was maximum for a zero day lag. The large variations in observed daily SSY indicate that the daily precipitation magnitude and intensity only have a marginal potential for estimating daily SSY. The variation could be because of the non-linear integrated response of the catchment, which may result in generation of markedly different runoff and hence SSY for the same daily precipitation amount and EI_{30} . Since runoff generation is directly influenced by the soil moisture in the surface soil layer (which in turn is influenced by meteorological forcings, antecedent hydrologic states,

and watershed properties), we explore if the variations in daily SSY with EI_{30} could be directly related to the prevailing soil moisture. To this end, data in the SSY vs EI_{30} plot are color coded based on simulated daily average soil moisture (Figure 2-7a). Based on the first glance, for an identical EI_{30} , SSY value appears to be larger for larger catchment-average soil moisture.

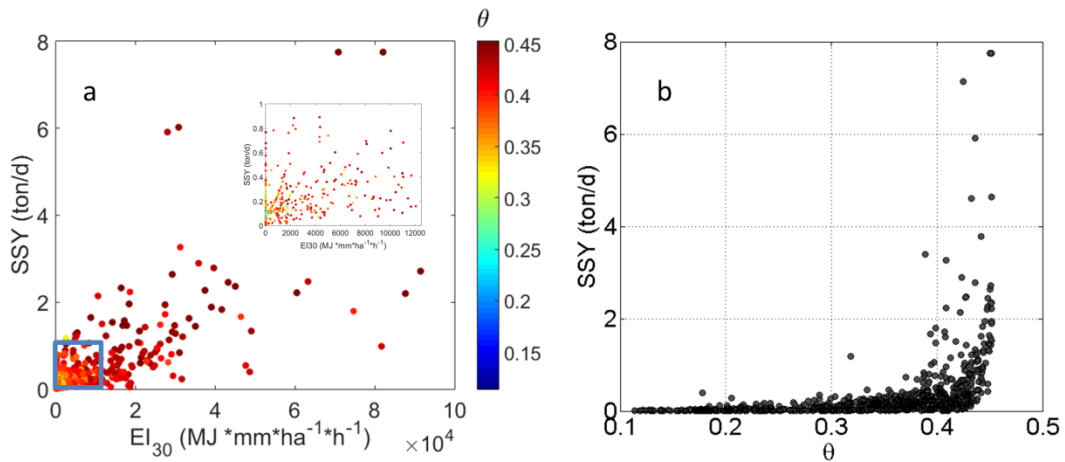


Figure 2-7 Scatter plot of daily observed SSY and EI_{30} , color coded with daily simulated catchment-average soil moisture; the inset figure is a zoom-in of daily observed SSY between 0-1 ton/d and EI_{30} between 0 – 1.2×10^4 $\text{MJ} \cdot \text{mm} \cdot \text{ha}^{-1} \cdot \text{h}^{-1}$; (b) Scatter plot of daily observed SSY from 2002 to 2003 and daily simulated catchment average soil moisture.

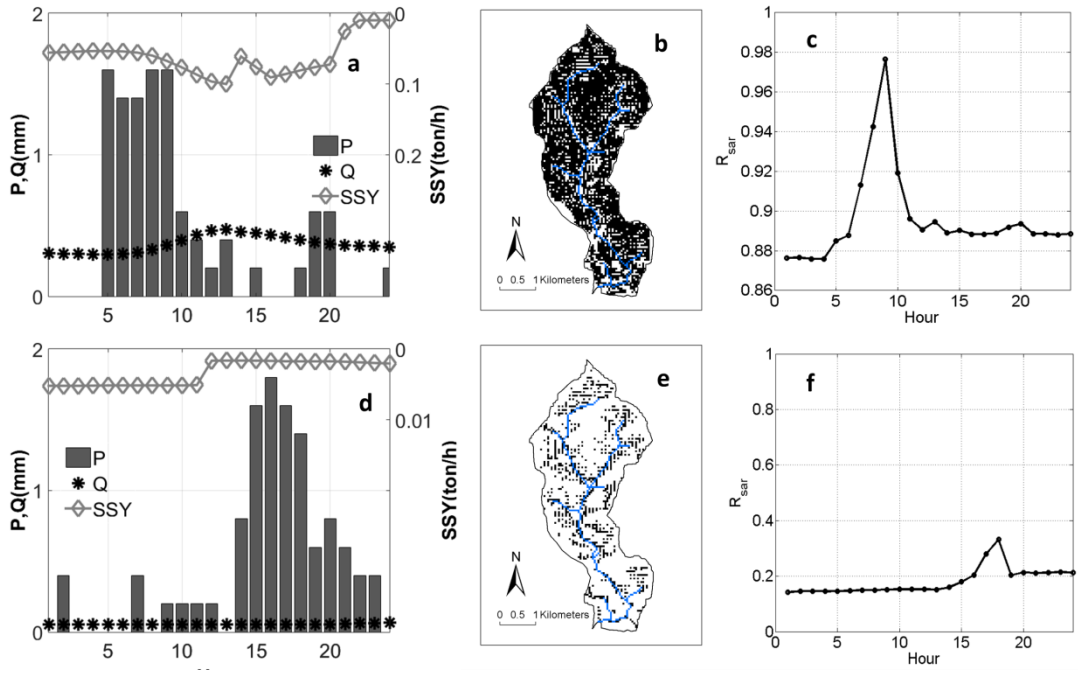


Figure 2-8 The hourly rainfall, observed discharge and SSY of two selected events (a,d); the simulated spatial distribution of soil loss area for two selected events (b,e), area with soil losses were black; the changes of saturated ratio of the simulated first layer soil moisture of the whole catchment (e,f); the plots for first event were on the top.

To explore this further, two daily events of similar magnitude but with very different moisture conditions were considered (Figure 2-8). The first event occurred on 2002/1/27 (identified in Figure 2-5) and delivered a total precipitation of 11 mm, a total measured streamflow of $1.3 \times 10^5 \text{ m}^3$ (modelled: $1.8 \times 10^5 \text{ m}^3$) and an event total suspended sediment yield (SSY) of 2.1 ton (modelled: 3.4 ton). The second event occurred on 2002/7/2 (identified in Figure 2-6) and delivered almost identical rainfall (11.6 mm in total) as the first event, but the total streamflow response and SSY at the outlet were much different. Streamflow response for the second event was measured at $1.1 \times 10^4 \text{ m}^3$

(modelled: $1.8 \times 10^4 \text{ m}^3$), while the event mean SSY was 0.066 ton (modelled: 0.054 ton). Notably, even though the rainfall volumes and intensities were similar for these two selected events, the first event lead to much larger runoff and SSY at the outlet (Figure 2-8a). The difference was mostly because of strong contrast in the antecedent moisture condition between the two cases (Figure 2-8c and Figure 2-8f). Around 88% of the catchment area was saturated at the start of event 1, with this fraction increasing to around 98% during the event. As a result almost the entire catchment participated in runoff generation leading to larger soil loss and larger mean SSY. This is not surprising as the catchment is fairly small. In contrast, only around 18% of the catchment area was saturated before event 2 and the fraction increased to around 36% during the event. Figure 2-9b and Figure 2-9d further reinforces the narrative that surface soil moisture influences SSY as it shows that event responses (both streamflow and SSY) were negligible for events from day-of-year (DOY) 200 to 290 in 2002, as the soil moisture was generally below saturation during this period (Figure 2-9c). By day 290, the water table was near the soil surface, which resulted in any additional precipitation to cause saturation excess runoff. To evaluate the variation of SSY with soil moisture across all events, a scatter plot between SSY and spatially averaged moisture conditions in the top soil layer (of thickness = 10cm) was drawn (Figure 2-7b). The figure suggests that runoff generation (from saturation excess or infiltration excess) and hence erosion per unit event magnitude is indeed larger when the top soil layer in the catchment is near

saturation. These results suggest that accurate prediction of spatial distribution of soil moisture is critical for generating temporally fine estimates of SSY. Notably, increase in soil saturation also increases soil cohesion which in turn may reduce erosion (see Equation (2.7)), but its impact is negated by large runoff generation for higher soil saturation cases. It is to be noted that the soil saturation of the top soil layer is a function of coupled surface water-groundwater-evapotranspiration interactions, and the parameters (such as topography, subsurface soil property, land cover etc.) that influence these processes. As such, the expressed role of surface soil moisture on SSY indirectly highlights the need for modeling of coupled processes in both space and time, much along the lines of process representations implemented in GEOtop.

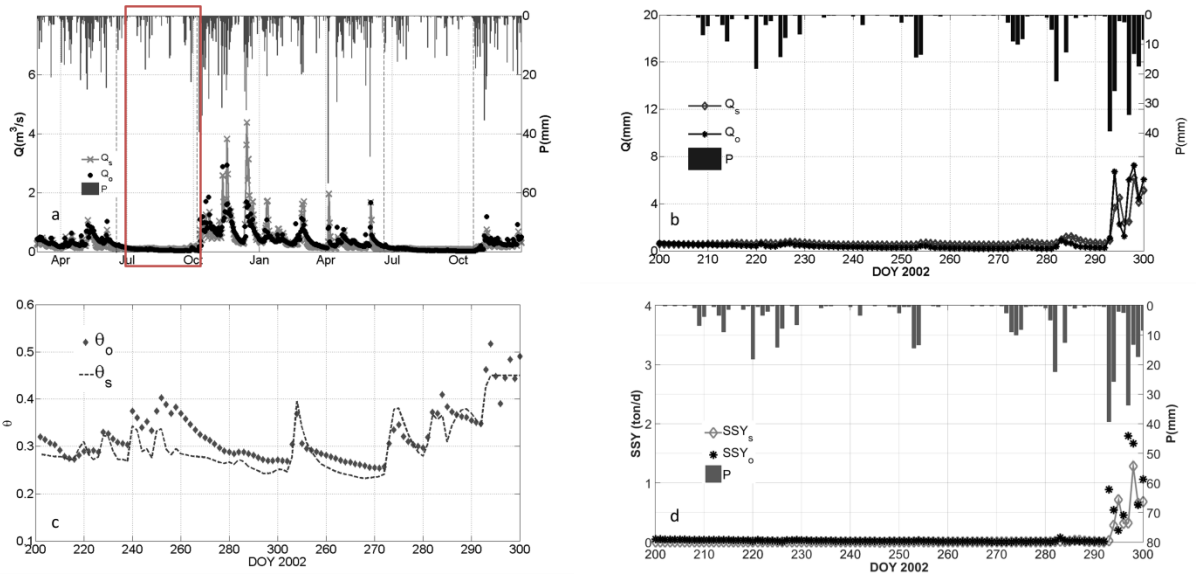


Figure 2-9 (a) The integrated model is able to capture occurrence of runoff events after a dry periods. The red box identifies the periods used in panel b, c, and d; (b) Observed and simulated flow rate; (c) Observed and simulated soil moisture (top 25 cm) (d)observed and simulated daily SSY

Suspended sediment yield from the catchment also showed ample variations between wet and dry periods. Even though the wet period (see Figure 2-6a) spanned only around 73% of the simulation time, it delivered 98.4% (99.9%, modeled) of the total sediment yield. This is in line with previously reported results from both field (Fu, 1989) and modeling experiments (Bartman et al., 2012; Zhang et al., 2012) that have shown that a few extreme events may contribute to a large portion of annual total soil erosion. Notably, our research area has a temperate weather and lacks extreme precipitation events, but nonetheless the dry period (~27% of the total simulation time) delivered only ~1% of the total SSY.

2.4.2 Spatially distributed estimates of erosion and deposition

Estimates of erosion and deposition simulated by the model displayed significant heterogeneity in both space and time. For example, for the two selected precipitation events with similar amounts of rainfall (Figure 2-8a, Figure 2-8d), the areal extent of soil loss and its spatial distribution locations were very different (Figure 2-8b, Figure 2-8e). The percentage area that participated in erosion loss was as high as 72% in event 1, while reaching only around 14% for event 2. Similarly the areal fraction of deposition areas were 14% and 7% respectively for the two events. A larger erosion loss area for event 1 can again be attributed to higher antecedent surface soil moisture in the catchment, which leads to a larger fraction of catchment area generating runoff. A larger volume of overland flow resulted in, higher shear stress and hence more soil loss from larger area. For the two years, the mean areal fraction of erosion and deposition was 27% and 8% respectively. Both erosion and deposition areal fraction were larger in wet periods than in dry periods. The variations of erosion and deposition areal portion were larger in wet periods (Table 2-6). Notably, the erosion and deposition areal fractions in the catchment were as large as 79% and 36% of the catchment area during the two year simulation periods. These statistics highlight that the source and sink areas in a catchment are very dynamic and change at both event and seasonal scales. Also, given the role of soil saturation area on runoff/erosion generation, dynamic mapping of

source/sink areas can benefit from spatially-explicit simulations of coupled hydrologic processes.

Table 2-6 The mean and standard deviation of erosion and deposition areas

	Mean erosional area fraction	Mean depositional area fraction	Standard deviation of erosional area fraction	Standard deviation of depositional area fraction
2002-2003	0.27	0.08	0.246	0.0859
Wet Periods	0.33	0.11	0.2476	0.0835
Dry Periods	0.11	0.02	0.1519	0.0585

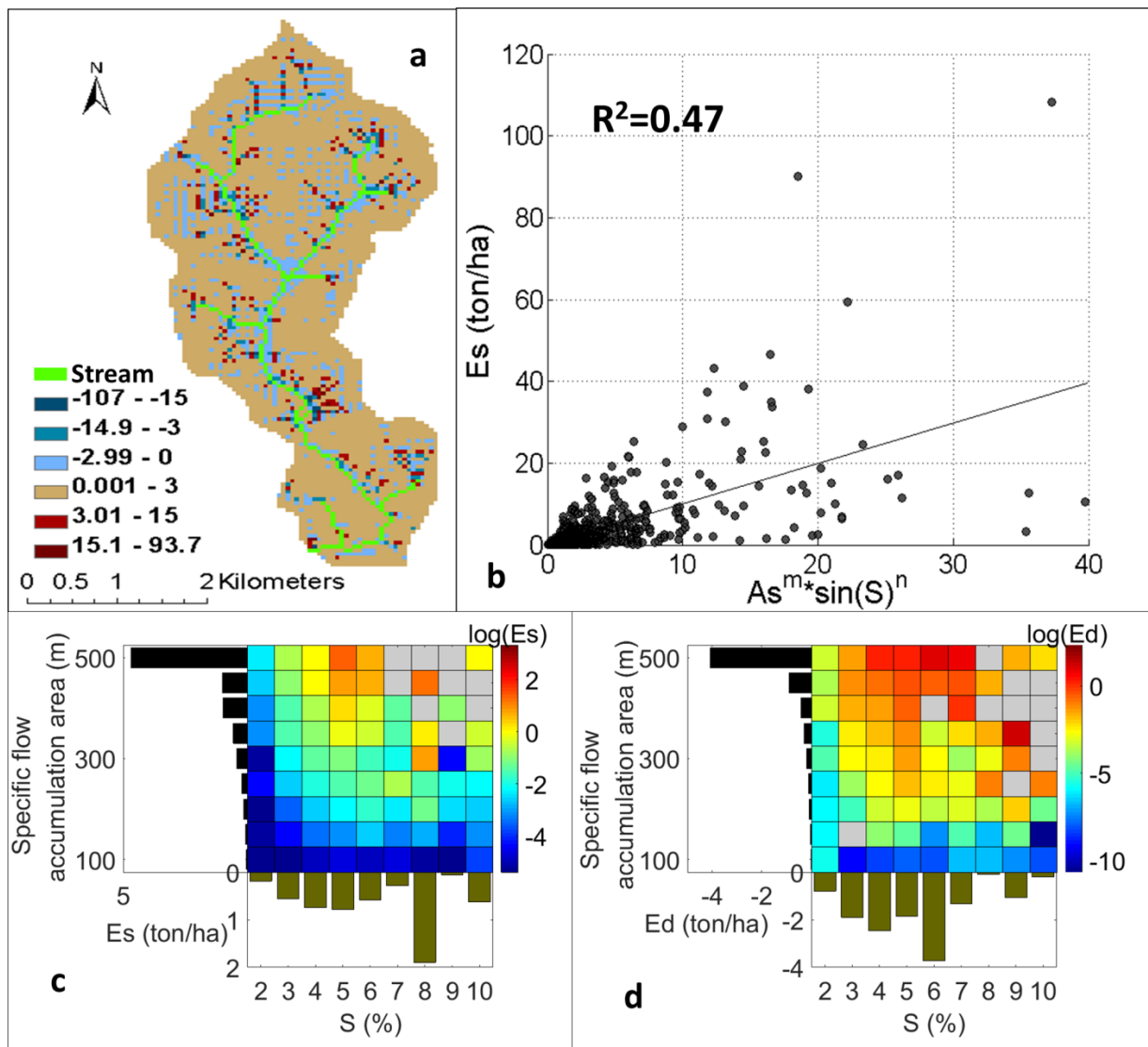


Figure 2-10 (a) Spatial map of soil erosion and deposition for each land pixel (unit:ton/ha/yr) for the entire two year simulation period; (b) Scatter plot between erosive loss(E_s) and slope-length factor for each land pixel; (c) Color chart of the logarithm of simulated erosive loss ($\log(\text{ton})$) for a range of slope (on x-axis) and specific flow accumulation area (on y-axis). Also included on the two axes are the bar plots of total erosive losses per unit area for different Slope and specific catchment area classes; (d) Color chart of the logarithm of simulated deposition ($\log(\text{ton})$). Also included on the two axes are the bar plots of total deposition per unit area for different Slope and specific catchment area classes. Note: grey cells in (c) and (d) are used to identify joint classes with no data.

At the annual scale, most deposition occurred near the riparian zone of the stream (dark blue color in Figure 2-10a), due to its relatively flat topography. Erosive losses were mainly located in the transition area between the hillslope and the riparian zone (dark red color in Figure 2-10a), which had both large flow accumulation area and relatively steep slope. The locations of erosion and deposition in terms of slope and specific catchment area are shown in Figure 2-10c and Figure 2-10d. Specific catchment area is the ratio of total contributing area of each land pixel and the pixel's width perpendicular to the flow direction. The bar plot of average erosion/deposition per unit area for different specific catchment areas shows that in general, erosion and deposition rates per unit area were larger with increasing specific catchment area. Areas with larger contributing areas generally had larger overland flow and hence larger transport capacity thus allowing more entrainment of soil particles (Figure 2-10c). Additionally, as more suspended sediment was transported to areas with large contribution area, the possibility that the suspended sediment concentration (SSC) exceeded the transport capacity, especially at flatter locations, also increased. This explains the increase in deposition with larger contributing areas (Figure 2-10d). Notably, total simulated soil erosive losses per unit area (E_s) did not show a monotonic trend with slope (Figure 2-10c). For flatter slopes, E_s is expected to be small because of the lower flow velocities. For larger slopes, while the local erosion at the cell under consideration is expected to be large, the incoming sediment input may either be small or large for a given contributing

area depending on the spatio-temporal extent of soil saturation area that determines runoff generation. As a result, E_s , which is an integrated net-erosional response from the contributing area and the pixel under consideration, may show non-monotonic variation with slope. This non-monotonic variation also has a tangible impact on the relation between the length-slope (LS) factor and the total simulated soil erosive losses per unit area (E_s). Model results suggest that while E_s shows an overall increasing trend with LS (Figure 2-10b), the relation is not one to one, and shows ample variations around the E_s - LS line ($R^2=0.47$, $\sigma^2=5.44$). While the result is based on only two years of simulation, it does highlight that the source efficiency or the erosion rates (in homogeneous watersheds/hillslopes with uniform soil property) is not just a simple function of contribution area and slope, and can be strongly influenced by the dynamic spatio-temporal distribution of soil moisture conditions.

2.5 Summary and Conclusions

In this study, we developed an open-source sediment erosion/deposition module for a 3D surface-subsurface hydrologic model, GEOtop, and evaluated its applicability in explaining the spatio-temporal distribution of erosion, deposition, and sediment yield dynamics at both plot and catchment scale. The model uses a physically-based representation of coupled surface-subsurface hydrologic processes and a comprehensive land-surface energy and water interaction scheme to simulate hydrologic response and consequent sediment dynamics. Because of its fully distributed nature, the model can

account for spatial heterogeneity in the watershed. As the model runs at an adaptive time interval determined by the dynamics of states, it can be used to perform simulations at event to inter-decadal scales. At the plot level, the model was evaluated at event time scale. Results show that the model was able to capture both the trend and the quantity of runoff and suspended sediment concentration (SSC) in response to events of varying intensity and duration. At the catchment level, after performing a global multivariate sensitivity analyses to identify sensitive parameters for hydrologic modeling (such as leaf area index, rill width ratio, depth of the first soil layer, Chezy's roughness coefficient, and vertical hydraulic conductivity of the first soil layer) and sediment dynamics (such as Chezy's roughness coefficient, soil median particle size, and rill width ratio), the model performance was evaluated at daily and seasonal time scales. In general, the model reasonably simulated both the timing and magnitude of stream flow and suspended sediment yield (SSY) from the catchment. Both streamflow and suspended sediment yield simulations showed better agreement with observed data during wet periods than in dry periods. The discharge volume was overestimated for dry periods and underestimated in wet periods, while the SSY was underestimated in both wet and dry periods. Notably, the biases in suspended sediment yield simulation were similar to that shown in streamflow simulation, thus highlighting that accuracy of flow simulations critically influences the estimation accuracy of SSY. While our research area has a temperate maritime climate and lacks extreme precipitation events, but still

dry period (~27% of the total simulation time) delivered only ~1% of the SSY. This underscores the importance of obtaining robust calibration parameter sets that at least perform well during wet periods, as is well documented in nutrient export studies (Jordan et al., 2005; Nasr et al., 2007; Ye et al., 2012). It is to be noted that the sensitivity analysis performed for Dripsy catchment could serve as a reference for future model applications, and for prioritizing observation of parameters to reduce the uncertainties in the erosion model.

Observed SSY from the catchment showed a non-monotonic variation with daily precipitation magnitude. Further examination of simulation results revealed that SSY per unit event magnitude varied proportionally with the prevailing soil moisture. The result indicates that accurate prediction of spatial distribution of soil moisture is critical for generating temporally fine estimates of SSY. Larger SSY per unit event magnitude for higher soil saturation also indicates that large runoff generation for wetter soil moisture conditions negated the impact of increase in soil cohesion with moisture content. The simulation results also showed that the source (erosion) and sink (deposition) areas in a catchment were heterogeneous and dynamic, and could change from one event to the next. Again, the extent of source/sink areas were found to be influenced by prevailing moisture conditions, which in turn determined the quantity of runoff generation. Model results also suggest that long-term erosion rate from a location was not a simple function of slope-length. In fact, the relation between erosion and slope-length showed ample

variations, thus highlighting that the source efficiency or the erosion rates (in homogeneous catchments/hillslopes with same rainfall forcing and uniform soil property) can be severely influenced by the dynamic spatio-temporal distribution of soil moisture conditions. Since the spatio-temporal dynamics of soil moisture is dependent on coupled process interactions such as evapo-transpiration, capillary rise and lateral groundwater flow, aforementioned results make a compelling case for spatially-explicit simulations of coupled hydrologic processes for estimation of erosion/deposition distribution and sediment generation.

The simulation results presented in this study do not account for uncertainty in parameters. Also, even though the parameters in the presented model are physically-based and can be obtained through measurements, because of the sparseness of observed data, disconnect between observation and model scale, and model uncertainty, these parameters still need to be calibrated. This is a big challenge for spatially-distributed models such as GeoTopSed, as they are computationally demanding. Further confidence in the modeled estimates could be built by obtaining field estimates of states (e.g. ground water, residence time etc.) and related parameters (e.g. rill width, soil cohesion etc.), and by implementing the model in varied settings. The presented model version does not account for bank-erosion processes, which limits its applicability to watersheds with small bank erosion w.r.t. total hillslope losses. It is to be noted that 1D representation of flow routing in channel especially limits the calculation of lateral

convective gradients and shear, thus hindering the development of a comprehensive sediment erosion and transport module. Also, as the GEOtop model uses kinematic wave scheme to solve for overland and channel flow, the model is not well suited for flow and sediment yield calculations in flow regimes with either Froude number smaller than 0.5 or Kinematic wave number smaller than 5(Vieira, 1983). For using the model as a predictive tool, vegetation dynamics in response to changes in meteorological forcings and hydrologic states need to be accounted for. In spite of aforementioned limitations, the open-source integrated modeling framework presented here offers the potential for its use both as an evaluation and retrospective-prediction tool, and as a virtual laboratory for understanding the role of hydrologic states and parameters on sediment dynamics.

3 Inter-comparing erosion, deposition, and sediment yield estimates using process representations ranging from empirical to physics-based

This chapter is a modified version of the manuscript currently in preparation:

Tan Zi, Mukesh Kumar, John Albertson, Inter-comparing erosion, deposition, and sediment yield estimates using process representations ranging from empirical to physics-based.

3.1 Introduction

Both empirical and physics-based models are widely used to estimate the erosion and sediment transport processes (Owoputi and Stolte, 1995; Tsara *et al.*, 2005; Licciardello, 2007; Pieri *et al.*, 2007; Ismail and Ravichandran, 2008; Terranova *et al.*, 2009; Kinnell, 2010). Empirical models generally provide erosion estimates at coarse temporal resolution, but have the advantage of using less number of input parameters and being computationally efficient (Millward and Mersey, 1999; Hao *et al.*, 2001; Terranova *et al.*, 2009; Renard *et al.*, 2010; Podmanicky *et al.*, 2011). These models often ignore the heterogeneity of forcing fields and assume that the properties of the watershed are stationary. In contrast, self-described physics-based erosion models often provide estimates at fine temporal resolution. These models have more detailed descriptions of erosion and sediment transport processes (DeRoo *et al.*, 1996; Wicks and Bathurst, 1996; Morgan *et al.*, 1998; Hessell, 2005; Jain *et al.*, 2005; Heppner *et al.*, 2006; Ran *et al.*, 2007; de Vente *et al.*, 2008; Kim *et al.*, 2013; Endrizzi *et al.*, 2014; Zi *et al.*, 2016), and are capable of

accounting for the spatial heterogeneity of geomorphology, topography, soil and land surface properties, and the temporal variations in meteorological inputs. However, these models are data and computation intensive. Also data acquisition and uncertainty estimation costs associated with these models are relatively large (Boardman, 2006). Many other pros and cons of empirical, semi-empirical and physics-based models vis-a-vis their input–output data requirements, model structure, uncertainty, and accuracy have been discussed in detail in several review studies (Merritt *et al.*, 2003; Aksoy and Kavvas, 2005; Kinnell, 2005; Kinnell, 2010).

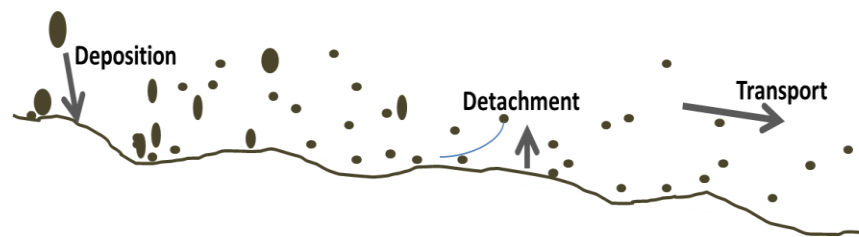


Figure 3-1 Three major processes for erosion and sediment transport

Irrespective of the model formulation, majority of the erosion and sediment transport models strive to capture the impacts of three primary processes viz. detachment, deposition, and transport (Figure 3-1). Notably, these processes may be represented in very different ways in empirical, semi-empirical and physics-based models (Table 3-1). For example, in empirical models, rainfall erosivity is a widely used variable to quantify the potential soil erosion (Wischmeier and Smith, 1978; Renard *et al.*, 1991), which may be caused by raindrop impact and/or from overland flow shear on the soil surface. Rainfall erosivity (R) is evaluated using :

$$R \propto EI_{30} \quad (3.1)$$

where E is rainfall energy, I₃₀ is maximum 30 minutes rainfall intensity. R implicitly captures the enhanced detachment during high intensity storms, both due to raindrop impact and shear stress from overland flow. Since antecedent conditions (Chen et al., 2014) may influence the generation of overland flow volume and peak, instead of only using the precipitation statistics, several models (Williams, 1975) directly used flow volume (Q) and peak flow rate (q_{peak}) for flow erosivity calculations:

$$R \propto f(Q, q_{peak}) \quad (3.2)$$

Overland flow data used for erosivity calculations in these models are often generated using SCS curve number method (Cronshey, 1986). Some physics-based erosion and sediment transport models, , such as GEOtopSed(Zi et al., 2016), tRIBS-OFM (Kim et al., 2013), use coupled surface-subsurface processes for the surface flow generation. While some other erosion models do not have strong coupling between surface and subsurface(Smith et al., 1995; DeRoo et al., 1996).. Both rain drops (D_r) and flow detachment (D_f) are generally explicitly evaluated in physically based models using:

$$D_E = D_r + D_f \propto f(E, (TC - C)) \quad (3.3)$$

where D_E is the total detachment, and TC and C are transport capacity and sediment concentration of flow. D_r is a function of rainfall energy (E), while D_f is a function of the gradient between TC and C. Assuming all other conditions to be the same, D_f is generally larger when flow sediment concentration is smaller than the transport capacity. Here TC is defined as the maximum concentration of sediment that can be carried with the flow. The gradient function used to calculate D_f is dependent on both flow characteristics such as velocity, volume and friction slope, and sediment grain properties such as its size and specific gravity (Bagnold, 1966; Govers, 1990). Flow properties used for estimation of D_f in physics based models are sometimes obtained using coupled interactions between surface, subsurface and ecological processes (Kim et al., 2013; Zi et al., 2016) and at other times based on simplified infiltration and flow routing processes. For instance, SWAT model uses SCS curve number method and WEPP model uses green-ampt method instead (Laflen et al., 1991; Smith et al., 1995).

As far as deposition and transport processes are concerned, empirical erosion and sediment yield models, e.g. USLE and RULSE, often do not explicitly simulate these processes at all. Application of these models for sediment yield simulations generally involves use of a linear multiplier called sediment delivery ratio (SDR) to account for the soil particle deposition during the sediment routing processes (Young et al., 1989). The SDR approximates the average portion of eroded soil particles that can eventually be transported out of the area of interest. In many other models (Beasley et al., 1980; Knisel,

1980) erosion estimated by USLE equations are routed downhill based on the transport capacity calculations. If transport capacity is smaller than the total amount of sediments, the “excess” sediment is deposited or else it is carried downstream. These models generally use long term (often annual) rainfall and peak flow statistics and topographic attributes to obtain transport capacity (Van Rompaey et al., 2001; Verstraeten et al., 2007; Bonumá et al., 2014). In physics-based models, the transport capacity of flow is calculated based on the dynamic hydrological state at a given location (Julien and Simons, 1985; Govers, 1990; Everaert, 1991), and is a function of flow velocity and volume, and friction slope.

The representation of erosion, deposition and transport processes in empirical, semi-empirical and physics-based models are not restricted to the example configurations discussed above. As is evident from Table 3-2, varied permutations of the process representations are often used. While studies focused on inter-comparison of sediment models exist (Jetten *et al.*, 1999; Shen *et al.*, 2009), the previous studies are more focused on comparing the model performances with respect to observed data. The role of differences in model structures was not investigated thoroughly.

Table 3-1 Varied representations of detachment, deposition and transport processes in sediment models

Process Representations		
Detachment	Deposition	Transport
<p>1. Dynamics driven by rain erosivity (e.g. EI30)</p> <p>2. Dynamics driven by flow erosivity (e.g. $f(Q, q_{peak})$)</p> <p>3. Explicit calculation of rainfall and flow detachment based on rainfall kinetic energy and flow shear stress.</p>	<p>A. No deposition calculation</p> <p>B. Limited by SDR</p> <p>C. Limited by TC</p> <p>-- C1. TC calculation based on rainfall erosivity, topographic factor.</p> <p>-- C2. TC calculation based on flow erosivity and topographic factor.</p> <p>-- C3. TC calculation based on explicit calculation of shear stress etc.</p>	<p>i. No routing calculation</p> <p>ii. Routing based on mass balance</p>

Table 3-2 List of sediment models and representation schemes of detachment, deposition and transport processes in them. See Table 3-1 for representation details.

Model	Representation of detachment	Representation of deposition simulation	Representation of transport simulation	Reference
AGNPS	1	C2	ii	(Young <i>et al.</i> , 1989)
ANSWERS	2	C2	ii	(Beasley <i>et al.</i> , 1980)
CASC2D-SED	2	C2	ii	(Johnson <i>et al.</i> , 2000)

CREAMS	1 and 2	C3	ii	(Knisel, 1980)
EROSION 2D/3D	3	C3	ii	(Schmidt, 1991)
EUROSEM	3	C3	ii	(Morgan <i>et al.</i> , 1998)
GEOtopSed	3	C3	ii	(Zi <i>et al.</i> , 2016)
GUEST	3	C3	ii	(Rose <i>et al.</i> , 1998)
HSPF	2	B	ii	(Donigian Jr <i>et al.</i> , 1995)
InHM	3	C3	ii	(Heppner <i>et al.</i> , 2006)
KINEROS	3	C3	ii	(Smith <i>et al.</i> , 1995)
KINEROS2	3	C3	ii	(Goodrich <i>et al.</i> , 2002)
LandSoil	2	C2	ii	(Ciampalini <i>et al.</i> , 2012)
LASCAM	2	C2	ii	(Viney and Sivapalan, 1999)
LISEM	3	C3	ii	(DeRoo <i>et al.</i> , 1996)
MHYDAS-Erosion	3	C3	ii	(Gumiere <i>et al.</i> , 2011)
MUSLE	2	A	i	(Williams, 1975)
PERFECT	2	A	i	(Littleboy <i>et al.</i> , 1992)
RUSLE	1	A	i	(Renard <i>et al.</i> , 1991)
RUSLE2	1	C2	ii	(Foster <i>et al.</i> , 2005)
SEDD	1	B	ii	(Ferro, 2000)
SHESED	3	C3	ii	(Wicks and Bathurst,

				1996)
SWAT	2	A	ii	(Arnold <i>et al.</i> , 1998)
SWRRB	1 and 2	C3	ii	(Arnold <i>et al.</i> , 1990)
tRIBS-OFM	3	C3	ii	(Kim <i>et al.</i> , 2013)
USLE	1	A	i	(Wischmeier, 1959; Wischmeier and Smith, 1978)
WASA-SED	1	C2	ii	(Medeiros <i>et al.</i> , 2010)
WATEM/SEDEM	1	C1	ii	(Van Oost <i>et al.</i> , 2000; Van Rompaey <i>et al.</i> , 2001)
WEPP	3	C3	ii	(Laflen <i>et al.</i> , 1991)

Because of the differences in representation of hydrologic processes, usage of data and calibration strategy between the considered models, it is not clear how the representation of detachment, deposition and transport processes may impact that spatial and temporal distribution of erosion, deposition, and sediment yield.

Here, we perform an inter-comparison experiment to evaluate the role of representation of erosion, deposition and transport processes on modeled estimates. Specifically, our goal is to evaluate the extent to which the spatio-temporal variations in states as modeled by the physics based models with coupled surface-subsurface interactions, are captured by simpler models. We also evaluate the differences in

sediment yield estimates and net-erosion and deposition areas from models that use varied representations of erosion, deposition and transport processes. Finally we explore the possible causes of these variations.

3.2 Method

3.2.1 Selected model representations

A total of six model configurations are considered (Table 3-3). RUSLE_SDR and MUSLE_S_SDR model configurations use RUSLE (Renard et al., 1991) and MUSLE(Williams, 1975) model schemes with sediment delivery ratio (SDR) factor to estimate sediment yield. Erosion calculation in RUSLE model uses:

$$E = \sum_i EI30_i * K * LS * C * P \quad (3.4)$$

where $EI30$ is a compound erosivity index of total storm kinetic energy and maximum 30 minutes rainfall intensity that is calculated on daily basis, K is soil erodibility, LS is length- slope factor, C is land cover-management factor and P is supporting-practice factor. The MUSLE model, on the other hand, uses erosion calculation, based on runoff volume and peak flow rate:

$$E = \sum_i (Q_i * q_{peak_i})^{0.56} * K * LS * C * P \quad (3.5)$$

Runoff volume (Q) in the above equation is often derived using SCS curve number method (Cronshey, 1986):

$$Q = \frac{(P - I_a)^2}{P - I_a + S} \quad (3.6)$$

$$S = 25.4 \left(\frac{1000}{CN} - 10 \right) \quad (3.7)$$

where I_a is the initial abstraction and CN is the curve number. The curve number is used to account for the effects of land cover and antecedent soil moisture on runoff generation. The peak flow rate (q_{peak}) is generally derived using rational formula:

$$q_{peak} = \frac{a_{tc} * Q * DA}{3.6 * t_{conc}} \quad (3.8)$$

where DA is drainage area, a_{tc} is the fraction of daily rainfall that occurs during the time of concentration (t_{conc}). These two model configurations do not explicitly account for the sediment transport. Also, they do not provide spatially-explicit estimates of sediment deposition. The SDR used to obtain sediment yield at the watershed outlet (and hence net deposition within the watershed) is calculated using the equation proposed by Williams (1977):

$$SDR = 1.355 * 10^{-11} DA^{-0.0998} rl^{0.3629} CN^{5.444} \quad (3.9)$$

where rl is the relief. Models that use `RUSLE_SDR` configuration include `SEDD` (Ferro, 2000), while `MUSLE_S_SDR` configuration has been used in `HSPF` (Donigian Jr *et al.*, 1995). The next three model configurations viz. `RUSLE_TC`, `MUSLE_S_TC`, and `MUSLE_G_TC`, again use `RUSLE` and `MUSLE` schemes but with transport capacity (TC) calculations, which allows estimation of both sediment yield at the watershed outlet and

a spatially-explicit distribution of erosion and deposition within the area of interest. The transport capacity is obtained using (Bonumá et al., 2014):

$$TC = ktc * R_i * K * DA^{1.4} * S^{1.4} \quad (3.10)$$

where ktc is a calibration factor. The erosivity (R_i) is obtained by:

$$R_i = \begin{cases} EI_{30_i}, & \text{RUSLE_TC} \\ ((Q_i \cdot q_{peak_i})^{0.56}), & \text{MUSLE_S_TC, and MUSLE_G_TC} \end{cases} \quad (3.11)$$

For RUSLE_TC, rainfall erosivity is used and flow erosivity is used in MUSLE_S_TC and MUSLE_G_TC. Models that use RUSLE_TC configuration include RSULE2(Foster et al., 2005), AGNPS(Young et al., 1989), and WASA-SED(Medeiros et al., 2010). MUSLE_S_TC configuration has been used in models such as LASCAM(Viney and Sivapalan, 1999), LandSoil(Ciampalini et al., 2012). MUSLE_G_TC is a sister configuration of MUSLE_S_TC with the only difference being that the flow variables in MUSLE_S_TC are obtained using SCS curve number based method, while it is obtained from a physics-based distributed hydrologic model, GEOtop model (Rigon et al., 2006; Endrizzi et al., 2014), in MUSLE_G_TC. The final model configuration is an integrated physics-based model of hydrology and sediment transport called GEOtopSed (Zi et al., 2016). GEOtopSed simulates soil moisture in each subsurface layer by solving the 3D Richards equation. After updated the soil moisture profile in each time step, the head gradient in the top soil layer is used to for estimation of infiltration/exfiltration flux. Then surface overland flow is routed based on the elevation gradient. A Similar

configuration has been used in several physics based models such as tRIBs-OFM (Kim et al., 2013).

Four of the selected model configurations can be used to obtain a spatially-explicit distribution of erosion and deposition within the area of interest, and also to simulate the sediment yield, including RUSLE_TC, MUSLE_S_TC, MUSLE_G_TC, and GEOTopSed. The four configurations use the precipitation and/or flow statistics in an optimal way, meaning that the statistics is used for both detachment and deposition calculations. For example in model configuration such as 1-C2-ii (see Table 3-1 for notations and Table 3-2 for examples), precipitation statics are used for detachment calculation whereas flow statistics, which is derived using the precipitation data, are used to obtain transport capacity for deposition estimation. Since, flow statistics are anyhow being modeled here and considering that they determine the erosion and entrainment of sediments, they are not being optimally utilized in 1-C2-ii. In contrast, in 2-C2-ii (or MUSLE_S_TC) flow statistics is used for both detachment and deposition calculation.

Table 3-3 Selected model configurations*

Model configurations	Detachment	Deposition	Transport	Spatial Comparison
RUSLE_SDR	EI30 (1)	SDR (B)	i	N
RUSLE_TC	EI30 (1)	TC (C1)	ii	Y
MUSLE_S_SDR	SCS (2)	SDR (B)	i	N
MUSLE_S_TC	SCS (2)	TC (C2)	ii	Y
MUSLE_G_TC	GEOTop (2)	TC (C2)	ii	Y
GEOTopSed	GEOTop (3)	TC (C3)	ii	Y

*: the process representation classification is in the parenthesis.

3.2.2 Site descriptions and model input data

A small experimental catchment, at Dripsey, Ireland (Figure 3-2) is used to test different model configurations. The Dripsey catchment is located approximately 25 km northeast of Cork, and has an area of 15 km². The elevation of this catchment ranges from 60 to 210 m. It is a beef and dairy producing agricultural catchment and is almost 100% covered by perennial ryegrass. The catchment slopes gently, with around 85% of the area having less than 3% grade. Gleys and podzols are the two major soil types. The experimental field site is managed by the Hydromet team of the University College Cork (UCC). The experimental field site is managed by the Hydromet team of the University College Cork (UCC). There is a meteorological flux tower at the top of the catchment (elevation 192 m) where radiation, wind speed, air temperature, surface temperature, relative humidity, and soil moisture (at five depths) have been measured at 30 minutes interval since 1998 (Albertson and Kiely, 2001). All the meteorological data from the site are archived in the FLUXNET repository (<http://fluxnet.ornl.gov>). At the catchment outlet (elevation 60 m), stream flow was monitored continuously at 30 minutes interval for a period of over two years (2002-2003). Flow-weighted water samples at the catchment outlet were collected using an ISCO 6712 auto-sampler with intake set at approximately 0.25 m above the streambed (Lewis, 2003; Lewis, 2011).

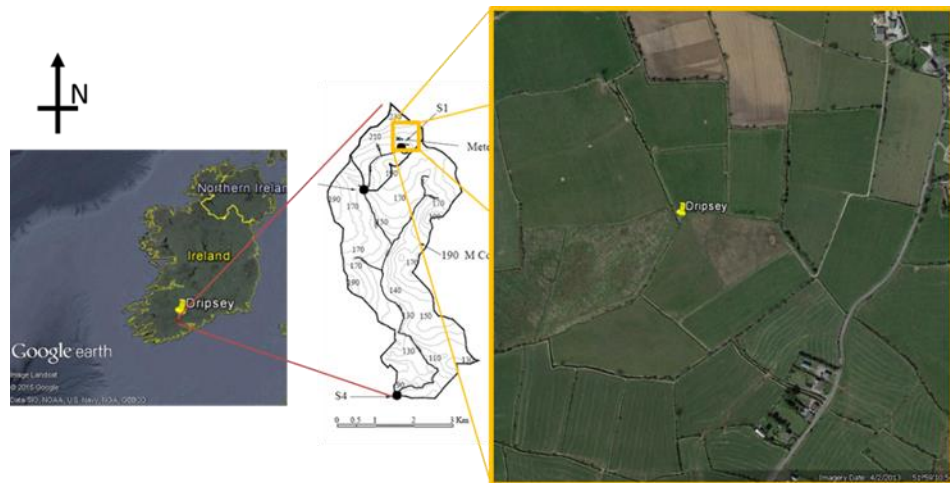


Figure 3-2 Location of Dripsey catchment in County Cork, Ireland. The yellow square is the location of flux tower.

The climate in the study region is temperate maritime, and is characterized by high humidity and a lack of temperature extremes during the year. The minimum daily temperature for years 2002 and 2003 was -0.2°C . The mean annual precipitation locally is approximately 1400 mm. Figure 3-3a shows the multi-year monthly average rainfall of Dripsey watershed. October to January have more rainfall than other months. All months have decent amount of rainfall occurred. Figure 3-3b shows the probability of daily precipitation. 75% of daily rainfall was less than 6.52mm and 95% was less than 18.4mm. Only 13 days during the 11 years have precipitation larger than 40mm, 5 of them have precipitation larger than 50mm.

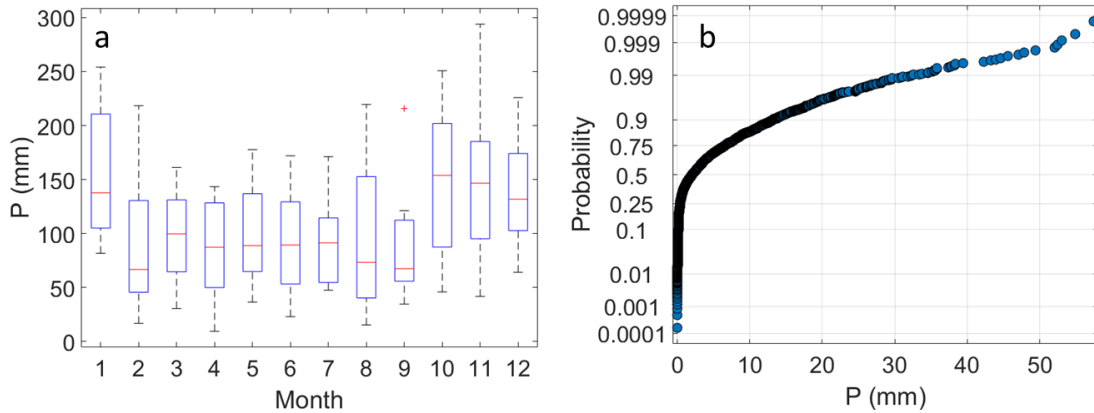


Figure 3-3 (a) Multi-year(2002-2012) monthly average rainfall Dripsey; (b) Daily rainfall probability plot.

Among the six considered model configurations, GEOtopSed in most data intensive. Data needs for other model configurations is just a subset of the input data set for GEOtopSed. GEOtopSed requires a digital elevation model (DEM), land use/land cover (LULC) map, and soil type map to simulate the hydrological processes for a catchment. The soil type map and soil parameters were obtained from Irish Forestry soils (IFS) database and in situ soil samples (Lewis, 2011). LULC parameters were derived based on classifications using the Corine land cover 2000 database and land use data observed in the catchment. The stream channel was delineated using DEM processing in GIS. The derived extent of stream was validated against the regional channel map. Geomorphic properties of the channel were defined based on the DEM data. All thematic maps were resampled at 50 m × 50 m spatial resolution. Meteorological data such as precipitation, temperature, incoming shortwave radiation,

air pressure, relative humidity, wind speed and direction in half-hourly time steps were collected at the HYDROMET flux tower at Dripsey. Because of the small size of the catchment (area = 15km²) and absence of any other precipitation data fine enough to resolve the heterogeneities within the watershed, the rainfall was assumed to be uniform within the catchment. The assumption is reasonable given the mild topographic relief and a uniform land cover within the catchment. Overall, the watershed is homogeneous in terms of parameters and forcing, and serves as an ideal test case to intercompare model configurations because of its simple setup. The stream flow and suspended sediment concentration data, collected by the water level recorder and water ISCO 6712 auto-sampler at the outlet of catchment, were used to both calibrate and validate the models..

3.2.3 Model calibration and validation

First, the calibration of GEOtopSed model was carried out using hourly flow data and suspended sediment concentration data from Jan 1st, 2002 to Mar 14th, 2002. The GEOtopSed model spin-up was performed using the meteorological data of Dec, 2001. Observed and simulated total discharge volumes per unit area over the calibration period were 411 mm and 472 mm, respectively (relative bias ~ 15%). The R2 and Nash-Sutcliff coefficient (NSE) were 0.76 and 0.48, respectively. In regards to the estimates of suspended sediment yield (SSY), the model also showed good agreement with the observations. The observed and modeled total suspended sediment losses were 72.76

and 79.94 tons, respectively, for the calibration period. The relative bias was 9.87%. R² and NSE were 0.79 and 0.65, respectively. The model was validated using data from Mar 15th, 2002 to the end of 2003. Observed and simulated total discharges per unit area were 1303.8 mm and 1287.7 mm. In general, the model reasonably simulated both the timing and magnitude of stream flow during the validation period (RMSE: 1.47mm/day; NSE: 0.5; and IOA: 0.9). The observed and simulated total annual suspended sediment losses were 170.66 and 132.48 tons, respectively. The total SSY of validation period simulation had a -22.37% relative bias. The erosion model did not miss any erosion events during the validation period. The model performances were summarized in Table 3-4.

For other model configurations, most of the parameters have reference values or can be derived. The calibration effort focused on the *ktc* parameter in the *TC* calculation (see equation (3.10)). A linear search calibration scheme was used to identify *ktc* that lead to minimum difference between long-term *SSY* simulated using RUSLE/MUSLE model configurations and that obtained from the GEOTopSed Model. Since the flow and suspended sediment concentration data in the watershed exists only for the period ranging from Jan 1st, 2002 to Dec 31st, 2003, long term calibration of USLE/MUSLE model configurations focused on obtaining *SSY* estimates that were close to one obtained using the calibrated GEOTopSed model.

Table 3-4 Performance of stream flow and total suspended sediment yield simulation in calibration and validation periods

	Calibration		Validation	
	Q	SSY	Q	SSY
<i>NSE</i>	0.48	0.65	0.5	0.32
<i>IOA</i>	0.92	0.93	0.9	0.86
<i>RB</i>	15%	9.87%	-1.2%	-22.37%
<i>RMSE</i>	3.03	0.83	1.47	0.41

3.2.4 Model comparisons

For this study, we focused on the comparison of models in regards to their ability to model *SSY* (an important variable for defining water quality) and spatial distribution of erosion and deposition (an important variable for soil sustainability assessment. The selected configurations of *RUSLE_SDR* and *MUSLE_S_SDR* will allow evaluation of the role of hydrological processes representations on *SSY* simulation, as these two configurations are incapable of return spatial specific results of erosion and deposition. The deposition processes were estimated indirectly by a multiplier (*SDR*). By applying *TC* methods, the other four selected configurations will allow highlighting the role of

explicit calculation of transport capacity, thus can calculate the location of erosion and deposition based on transport limitation assumption. The MUSLE-G-TC configuration uses the same hydrological inputs as GEOTopSed model, thus can highlight the differences in erosion calculations between MUSLE based method and physically based method. The comparison of spatial distribution of soil erosional loss and deposition among different models focused on identifying if the locations of erosional and depositional area predicted by models were the same. Long term (longer than or equal to annual scale) accumulated erosion and deposition spatial distribution were compared using the spatial maps obtained from GEOTopSed model as a reference.

3.3 Result

Here we present the inter-comparison results from both temporal and spatial aspects.

3.3.1 Temporal comparisons

Inter-comparison results of *SSY* at different temporal scales are shown in Figure 3-4. The scatter plots show the *SSY* for different model configurations against the ones obtained by GEOTopSed. Fisher approximate unbiased estimator (Fisher, 1915) was used to evaluate the correlation between models to account for the different sample sizes:

$$P = r + \frac{1-r^2}{2N}r. \quad (3.12)$$

Large correlation between different models indicates higher degree of agreement in the *SSY* estimates. The *RUSLE* based model showed the largest discrepancies comparing with *GEOtopSed* results. At the annual scale (Figure 3-4), *SSY* estimates from the rest five model configurations appear to vary linearly with the *SSY* estimates obtained from *GEOtopSed*, except for a few years (e.g. 2008, 2010). If the year 2010, for which all model representations grossly underestimate the *SSY* w.r.t. *GeoTopSed* (Figure 3-4), is not considered, the Fisher estimator between the *GEOtopSed* model and other model representations are all larger. The Fisher estimator for three *MUSLE* based model were all larger than 0.9 at annual scale. This implies that in *Dripsey* catchment, for most of the years the estimates of *SSY* obtained using simpler models based on *MUSLE* schemes can match the estimates from data and computationally intensive physics-based models. The *RUSLE* based model however did not show the similar responses, which implies the erosion estimation only based on rainfall may be very different with other type of models. The reasons for bias in the model performance in 2010, which received more than 112 mm rainfall within 10 days in January, is presented later in this section. At finer temporal scales (daily to seasonal), *SSY* estimates from *MUSLE_G_TC* model showed a power law relation with the *SSY* estimates from the *GEOtopSed* model. For other four model configurations, the Fisher estimator reduced significantly from annual to intra-annual scales (Table 3-5). The correlation between

GEOtopSed to other model representations is larger than 0.6 at seasonal and monthly scales also, as long as the year 2010 is excluded. At daily scale, the correlation for all model representations (except MUSLE_G_TC) is less than 0.26 with 2010 data and less than 0.3 without 2010 data (Figure 3-4). The results imply that: (a) models such as MUSLE_G_TC which has the same hydrological input as the GEOtopSed model can capture the SSY variations reasonably well at a wide range of temporal scales; (b) models with relatively simple hydrological representations such as based on SCS curve number method did not capture the temporal variation at daily event scale, but the model correlation improves as the time scale of comparison is coarser; and (c) model with MUSLE scheme is prone to underestimate the SSY responses to rainfall for large SSY events and overestimate for small SSY events with respect to GEOtopSed model even using the same hydrological inputs.

Table 3-5 Fisher approximate unbiased estimator of SSY modeling at different temporal scales (values in parenthesis are Fisher estimator without data in 2010)

	Annual	Seasonal	Monthly	Daily
RUSLE_SDR vs GEOtopSed	0.04(0.25)	0.15(0.16)	0.15(0.15)	0.13(0.14)
MUSLE_S_SDR vs GEOtopSed	0.64(0.93)	0.59(0.70)	0.57(0.65)	0.26(0.29)
RUSLE_TC vs GEOtopSed	0.04(0.25)	0.15(0.16)	0.15(0.15)	0.13(0.14)
MUSLE_S_TC vs GEOtopSed	0.64(0.93)	0.58(0.70)	0.56(0.65)	0.26(0.28)
MUSLE_G_TC vs GEOtopSed	0.67(0.93)	0.77(0.84)	0.74(0.81)	0.63(0.68)

Between model configuration using RUSLE and MUSLE schemes, MUSLE based models such as MUSLE_S_SDR and MUSLE_S_TC have better correlations with GEOTopSed model than RUSLE based schemes. There was no obvious improvement in the correlation depending on if the SSY estimation used an explicit routing method such as MUSLE_S_TC or a SDR based method such as MUSLE_S_SDR. However, the correlation between MUSLE_G_TC model configuration and GEOTopSed is significantly better than other model configurations. The results suggest that choice of hydrologic model for generation of runoff volume and peak can significantly influence the model performance at daily scales and moderately at monthly and seasonal scales.

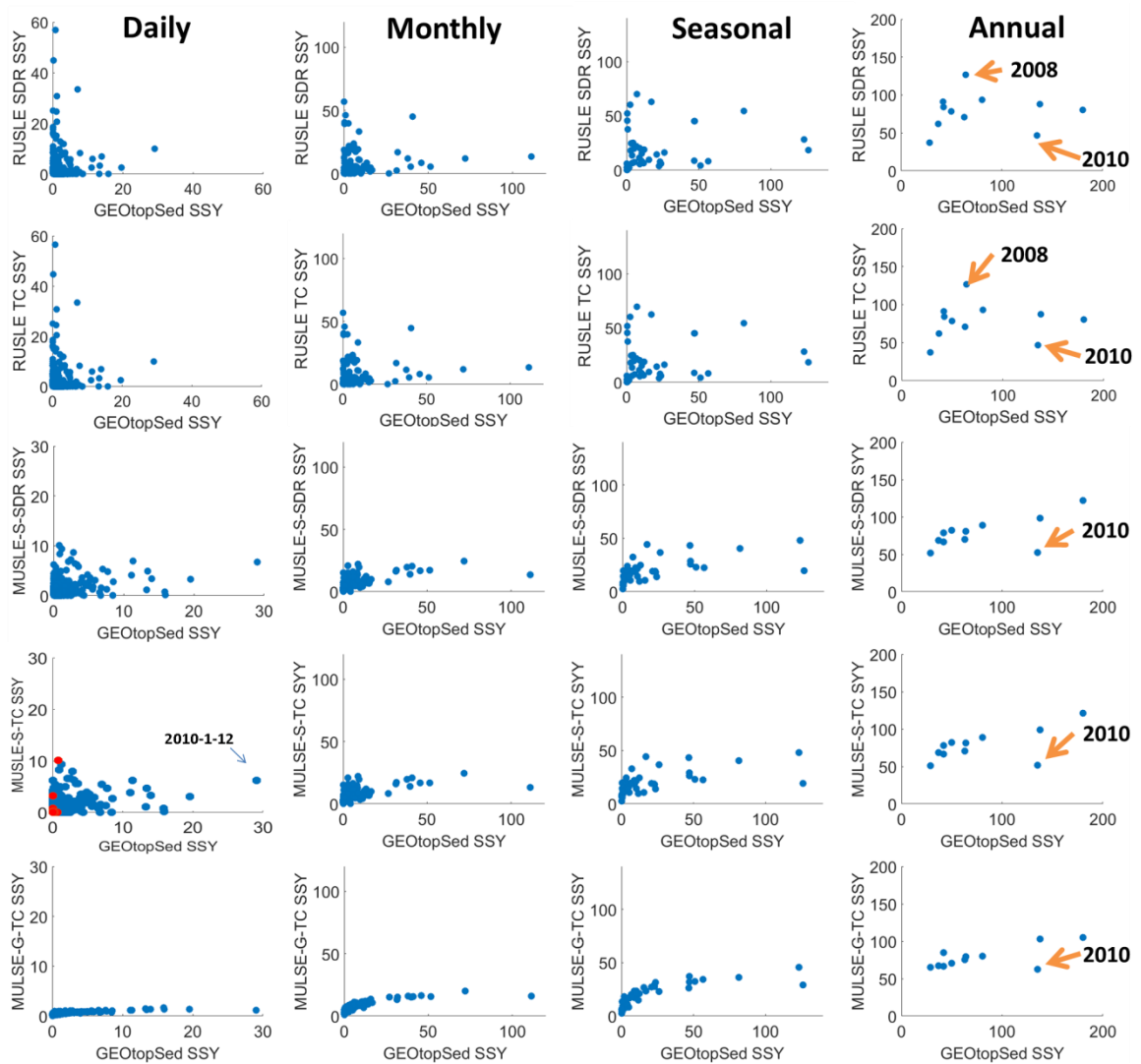


Figure 3-4 Scatter plot for SSY comparison with different model representations and temporal scales (from left to right: daily, monthly, seasonal, and yearly). Points with red color were points of case one in later discussion.

The different model structures used to calculate erosion and the differences in hydrological inputs/representations are two major reasons causing the disagreement in erosion responses from the selected model configurations. The discrepancies at monthly, seasonal, and annual scales are the sum of discrepancies at daily scale. The MUSLE-G-

TC model scheme used the hydrological statistics from GEOTop model, thus have almost the same driving forces for erosion calculation. The major disagreement between MUSLE-G-TC and GEOTopSed model are brought by the erosion calculation. Sediment generation and routing in GEOTopSed model are both related to transport capacity of the flow. Julien and Simons (1985) summarized different methods used to calculate sediment discharge based on transport capacity. The generated sediment discharge is usually a power law function of discharge. The index of the power varied from 0.5 to 2.42. With the wide range of derived index of power, the index of the power chosen to calculate transport capacity are different for GEOTopSed model and other model representations. Figure 3-5 showed the different erosion responses from the two model configurations to the same hydrological forces. The MUSLE-G-TC model generated more erosion than GEOTopSed model when the volume of daily discharge (Q) is less than 6 mm per unit area. When the flow volume increased beyond the threshold, GEOTopSed model generated more soil losses per unit discharge than MUSLE-G-TC model. The differences in the index can result in huge differences in soil erosion simulation if the volume of discharge is large, as shown in Figure 3-5.

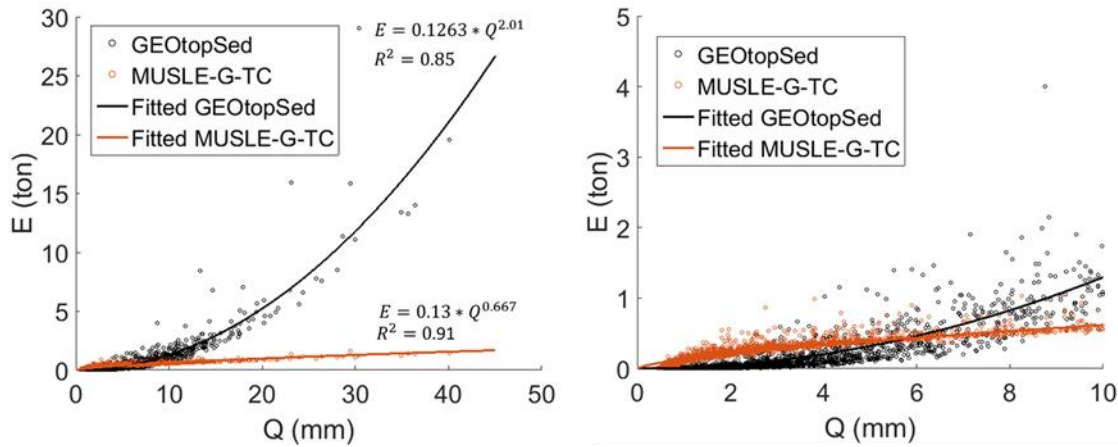


Figure 3-5 The scatter plot of Q and E for two models (left) and zoom-in scatter plot (right)

Besides the different equations used to calculate erosion, for model configurations with MUSLE-SCS frame and RUSLE frame, another big difference is the driving force. The flow simulated by SCS curve number method addresses the antecedent soil moisture condition by changing initial abstraction. The initial abstraction is adjusted by 5-day cumulative rainfall based on the method proposed by Sahu *et al.* (2010). Even though the proposed method was used to address the antecedent soil moisture condition, the coefficient of variation (CV) for initial abstraction (0.03) is much smaller than the CV of soil moisture content (0.27) simulated by GEOTopSed. This implies the 5-day cumulative rainfall method can only provide limited adjustments on initial abstraction. The simplification of hydrological processes representation in curve number method resulted in large discrepancies in generated overland flow (Q_s) to the overland flow generated by GEOTopSed (Q_G) as shown in Figure 3-6a.

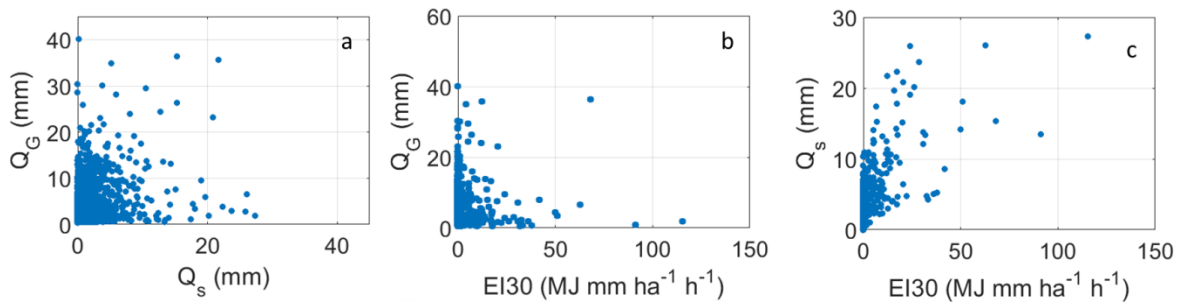


Figure 3-6 (a) Scatter plot of overland flow simulated by curve number method and GEOTopSed; (b) scatter plot of rainfall erosivity versus overland flow simulated by GEOTopSed; (c) rainfall erosivity versus overland flow simulated by curve number method;

Model configurations with RUSLE frame directly used precipitation as driving force. Some crucial hydrological processes, such as antecedent soil moisture condition, infiltration processes, and runoff generation were not accounted for in the erosion estimation. The rainfall erosivity used in RUSLE model has a poor correlation with overland flow predicted by GEOTopSed model (Figure 3-6b). RUSLE model uses 12.5mm as a threshold for erosive rainfall. The soil losses during small rainfall events were neglected. Figure 3-6b also showed zero rainfall erosivity for a range of overland flow generated by GEOTopSed model. Figure 3-6c showed a better correlation between the rainfall erosivity and the overland flow simulated with curve number method than Figure 3-6b. This indicates the similarities in erosion calculations between these two model configurations to the same rainfall.

Another feature of GEOTopSed model would result in differences in erosion simulation. GEOTopSed takes account for soil moisture impact on soil cohesion according to (Kemper and Rosenau, 1984):

$$\zeta_s = \left(\frac{\theta}{\theta_s}\right)^2 \zeta_{ss} \quad (3.13)$$

where ζ_s , ζ_{ss} are bare soil cohesion, saturated bare soil cohesion respectively, θ and θ_s are the soil moisture and saturated soil moisture contents.

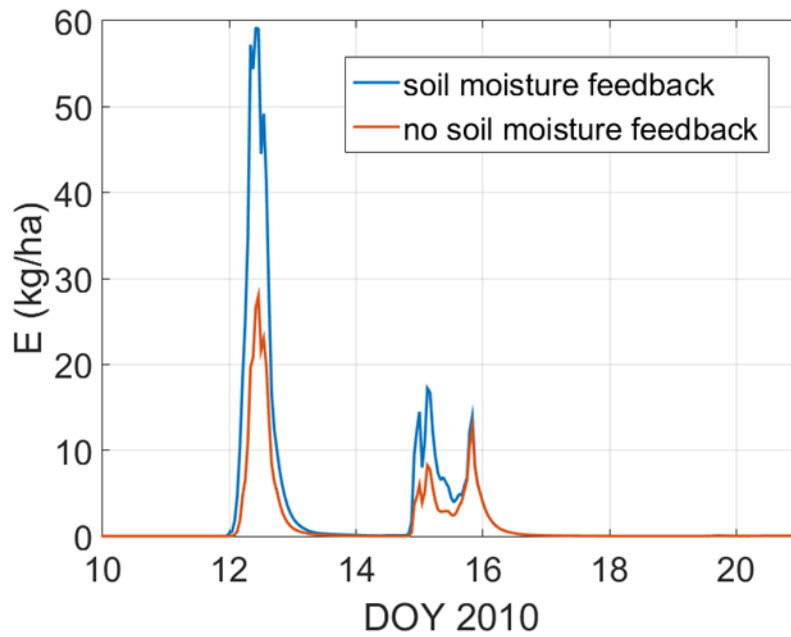


Figure 3-7 Comparison simulations with and without soil moisture feedbacks on soil cohesion

Comparison GEOTopSed simulations were run with and without the soil moisture feedback on soil cohesion. Figure 3-7 shows the soil moisture feedback on soil cohesion can increase the event SSY by two folds, if soil moisture is low.

The differences between soil loss values from the selected MUSLE based model configurations and GEOTopSed model (Δ SSY) was caused by the joint influences of the differences in hydrological processes representations and the different erosion processes

calculation. Among all the differences, varied equations used in erosion calculation, hydrological forces (overland flow simulation or erosivity calculation), and soil moisture dynamics are three major factors caused the disagreements between different model configurations. Figure 3-8 shows the scatter plots of daily Δ SSY versus Q_G , color coded with normalized antecedent soil moisture $\hat{\theta}$ from GEOtopSed simulation, between model configurations and GEOtopSed. The points were surrounded by black circles in Figure 3-8a and Figure 3-8b if the curve number method underestimated the surface runoff with respect to GEOtopSed.

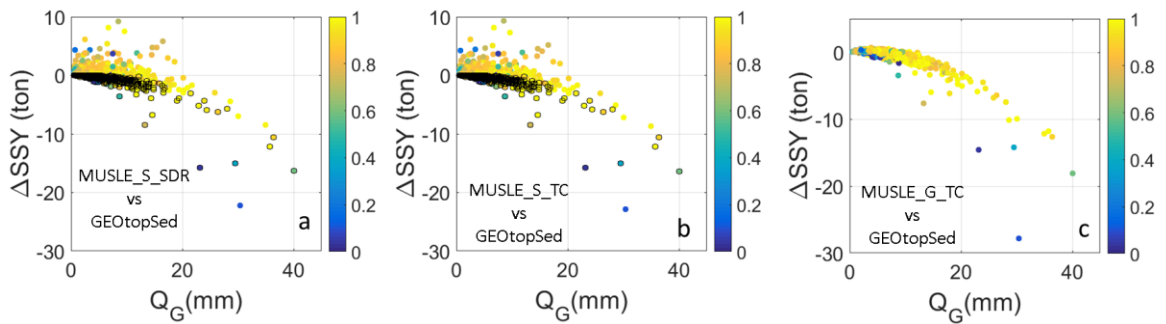


Figure 3-8 Scatter plots of overland flow simulated by GEOtopSed versus the differences of SSY. The points were color coded with normalized watershed average antecedent soil moisture ($\hat{\theta}$). The points with black edges indicate underestimation of Q by other model configurations w.r.t. GEOtopSed.

The differences between MUSLE-G-TC and GEOtopSed in Figure 3-8c were mainly caused by the different erosion calculation equations and the soil cohesion dynamics in GEOtopSed model. As Q_G increases, the probability of underestimation of SSY by MUSLE-G-TC model with respect to GEOtopSed model increases. This trend is due to the different soil loss responses from model structures as shown in Figure 3-5.

The soil cohesion decreasing at low soil moisture condition in GEOtopSed model also increased the SSY differences. A few blue points at the lower right corner indicate the soil cohesion effect. Figure 3-8a and Figure 3-8b showed similar trends as Figure 3-8c, underestimation became dominant as Q_G increases. The variations of SSY differences for those four pairs are larger than Figure 3-8c, especially when Q_G are small. The increased variations were caused by different hydrological representations between models.

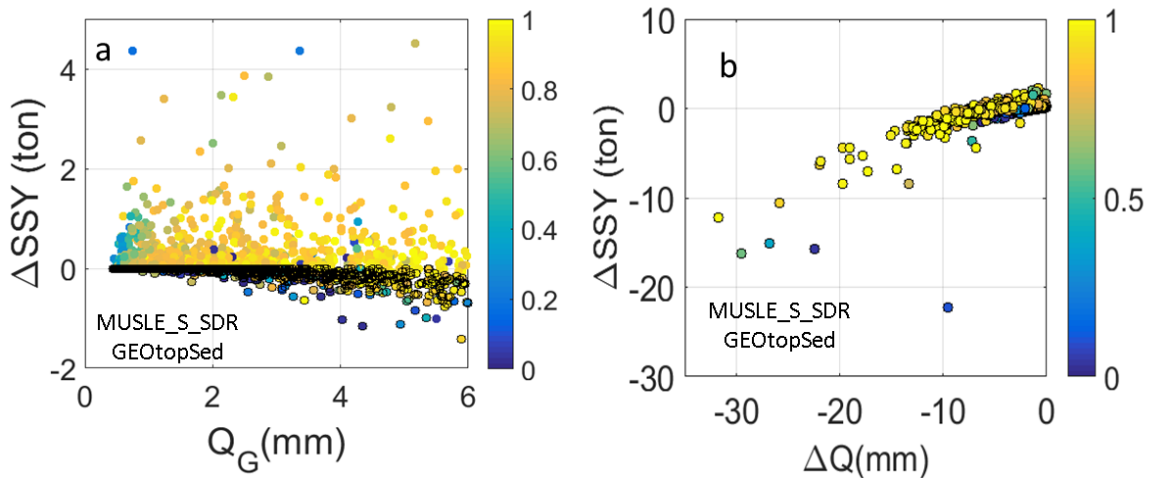


Figure 3-9 (a) Zoomed-in scatter plots of Δ SSY versus Q_G for $Q_G < 6$. (b) the scatter plots of Δ SSY versus ΔQ when $Q_G < 6$ and $\Delta Q < 0$. All plots were color coded with normalized watershed average antecedent soil moisture ($\hat{\theta}$).

Figure 3-9a and Figure 3-9c are zoomed-in scatter plots of Δ SSY versus Q_G for MUSLE-S-SDR and MUSLE-S-TC versus GEOtopSed when $Q_G < 6$ mm. When $Q_G < 6$ mm, the model configurations with MUSLE frames tend to overestimate SSY w.r.t. GEOtopSed if the hydrological driving forces were equivalent as shown in Figure 3-5. If the curve number method overestimate surface runoff w.r.t. GEOtopSed model, there's large possibility that they also overestimate the SSY. As shown in Figure 3-9a, most of

the points without black edges are above X-axis. If the overland flow is underestimated by curve number method, the influences from differences in erosion calculation equations and hydrological driving forces were from two opposite directions. If ΔQ is small enough, then the underestimation of hydrological driving force will dominant and result in $\Delta SSY < 0$. Otherwise, if the bias in hydrological driving force is not large enough and cannot compensate the bias brought by erosion equation differences, MUSLE based model would overestimate the SSY w.r.t. GEOtopSed model. As shown in Figure 3-9b, if $\Delta Q < -6$ mm, underestimation of SSY is always observed.

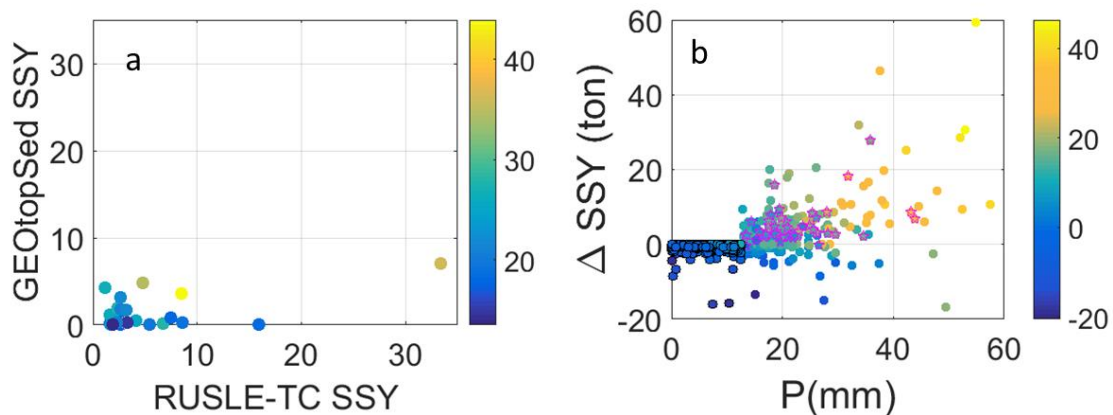


Figure 3-10 (a) scatter plots of SSY by GEOtopSed and RUSLE-TC, color coded with precipitation, only average antecedent soil moisture ($\hat{\theta} > 0.95$) were showed. (b) the scatter plot for ΔSSY and P, color coded with $(P - Q_G)$. Circles with black edge represent $P < 12.5$ mm, pentagrams with pink edge were points showed in (a).

As P increases, the probabilities of RUSLE base models overestimate SSY increase. Figure 3-10a is the scatter plots of the SSY simulated by GEOtopSed model versus the SSY simulated by RUSLE_TC model, when $\hat{\theta} > 0.95$. Near full saturate soil moisture condition implies the least impacts from the differences of hydrological driving

forces applied to the two models. The RUSLE-TC model overestimates SSY w.r.t. GEOtopSed when soil is very close to saturation if the rainfall is larger than the erosive rainfall threshold (12.5mm). This is mainly due to the differences in models. The RUSLE based model also ignores small rainfall showers below the threshold, which can cause erosion in GEOtopSed model. Thus it is observed from Figure 3-10b that RUSLE_TC model always under predicts SSY w.r.t. GEOtopSed when the differences between P and Q_G is smaller than 12.5 mm. Large difference between P and Q_G implies the differences of hydrological driving forces used for two models. Large positive values of differences between P and Q_G means high possibility that RUSLE based model over predicted the hydrological driving forces w.r.t GEOtopSed. The overestimations of hydrological driving forces combined with the model differences caused the overestimation in Figure 3-10b.

Here we selected two cases to highlight the role of hydrological processes representations on SSY simulations. Case one (2008-7-13 to 2008-8-7) was highlighted in red and case two (2010-1-10 to 2010-1-19) was identified with text in Figure 3-4.

Case one is an example of curve number method overestimate and underestimate overland flow w.r.t GEOtopSed model. Figure 3-11 showed the time series of rainfall, overland flow, soil moisture and the differences of SSY estimates of the selected period.

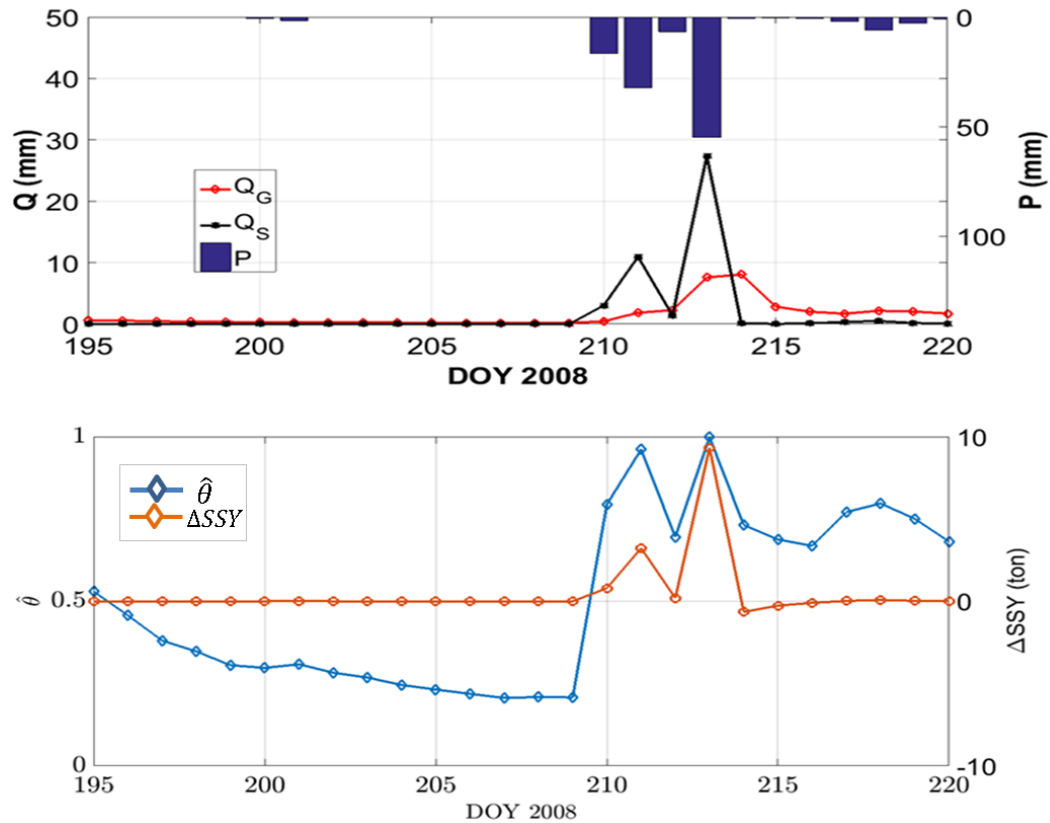


Figure 3-11(a) Time series of P and Q for case one; (b) time series of normalized soil moisture and ΔSSY .

The quite huge different responses between runoff generated by curve number method based models and GEOTopSed to the same amount rainfall were showed in Figure 3-11a from DOY 211 to DOY 213. The main reason is that by simulating soil moisture dynamics, the storage of the watershed is predicted low before rainfall occurred at DOY 210 by GEOTopSed model. This prediction reduces the runoff volume and then reduces the SSY. The Q simulated by SCS curve number method at 2008/7/31 is 27.34 mm and only 7.59mm by GEOTopSed. The SCS curve number method lacks the flexibility to adjust initial abstraction based on the soil moisture variation. The initial

abstraction is adjusted by 5-day cumulative rainfall and the variation of coefficient is not as large as soil moisture dynamics from GEOtopSed. The simple adjustment cannot reflect fully the variation of runoff generation process to the soil moisture dynamics. Thus the curve number based models showed significant overestimation on the peaks of runoff at DOY 211 and DOY 213, which also caused overestimation in SSY estimation (Figure 3-11b).

The curve number method has instantaneous response to the rainfall. The surface runoff generated by curve number method disappears after precipitation stops. The GEOtopSed model, on the other hand, has a comprehensive representation on rainfall-runoff process. Antecedent soil moisture is simulated and is used to adjust the infiltration and runoff generation processes. The surface flow was routed based on kinematic wave approximation following the direction of elevation gradient. Thus, when the volume of surface flow is small, the surface runoff process could last longer than the rainfall events due to the slow flow rate. The erosion process could also be observed during the recession period while no rainfall was occurred during that time. This explains the underestimation of SSY in Figure 3-11. This example event reveals that the MUSLE model with curve number method could overestimate the soil loss due to overestimate the runoff peak caused by lack the ability to capture soil moisture dynamics. The curve number based erosion model also could ignores the erosion happens during the recession period due to the simplification of surface flow routing

process. Rainfall erosivity based RUSLE model also lacks the ability to adjust the hydrological driving force based on soil moisture dynamics, neither can it capture the soil loss occurred during recessing period. Thus the SSY estimation from RUSLE based models has similar trend as MUSLE and curve number based models. It is also to be noted, if delay factors were added to the curve number method, such as SWAT (Arnold *et al.*, 1998), the performance of model could be improved.

Case two is an example for the impact of soil moisture on erosion calculation by reducing soil cohesion. In the right most column of Figure 3-4, one point (year 2010) is largely underestimated by other model configurations. This is due to the GEOtopSed model generated much more SSY than other model representations in that year. The overestimation of SSY w.r.t. other models was largely due to overestimation occurred during the winter. Figure 3-12 shows the rainfall, GEOtopSed generated runoff, soil moisture SSY time series of year 2010.

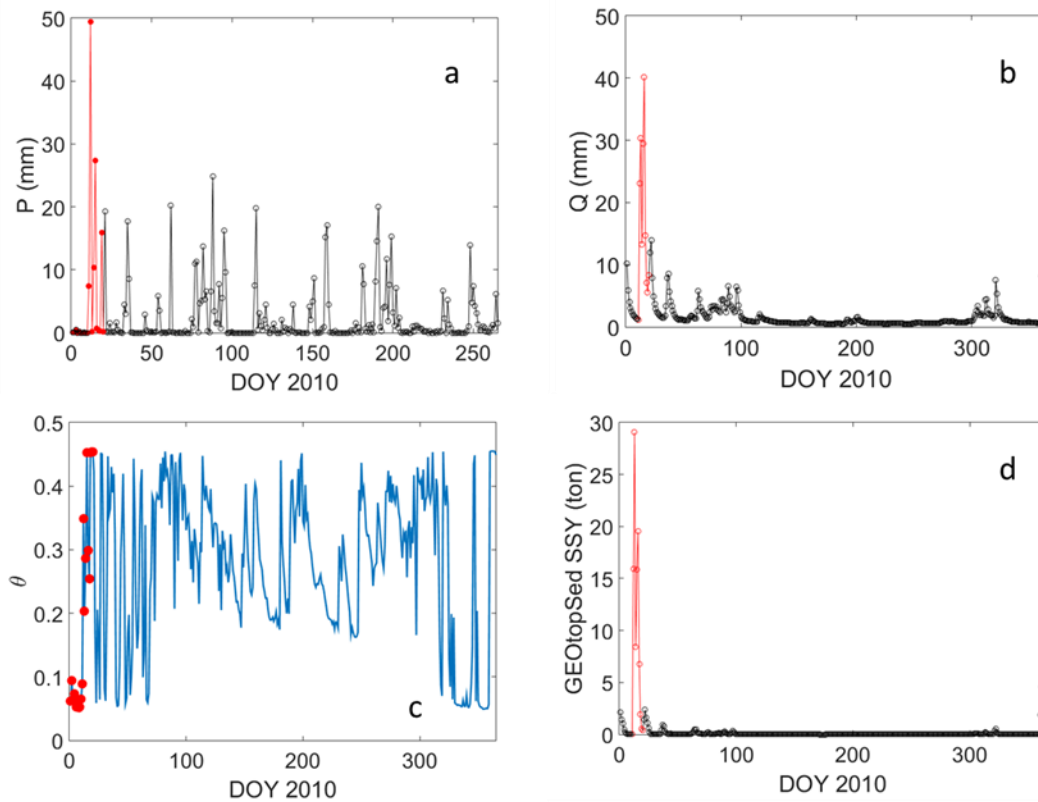


Figure 3-12 Rainfall (a), surface flow (b), soil moisture (c) and SSY (d) generated by GEOTopSed model in 2010

The period DOY 10 to DOY 19 at the beginning of year 2010 had more than 112mm rainfall for ten days with maximum daily precipitation 49.4mm (6th largest daily rainfall during the whole simulation period). The rainfall events between DOY 10 to DOY 20 generated 72.92% SSY of year 2010 (simulated by GEOTopSed model). SSY portion for RUSLE_TC, MUSLE_S_TC and MUSLE_G_TC are 11.55%, 22.41%, and 14.28% respectively. The EI30 is 11.55% of the annual EI30 for 2010. The antecedent soil moisture before precipitation is low (Figure 3-13c), thus the soil cohesion is small (Figure 3-13d), which increases soil erodibility when the raindrops impact and flow shear stress

acting on the land surface. Sensitivity analysis experiment on soil cohesion (Zi *et al.*, 2016) showed for GEOTopSed model, if the soil cohesion is less than 15 KPa, the SSY is really sensitive to the soil cohesion value (Figure 3-13b). When the extreme rainfall occurred, the soil cohesion value is below 15 KPa most of the time, thus exacerbate the soil loss generated by GEOTopSed model.

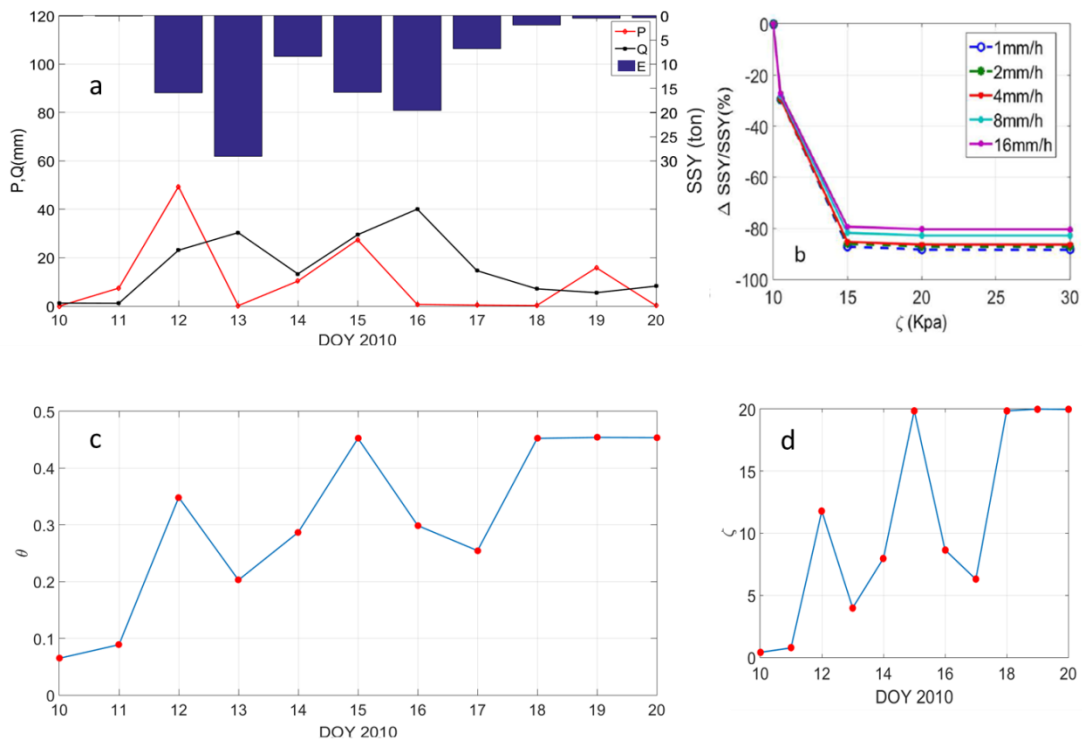


Figure 3-13 (a) P,Q and SSY time series, (b) the sensitivity analysis on soil cohesion, (c) changes of the soil moisture during the selected period, (d) changes of the soil cohesion during the selected period

Low antecedent soil moisture condition causes the first runoff peak smaller than the second one, even though the rainfall during the first peak is larger than the second one. However the reduced soil cohesion compensated the smaller peak flow rate and

resulted larger SSY than the second flow peak. The two selected cases showed the impacts of hydrological process representations on erosion simulation.

3.3.2 Spatial distribution

For spatial comparison of erosion and deposition areas, four out of six model representations from Table 3-3 were selected. Model representations with SDR based sediment routing were not considered for this analyses as they do not explicitly account for the spatial distribution of deposition within the watershed.

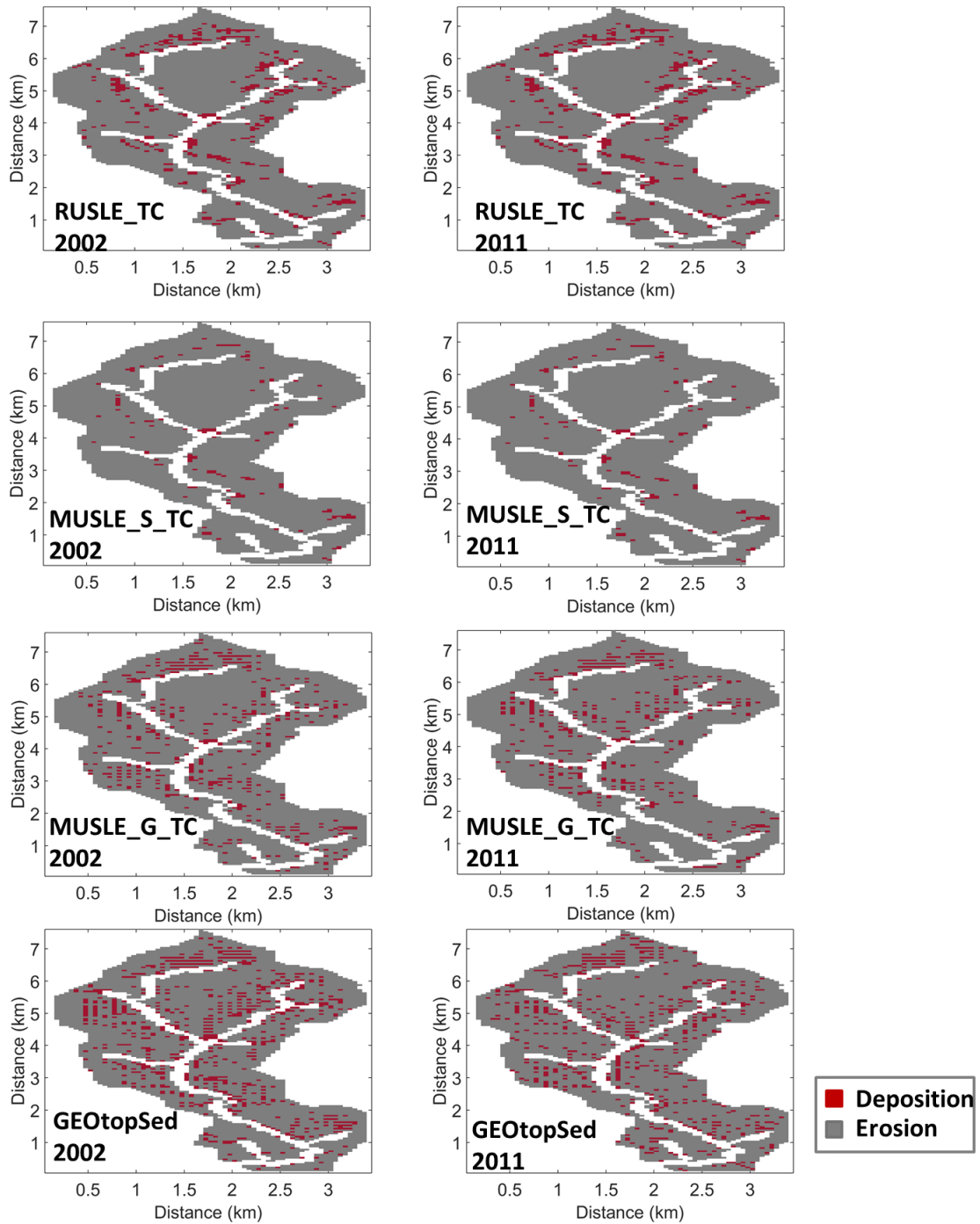


Figure 3-14 Spatial distribution of annual aggregated erosion, deposition area of different models. Grey color identifies the erosional area and red color shows the depositional area.

Figure 3-14 shows the spatial distribution for erosion and deposition from different model representations. The spatial distribution of RUSLE_TC and MUSLE_S_TC almost remains the same across different years. Because the spatial variation of erosion was mainly captured by LS factor in the calculation for RUSLE model. RUSLE model is designed to estimate the steady state of soil loss for a region and is not suitable for capturing the inter-annual variations on spatial distribution of erosion and deposition areas if the assumption of identical precipitation distribution between different years is assumed. The MUSLE model representation has a simplified runoff generation process (e.g. SCS), and it cannot show inter-annual variations of spatial distributions. For MUSLE_G_TC and GEOTopSed, we show spatial distribution maps for both dry (2011) and wet (2002) years. In general, all models showed similar spatial pattern of soil erosion and deposition. MUSLE_S_TC model had least deposition area and the results from GEOTopSed had the largest area of deposition.

Table 3-6 Area portion statistics

Models	Wet year		Dry year		Wet Day		Dry Day	
	Erosional area (%)	Depositional area (%)						
RUSLE_TC	91.47	8.53	91.47	8.53	91.5	8.5	91.5	8.5
MUSLE_S_TC	97.25	2.75	97.25	2.75	97.3	2.7	96.9	3.1
MUSLE_G_TC	90.91	9.09	92.81	7.19	93.0	7.0	94.0	6.0

GEOtop Sed	85.84	14.16	80.38	19.62	77.4	22.6	73.6	26.4
---------------	-------	-------	-------	-------	------	------	------	------

Table 3-6 shows the erosional and depositional area portion for different model representations. All representations had more than 80% erosion area within the watershed at annual scale. The larger change in the erosion and deposition area between wet and dry year in GEOtopSed model simulation indicates that it is more sensitive to inter-annual variability than MUSLE based model. The depositional area increases for GEOtop model. The erosional area increases for MUSLE_G_TC model when the climate condition is getting dryer which is counter-intuitive and implies simple model representations may not correctly redistribute soil sediment during erosion event. For shorter temporal scale (daily scale), GEOtopSed model showed the most sensitive to the changes of antecedent soil moisture condition, while other models were not as sensitive as GEOtopSed model.

The simulation results of locations of erosion and deposition within the watershed were compared to each other, using GEOtopSed as a reference. Year 2002 (wettest year during the simulation period) and 2011 (the second driest year during the simulation period) were selected to evaluate differences during both dry and wet years. 2010 is the driest year during the simulation period, but the SSY results from other models on that year have large bias with GEOtopSed which was discussed in previous section. Figure 3-15 and Table 3-7 show the agreements and disagreements between

different models. The percentage in Table 3-7 is based on the erosional area and depositional area of GEOtopSed model. All model representations have very good agreement on erosion area. Larger than 91% erosional area from GEOtopSed model were also predicted as erosional area in other model representations. However, the depositional area has poor agreement. More than 51% depositional area from GEOtopSed model was predicted as erosional area by other models. The MUSLE_G_TC has the most depositional area predicted as erosional area (87.7%) at year 2011 and The MUSLE_S_TC model has the least of 51.5%. MULSE_G_TC has the lowest erosional area agreement at year 2002 (91.6%) and the MUSLE_S_TC has the highest at year 2011 (98.4%). Red color in Figure 3-15 identified the disagreement between different models. The Cohen's Kappa coefficient (Cohen, 1960) is used to check the agreement in spatial distributions of erosion and deposition between models. Kappa coefficient equals to one indicates a complete agreement between two parties. If the Kappa value is smaller than zero, it implies the agreement between two parties is less than the agreement by chance. The negative values in Table 3-7 reveal that none of the model representations has a good agreement in spatial distribution of erosion and deposition, maybe due to the large discrepancies in the deposition locations.

Table 3-7 Agreement and disagreement percentage and Cohen's Kappa coefficient(Cohen, 1960) between different models. R is short for RUSLE_TC, M is short for MUSLE_S_TC and MUSLE_G_TC, G is short for GEOtopSed, "+" stands for erosion, "-" stands for deposition

	R,M(+)/G(+)	R,M(-)/G(-)	R,M(-)/G(+)	R,M(+)/G(-)	Cohen's kappa Coefficient
RULSE_TC vs GEOtopSed 2002	94.57	45.37	5.43	54.63	-0.48
RULSE_TC vs GEOtopSed 2011	93.41	31.83	6.59	68.17	-1.04
MULSE_S_TC vs GEOtopSed 2002	98.35	48.53	1.65	51.47	-0.65
MULSE_S_TC vs GEOtopSed 2011	97.77	28.68	2.23	71.32	-1.04
MULSE_G_TC vs GEOtopSed 2002	91.60	20.71	8.40	79.29	-1.12
MULSE_G_TC vs GEOtopSed 2011	91.96	12.28	8.04	87.72	-1.76

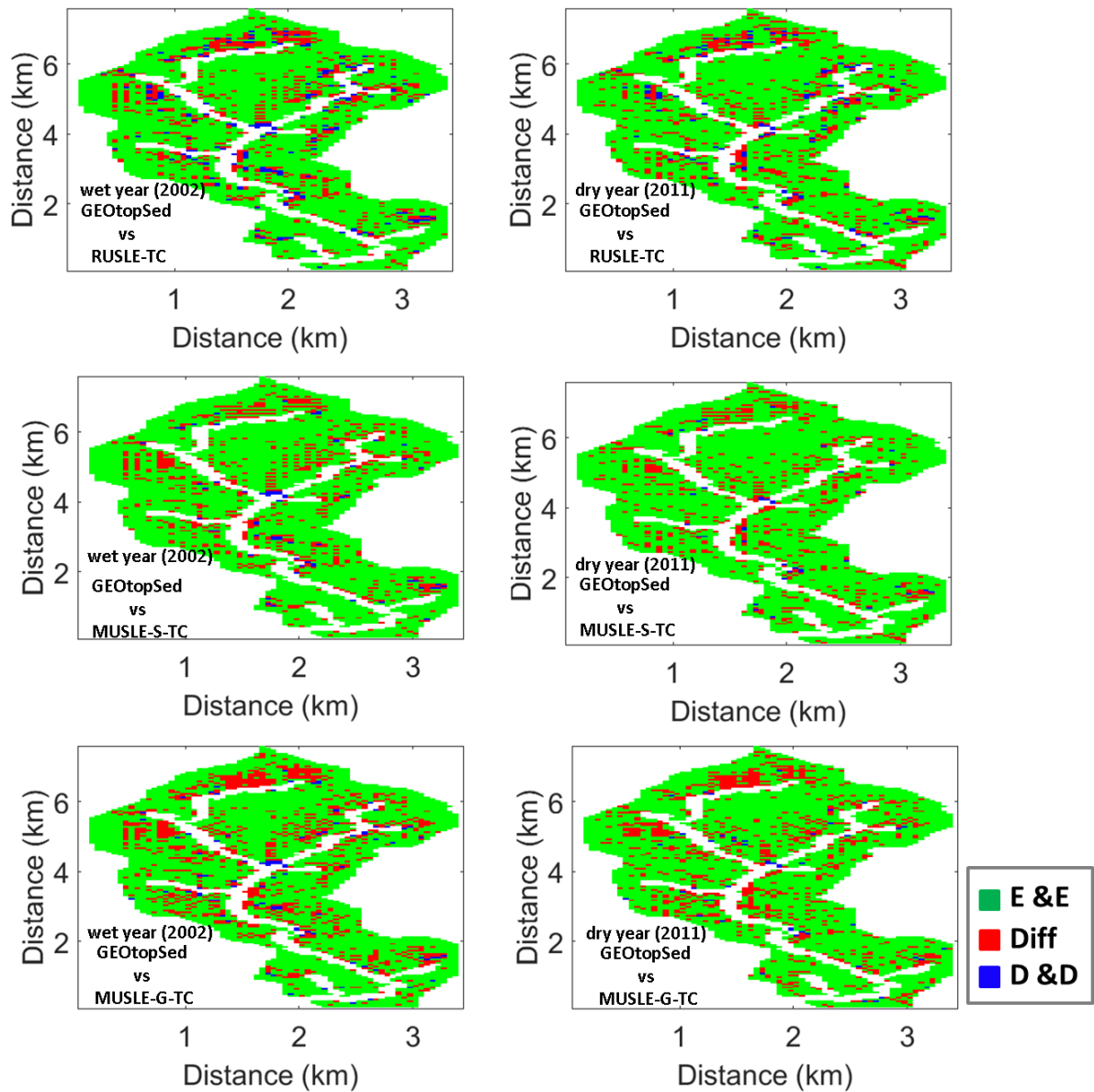


Figure 3-15 Comparison of erosion/deposition locations between different models.

Next we explore the topographic characteristics of locations that are identified as erosion or deposition by both GeoTopSed and the models under consideration. Table 3-8 to

Table 3-10 shows the statistics of agreement and disagreement area between different models. Some general trends were found across different model representations. For locations with small drainage areas (~1ha), all models predict these places have soil losses due to water erosion, while for locations that all models predicted as deposition zone, the drainage area is relatively large (~4 ha). The disagreement locations between varied model representations have moderate drainage area, soil moisture and LS factor. These findings implied that different models have good agreement for either headwater area or locations have large drainage area. The headwater area has relatively simple hydrological responses; none or few tributaries, thus the transport path of flow and suspended sediment are simple. Models with simplified hydrological representations can be used to compare with physically based representations. At locations with large drainage area, the hydrological states reflect the characteristics of watershed or subwatershed. Simple hydrological representations which are designed to capture the average hydrological states can be used to substitute more complex model representations. At the area in between, the hydrological processes can be influential to erosion simulation, which more detailed hydrological representations are needed. The trends among different models are similar. This implies the transport capacity is a crucial part in simulations for spatial distribution of erosion and deposition. For a transport limited case, since all three simplified models (RUSLE_TC, MUSLE_S_TC, MUSLE_G_TC) applied similar transport capacity

calculation (equation (3.10) and (3.11)), thus the simulated spatial patterns of erosion and deposition are similar (Figure 3-14). The differences in statistic values were related to the differences in transport capacity values and predicted soil losses from different methods. Figure 3-16 clearly showed that the modes and distributions of agreed erosional and depositional area are different. The agreed erosional area were concentrated at area with smaller drainage area while the depositional area have a wider range and larger drainage area in general.

Table 3-8 Statistics of agreement and disagreement area between RUSLE_TC and GEOTopSed (dry year)

RUSLE_TC vs GEOTopSed	\bar{S}	\overline{DA}	$\overline{DA * S}$	\overline{LS}	$\bar{\theta}$	$CV(\bar{\theta})$
R(+),G(+)	2.86	1.10	3.12	0.14	0.27	0.25
R(-),G(-)	2.61	3.97	9.43	0.27	0.33	0.15
R(+),G(-)	3.27	2.74	8.00	0.26	0.31	0.18
R(-),G(+)	2.34	3.91	8.58	0.25	0.32	0.16

Table 3-9 Statistics of agreement and disagreement area between MUSLE_S_TC and GEOTopSed (wet year)

MUSLE_S_TC vs GEOTopSed	\bar{S}	\overline{DA}	$\overline{DA * S}$	\overline{LS}	$\bar{\theta}$	$CV(\bar{\theta})$
MS(+),G(+)	2.84	1.21	3.35	0.14	0.33	0.31
MS(-),G(-)	2.04	5.18	10.50	0.27	0.41	0.23
MS(+),G(-)	3.16	2.93	8.25	0.26	0.38	0.27
MS(-),G(+)	2.14	4.80	10.04	0.27	0.41	0.23

Table 3-10 Statistics of agreement and disagreement area between MUSLE_G_TC and GEOtopSed (dry year in parenthesis)

MUSLE_G_TC vs GEOtopSed	\bar{S}	\overline{DA}	$\overline{DA * S}$	\overline{LS}	$\bar{\theta}$	$CV(\bar{\theta})$
MG(+),G(+)	2.86(2.87)	1.07(1.06)	3.04(3.02)	0.13(0.13)	0.36(0.26)	0.25(0.49)
MG(-),G(-)	2.63(2.1)	4.51(4.92)	9.63(9.77)	0.26(0.26)	0.4(0.32)	0.18(0.44)
MG(+),G(-)	2.97(3.11)	3.21(2.56)	8.835(7.28)	0.27(0.24)	0.41(0.31)	0.16(0.45)
MG(-),G(+)	2.94(2.48)	2.99(3.63)	7.61(8.53)	0.25(0.26)	0.38(0.3)	0.22(0.46)

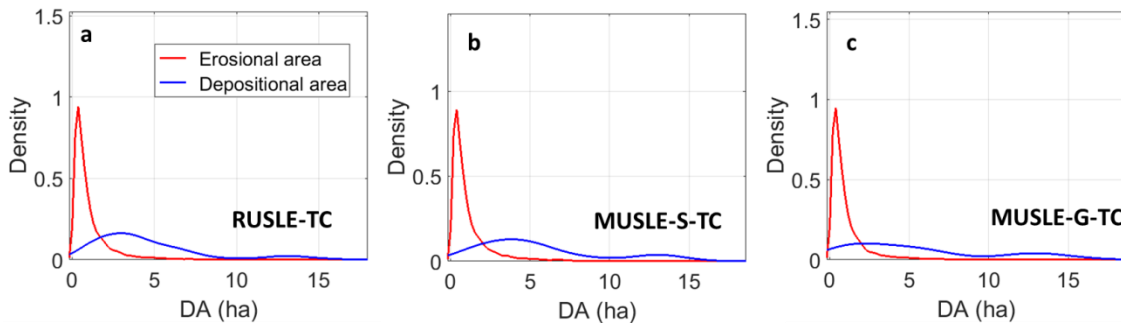


Figure 3-16 PDFs of drainage area (DA) for agreed erosional and depositional area of different model pairs.

3.4 Conclusion

In this chapter, we compared erosion/sediment transport model with different representations, from simple to complex. Two key aspects were focused on, the SSY at outlet of watershed and the spatial distribution of erosion and deposition. By applying models at a watershed located at maritime climate region, we found that the models with simplified hydrological representations can still have similar performance on SSY simulation at annual scale with the complicate model, but show fair amount of

discrepancies at shorter temporal scales. Model with hydrological input from complicate hydrological model, even though has simplified sediment generate and transport processes, still can have similar performances on SSY with complicated erosion model across all selected temporal scales. We compared the spatial distribution of erosion and deposition between different models. The agreement percentages for erosion area are above 90%. The location of depositional area varied among model representations. The model representations have good agreement at locations with small or large drainage area. The disagreement occurs at locations with moderate drainage area, LS factor and average soil moisture. This finding implies that simple erosion model representations could be substitutions for complicated representations on long-term (longer than annual scale) at headwater region and foot of hills.

4 The role of hydrologic feedback to the suspended sediment yield responses to different precipitation regimes: Implications on the evaluation of climate change impacts on erosion

This chapter is a modified version of the manuscript currently in preparation:

Tan Zi, Mukesh Kumar, John Albertson, The role of hydrologic feedback to the suspended sediment yield responses to different precipitation regimes: Implications on the evaluation of climate change impacts on erosion.

4.1 Introduction

Storms are the major mechanism that responsible for soil water erosion. Rainfall intensity is closely related to the soil water erosion process. High intensity rainfall can detach more soil particles because the raindrops have larger kinetic energy (van Dijk et al., 2002). More extreme rainfall can also lead to more infiltration excess runoff, thus causing more entraining soil particles from soil surface into the flow and keeping them in transport(Holden and Burt, 2002). The future climate projections show the amplification of the hydrological cycle, which will lead to a worldwide increase in heavy rainfall events and longer intervals between events (Ipcc, 2014). The rainfall intensity was found to increase in all over US too (Palecki et al., 2005). The increasing rainfall variability has both positive and negative impacts on terrestrial ecosystem (Knapp et al., 2008). Increase of the duration and severity of soil water stress are expected as intervals between rainfall events increase (Porporato et al., 2004). These researches implies

nonlinear responses of precipitation controlled soil erosion, given the nonlinearity feedbacks of some erosion related hydrologic factors such as runoff, soil moisture.

A number of researches evaluate the impact of climate change on soil water erosion potential based on the projected change of rainfall erosivity (Nearing, 2001; Sun et al., 2002; Yang et al., 2003; Hammad et al., 2006; Capolongo et al., 2008; Diodato and Bellocchi, 2009). Rainfall erosivity is a factor predicting the soil erosion risk with rainfall kinetic energy and peak rainfall intensity (Wischmeier and Smith, 1960). As a simple indicator, rainfall erosivity can be easily applied to different regions and climate scenarios. However, due to its simplicity, the impact of precipitation changes on erosion may not exclusively reflected by erosivity.

The ways that climate changes affecting soil erosion are quite complicated. Changes in vegetation cover, plant root and residues, soil chemical and physical properties, hydrologic factors such as evapotranspiration and soil moisture changes, surface roughness factors, and others can all affect the soil erosion responses to climate changes. Several modeling studies tried to predict soil erosion responses by considering as many factors as the models can account for (Williams et al., 1996; Favis-Mortlock and Guerra, 1999; Pruski and Nearing, 2002; Pruski and Nearing, 2002; Nearing et al., 2005; O'Neal et al., 2005). Two major uncertainties were to be noted for these researches: 1) the uncertainties in parameters and forcing; 2) the uncertainties in the interactions among

parameters. With those uncertainties, the prediction results could still be “right answer with wrong reasons”.

In this study, we limited the influencing factors to the hydrologic feedbacks. The unit plot assumption was applied to remove other factors such as vegetation cover and land uses. A physically based erosion model with a comprehensive hydrological process description was utilized to do the erosion simulation. More aspects of rainfall impacts on hydrological processes and erosion generation process, directly and indirectly, can be evaluated from the model. The model simulations results were then used to compare with the erosion prediction based on erosivity method. By comparing the two types of results, we are trying to address following questions: 1) For different precipitation regimes, do the models show different responses on the changes of hydrological forces to erosion? 2) What is the role of hydrologic feedback to the SSY responses to different precipitation regimes in varied hydroclimatic settings? 3) What is the implication on climate change impact evaluation on soil erosion?

4.2 Data and Methodology

4.2.1 Physically based erosion model

In this study, an open-source sediment erosion/deposition model, GEOtopSed (Rigon et al., 2006; Endrizzi et al., 2014; Zi et al., 2016), was selected as the representative physically based erosion model. This model has a comprehensive description for

hydrological processes, such as evapotranspiration, infiltration, surface and subsurface flow, etc. This model was evaluated at both plot and catchment scale. Both short term (sub-event) simulations and long term simulations (multiple years) have been conducted using this model. The GEOtopSed model uses a state-of-the-art representation of coupled surface-subsurface hydrologic processes. The comprehensive land-surface energy and water interaction scheme and detailed description of hydrologic processes within the GEOtop model can simulate both fast and slow responses in energy and water dynamics, which ensures the coupled erosion model, can be applied across a wide range of temporal scales.

4.2.2 Experiment design

Suspended sediment yield (*SSY*) from the unit plot were estimated using the aforementioned two methods. In this study, seven different locations were selected to represent different climate regions. For each region, nine different rainfall scenarios were generated for the two methods. The frequencies of extreme precipitation from nine scenarios increase monotonically. 50-year ensemble simulation results were used to represent results for each scenario.

The multi-year average annual soil loss from the unit plot using rainfall erosivity method is a reference for soil erosion estimation. This concept was used to determine how the conditions of actual plots related to the unit plot by multiplying other limiting factors. To compare two methods, the Unit Plot concept was applied to the physically

based erosion model. A unit plot was created with the dimension of 22m* 2m*5m with a 9% slope. The spatial resolution for each cell is 1m*1m. The soil parameters were assigned for silt loam taking the SSURGO database as a reference (<http://websoilsurvey.nrcs.usda.gov/>). No vegetation was set for the GEOtopSed model. The GEOtopSed model was set to run all scenarios at all stations each for 55 years at daily time step. The first five years were treated as a spin-up time for the model.

4.2.3 Experiment sites for different climate regions

Karl and Koss (1984) proposed nine climate regions for continental US. The Northern Rockies and Plains region and the Upper Midwest region were excluded due to the snowy winter. For the other seven climate regions, seven weather stations from Global Historical Climatology Network (GHCN) were selected as the reference stations. The climate data from these stations were downloaded from National Climate Data Center (NCDC, <http://www.ncdc.noaa.gov/>). All of the selected weather stations have daily weather records longer than 125 years and missing data were all less than 3% for the whole observation durations. Linear interpolation method was used to fill gaps of missing temperature and relative humidity records. The missing precipitation records were filled with zero.

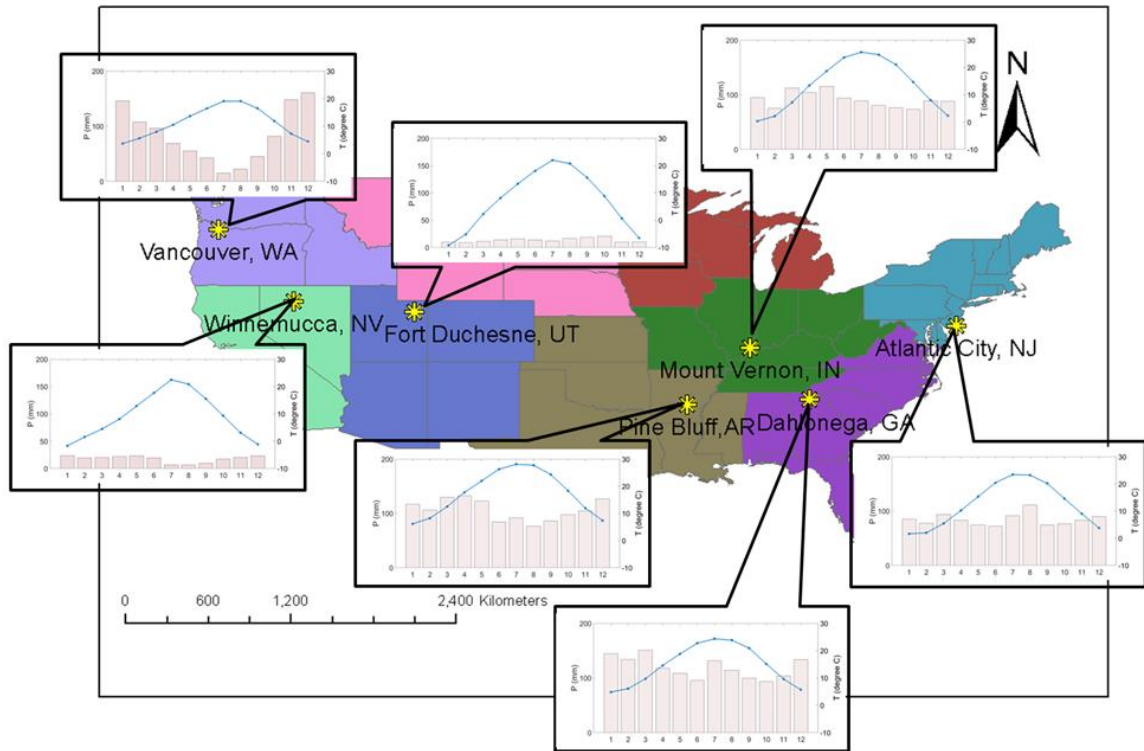


Figure 4-1 Selected weather stations in this study. The bars are monthly rainfall for each station and the blue line is the monthly average temperature. Different colors for states identifies different climate regions proposed by National Climate Data Center(Karl and Koss, 1984).

Figure 4-1 and Table 4-1 show the location and climate conditions for the seven selected weather stations. The mean annual precipitation (MAP) records of the seven stations were from 178.85mm to 1584.1mm. To exclude the impact of snow, all the selected sites have no more than 8% snow day ratio. Figure 4-1 also shows the seasonality of precipitation for different locations.

Table 4-1 Information of selected weather stations

Weather Station	Köppen Climate Classification	ELEV (m)	LAT	LON	MAP (mm)	Snow day ratio (%)	ATMAX (degC)	ATMIN (degC)	Miss data ratio (%)
Atlantic City, NJ (AC)	Warm Continental	15.8	39.367	-74.41667	1029.3	2.73	16	9	1.74
Dahlonaga, GA (DA)	Warm Oceanic	457.2	34.533	-83.983	1584.1	0.40	20.8	8.5	0.47
Fort Duchesne, UT (FD)	Warm Semi-arid	1521	40.283	-109.85	178.85	4.25	16.3	-1.59	2.78
Mount Vernon, IN (MV)	Warm Continental	125	37.933	-87.9	1105.95	2.98	19.86	7.86	1.39
Pine Bluff, AR (PB)	Warm Oceanic	65.5	34.2	-92	1303.05	0.28	23.6	11.5	2.1
Vancouver, WA (VA)	Temperate Mediterranean	11.6	45.633	-122.65	992.8	1.25	16.74	6	0.66
Winnemucca, NV (WI)	Warm Semi-arid	1324.1	40.967	-117.717	208.05	7.07	18	0.41	0

4.2.4 Weather generation

Nine precipitation scenarios were simulated using a combination of the first order Markov Chain model and variant Gamma distributions. The first order Markov Chain method was used to simulate the occurrence of rainfall events. Two conditional probabilities were calculated for each month of each station:

$$p_{01} = \Pr\{\text{precipitation on day } t \mid \text{no precipitation on day } t - 1\} \quad (4.1)$$

and

$$p_{11} = \Pr\{\text{precipitation on day } t \mid \text{precipitation on day } t - 1\} \quad (4.2)$$

where p_{01} is the probability of rainfall events on day t if no rainfall occurred on day $t-1$ and p_{11} is the probability of rainfall events on day t if rainfall occurred on day $t-1$. For each simulation day, a random number u is drawn using a uniform distribution from the interval $[0, 1]$. Based on the status of the previous simulated day, the judgment would be made whether the value of u is larger or smaller than p_{01} (p_{11}). The day is simulated to be wet if $u \leq p_{01}$, otherwise, the day is simulated to be dry. According to the current status of simulated day, the occurrence of precipitation for the next simulation day would be assigned.

The nine scenarios were then obtained by changing the coefficients (β_i and α_i) of the gamma distribution for precipitation event amounts to $N^* \beta_i$ and α_i / N , respectively. This ensured that the simulated precipitation events for scenarios with different N had the same mean ($\alpha_i \beta_i$) but different variance ($N \alpha_i \beta_i^2$). Here N ($N = 0.5, 1, 2, 4, 6, 8, 10, 12,$ and 14) is a scaling factor that was used to adjust the intra-seasonal variability of precipitation events to generate nine scenarios. Each scenario entailed 55 random realizations of a precipitation series and they were used to assess the average and variance changes in soil losses due to water erosion. The frequencies of extreme

precipitation from Scenario 1 to 9 were 3.3%, 5.0%, 6.7%, 8.3%, 9.6%, 10.2%, 10.6%, 10.9%, and 11.0%, respectively. Here, extreme precipitation was defined as a daily amount larger than the 95th percentile in the base scenario (Scenario 2). In relation to the base frequency (Scenario 2), the frequency of extreme precipitation ranged from -35% (Scenario 1) to 120% (Scenario 9), generally within the range of change in reported extreme precipitation for the US (Madsen and Figdor, 2007).

With the first order Markov Chain method, the general precipitation seasonality at different locations was captured by the base scenario (Figure 4-2). The gamma distribution also fits well with the observed precipitation distribution.

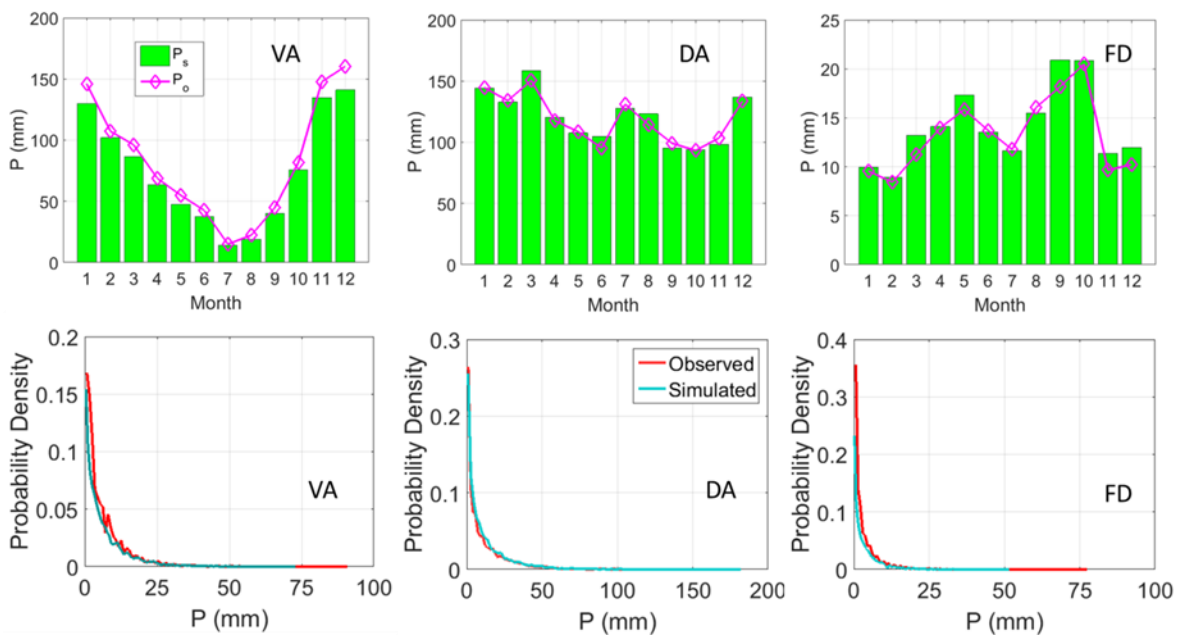


Figure 4-2 (a) Observed and simulated monthly precipitation (base scenario) for three different weather stations, (b) Observed and simulated precipitation probability density functions for three different weather stations

The annual temporal dynamics of the generated temperature is identical for different years at each station. So does the generated relative humidity time series. The relative humidity was changed to the maximum relative humidity record from observed records if rainfall occurred at the same day. The general trend of generated temperature and relative humidity for each year were derived from the best-fit functions of long term observed values (Figure 4-3).

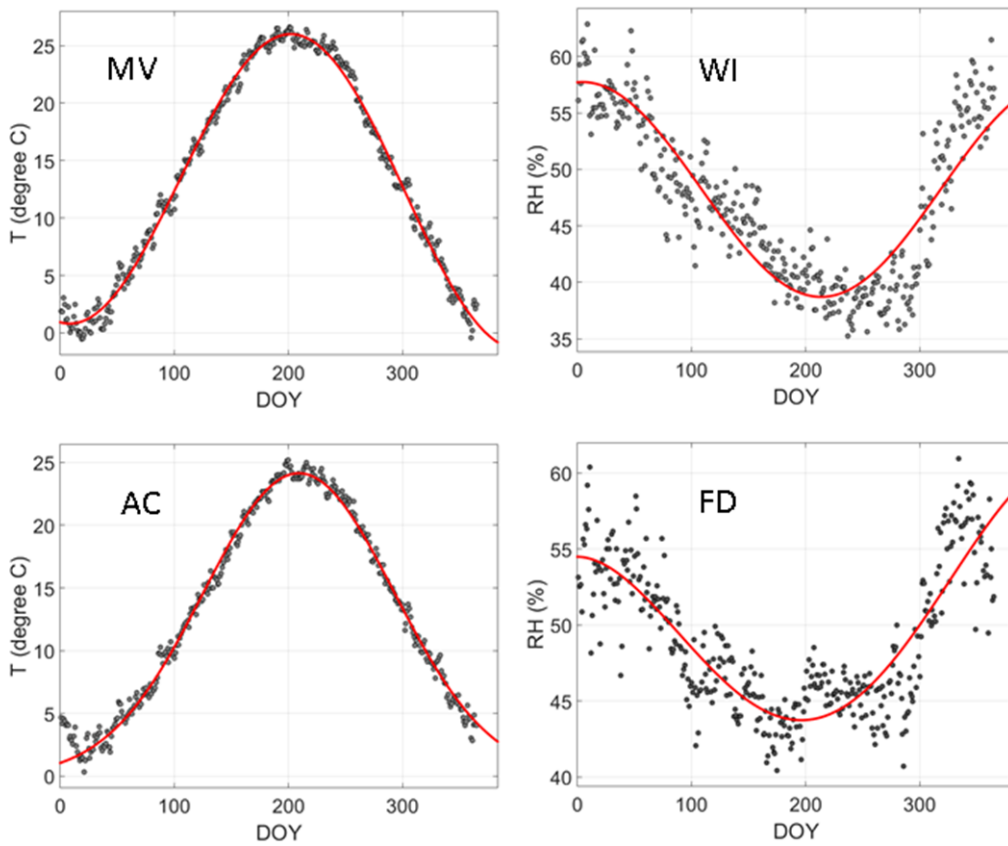


Figure 4-3 Fitted and observed temperature and relative humidity time series for four stations

4.3 Results

The responses of different sites to the changes of rainfall extremes are very different between the two methods (Figure 4-4). The changes of magnitude of soil loss simulated by GEOtopSed are much smaller than the changes of rainfall erosivity. The rainfall erosivity method predicts the monotonic increasing of soil loss rate for different climate regions as the rainfall becomes more extreme (only two exceptions for all the cases), while the trends simulated by GEOtopSed are more complex. It is noted that for different location, the soil loss varied from 3.43 ton ha⁻¹ yr⁻¹ to 13.57 ton ha⁻¹ yr⁻¹ for GEOtopSed simulation, and from 3.42 ton ha⁻¹ yr⁻¹ to 47.56 ton ha⁻¹ yr⁻¹ for rainfall erosivity method. The big difference in the range of soil loss predicted by rainfall erosivity method and GEOtopSed method indicates the hydrological responses of soil erosion as the rainfall become more extreme can greatly impact erosion simulation. Three different trends were shown in the results of GEOtopSed model. The soil loss at Winnemucca (WI) and Fort Duchesne (FD) sites showed both increasing and decreasing trends as the rainfall is more extreme. The soil loss at Pine Bluff (PB) did not show obvious increasing (~4%) trend as the rainfall became more extreme. Soil loss at other four selected sites showed increasing trends given the changes of extreme precipitation regimes. The magnitudes of increasing are smaller than rainfall erosivity method.

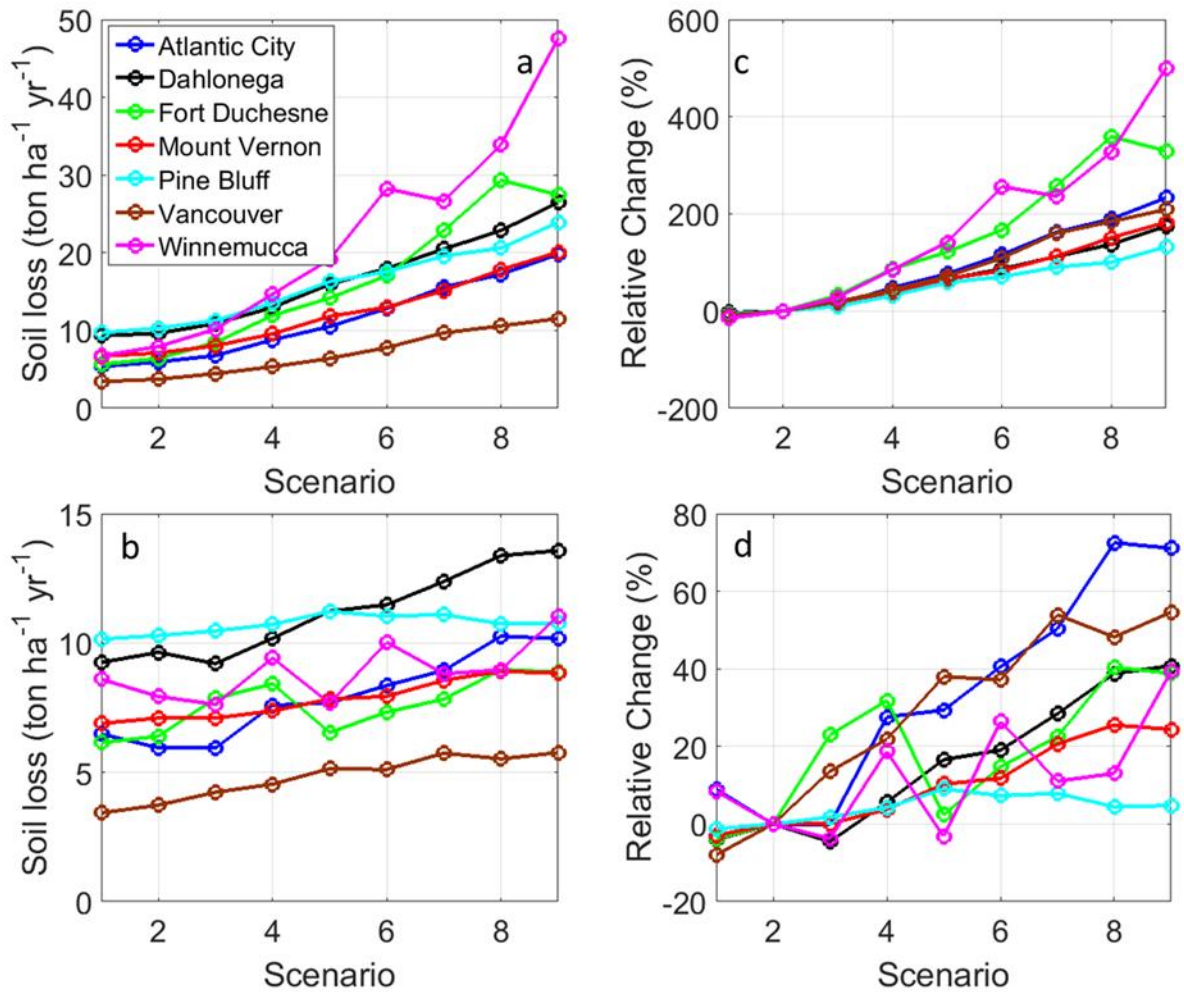


Figure 4-4 Absolute soil loss (left) and relative change of soil losses (right) based on Scenario 2 (a,c Erosovity method, b,d GEOTopSed) for different sites and different scenarios

Table 4-2 and Table 4-3 showed the mean annual soil loss for each station and each scenario and their coefficient of variation. The mean annual soil losses estimated with rainfall erosivity method are 1.95-4.3 folds of the soil losses estimated with GEOTopSed model for the most extreme scenario (scenario 9) for different locations. In general, the soil losses predicted by rainfall erosivity method are more than the

estimation of GEOTopSed model, the differences between two methods increase as the rainfall getting more extreme. The CV of mean annual soil losses estimated by erosivity method increase as the rainfall events became more extreme. This trend identified soil erosion values have larger variation year to year in future according erosivity method. Similar to the mean annual soil losses results, the CV of annual soil losses from GEOTopSed model also showed complex trends. The CV of annual soil losses predicted by GEOTopSed model can increase or decrease as the change of rainfall regimes. This implies the increase of rainfall variation does not cause increase of variation in soil loss predicted by GEOTopSed model.

Table 4-2 Mean soil loss (ton ha⁻¹ yr⁻¹) of unit plot for different scenarios with different methods(G: GEOTopSed, E: rainfall erosivity)

Mean Soil Loss	Metho d	1	2	3	4	5	6	7	8	9
Atlantic City,NJ	G	6.48	5.95	5.94	7.59	7.69	8.36	8.94	10.26	10.17
	E	5.38	5.95	6.77	8.79	10.51	12.85	15.59	17.21	19.79
Dahlonega,GA	G	9.25	9.64	9.20	10.18	11.23	11.48	12.38	13.38	13.57
	E	9.31	9.64	10.88	12.97	15.94	17.97	20.47	22.86	26.46
Fort Duchesne,UT	G	6.15	6.39	7.86	8.42	6.54	7.33	7.83	8.97	8.87
	E	5.65	6.39	8.46	11.93	14.17	17.06	22.87	29.34	27.44
Mount Vernon,IN	G	6.89	7.10	7.10	7.37	7.83	7.94	8.56	8.91	8.83
	E	6.70	7.10	8.04	9.55	11.81	12.99	15.13	17.82	20.07

Pine Bluff,AR	G	10.1 5	10.29	10.4 7	10.7 2	11.2 2	11.0 4	11.1 0	10.7 4	10.7 8
	E	9.71	10.2 9	11.2 8	13.5 5	16.2 9	17.5 6	19.5 9	20.6 1	23.8 9
Vancouver, WA	G	3.43	3.73	4.23	4.54	5.14	5.11	5.74	5.52	5.76
	E	3.42	3.73	4.44	5.34	6.40	7.80	9.70	10.5 9	11.5 2
Winnemucca, NV	G	8.60	7.93	7.63	9.42	7.67	10.0 3	8.81	8.96	11.0 5
	E	6.74	7.93	10.1 7	14.6 8	19.1 4	28.2 5	26.6 7	33.8 9	47.5 6

Table 4-3 Coefficient of variation (CV) of soil loss of unit plot for different scenarios with different methods(G: GEOTopSed, E: rainfall erosivity)

CV	Method	1	2	3	4	5	6	7	8	9
Atlantic City,NJ	G	0.58	0.31	0.37	0.53	0.44	0.33	0.30	0.57	0.41
	E	0.26	0.25	0.35	0.38	0.49	0.70	0.67	0.65	0.99
Dahlonega,GA	G	0.35	0.30	0.22	0.24	0.24	0.26	0.25	0.38	0.37
	E	0.27	0.38	0.34	0.44	0.67	0.44	0.68	1.06	1.01
Fort Duchesne,UT	G	0.67	0.58	0.69	0.55	0.69	0.58	0.59	0.65	0.72
	E	0.00	0.00	0.01	0.02	0.03	0.01	0.01	0.09	0.02
Mount Vernon,IN	G	0.24	0.36	0.25	0.27	0.25	0.21	0.31	0.27	0.25
	E	0.56	0.71	0.99	1.28	1.34	1.70	1.93	1.73	1.88
Pine Bluff,AR	G	0.16	0.17	0.18	0.18	0.19	0.19	0.18	0.21	0.20
	E	0.74	0.81	1.02	1.18	1.44	1.53	1.51	1.76	2.01
Vancouver, WA	G	0.13	0.18	0.14	0.15	0.19	0.20	0.21	0.25	0.22
	E	0.20	0.43	0.68	0.78	1.22	1.51	1.52	2.14	1.64
Winnemucca, NV	G	0.60	0.72	0.47	0.56	0.70	0.58	0.63	0.72	0.60
	E	0.00	0.02	0.05	0.11	0.12	0.18	0.16	0.19	0.21

4.4 Discussion

The probability density functions (PDF) were shown in Figure 4-5 for scenario 1 and scenario 9 at three sites from dry area to humid area. The vertical gray dash lines identified the 12.5mm threshold. The threshold for erosive rainfall (12.5mm) applied by the rainfall erosivity method is relatively high as most of the rainfall showers for the three selected sites were under the threshold even for the most extreme rainfall scenario. As the rainfall regimes changing from the least extreme to the most extreme, the shapes of rainfall PDFs revealed that more intensive extreme rainfall showers and less small or moderate rainfall showers were expected. The thresholds for extreme rainfall and small/moderate rainfall varied site by site and scenario by scenario.

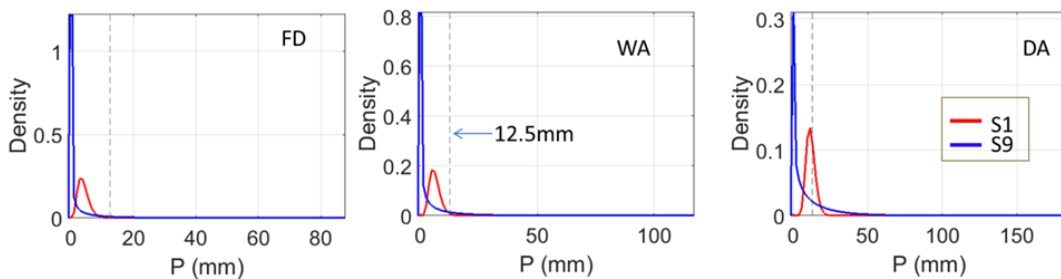


Figure 4-5 Rainfall PDFs of scenario 1 and scenario 9 for three different sites

Unlike rainfall erosivity method, GEOtopSed model does not only rely on the rainfall changes to predict erosion changes. Both raindrop impact and shear stress from overland flow are considered as driving forces of soil erosion. More comprehensive hydrological processes were included in the GEOtopSed model, such as infiltration excess flow, saturation excess flow, surface flow etc, to facilitate erosion simulation.

GEOtopSed model solves 3D-Richards equation every time step and updates the soil moisture for the whole soil profile.

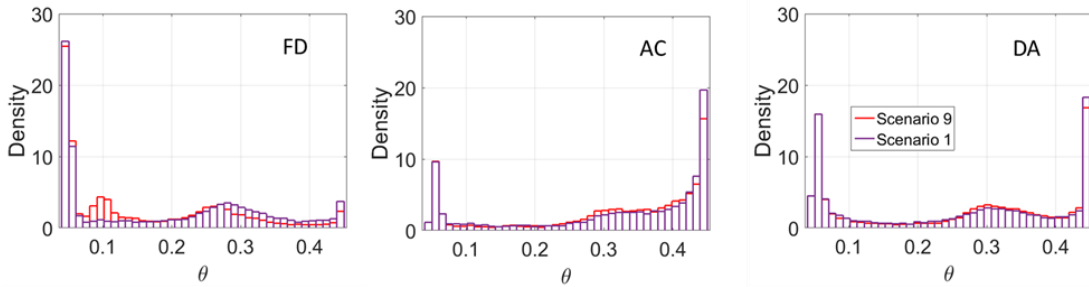


Figure 4-6 Probability densities of the first layer soil moisture for three locations

Figure 4-6 shows the probability densities for the first layer soil moisture simulated by GEOtopSed model. For dry climate region, the more extreme scenario results a larger portion of dry soil condition (soil moisture between 0.05 and 0.15). While for humid area, the more extreme scenario results in a smaller probability of soil saturate condition (soil moisture ~ 0.45). The probability of soil moisture between 0.27 and 0.43 increased a little for humid area when the rainfall is more extreme. The climate region with moderate rainfall showed the similar pattern of the soil moisture change as the rainfall changes. The runoff generation process is based on the soil moisture simulation. Thus the influences of more intensive extreme rainfall showers and less small or moderate rainfall showers on soil moisture, then on runoff and erosion can be accounted for in GEOtopSed model. The drier soil moisture condition had a tradeoff effect that reduces erosion days due to larger soil moisture deficit to generate runoff. The changes of total runoff volumes thus are smaller than the changes of rainfall erosivity because

some small rainfall events would not generate any runoff in more extreme rainfall setting. Thus less erosion days were predicted by GEOtopSed model. This eventually resulted in less magnitude of changes in erosion than rainfall erosivity method as rainfall became more extreme.

Table 4-4 showed that as the rainfall became more extreme, the soil moisture conditions became drier in average for the selected climate regions. For all selected regions, the erosion events decreased when the rainfall became more extreme. The volumes of runoff generated in more extreme rainfall setting are larger but the relative changes are not comparable to the relative changes of rainfall erosivities. Only models with comprehensive hydrological processes representations like GEOtopSed can account for these changes brought by changes of rainfall regimes.

Table 4-4 Changes of average annual runoff, average soil moisture and erosion days per year between two scenarios

	Scenario 1			Scenario 9		
	θ	Erosion days per year	Q (m ³ /yr)	θ	Erosion days per year	Q (m ³ /yr)
Atlantic City, NJ	0.37	118	17.35	0.36	85	18.96
Dahlonega, GA	0.36	129	25.58	0.37	102	29.52
Fort Duchesne, UT	0.29	26	2.65	0.23	12	2.81
Mount Vernon, IN	0.38	120	22.99	0.39	100	24.85

Pine Bluff, AR	0.41	126	29.15	0.41	115	29.59
Vancouver, WA	0.42	121	25.47	0.4	89	24.47
Winnemucca, NV	0.24	19	2.81	0.19	9	3.48

The above discussion showed that the soil layer acted as a buffer to adjust the hydrological driving forces. As shown in Figure 4-7, the heavy tail of precipitation PDF curve were filtered out by soil moisture adjustment. The PDF curve of $P-\theta_d$ did not have a heavy tail above zero, which indicates that with the adjustment of soil, the impacts from extreme rainfall events reduced. The alternative hydrological driving force $P-\theta_d$ is relevant to both the rainfall characteristics and the soil moisture dynamics. The impacts of the hydrological processes on erosion are highly correlated to the local climate and soil conditions. Erosion estimation methods only considering the rainfall changes (eg. Erosivity method) cannot capture the impact of soil adjustment, thus are not suitable for areas where soil have strong adjustment capabilities.

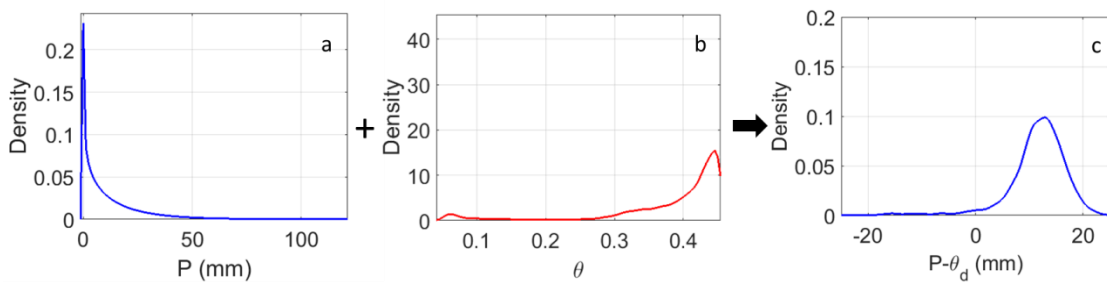


Figure 4-7 The buffer effect of soil on hydrological driving force

4.5 Conclusion

In this study, we showed the role of hydrologic processes on erosion response to extreme precipitation regimes in varied hydroclimatic settings with the simulation results using a physically based erosion model, GEOtopSed. The responses of erosion to different extreme precipitation regimes varied with hydroclimatic settings. Nine different extreme precipitation regimes were generated in seven selected climate regions of US according to the local climate characteristics. 50 years ensemble simulations were conducted for each of the rainfall regimes using the physically based GEOtopSed model on a unit plot setting. With a more comprehensive description of hydrological processes, the GEOtopSed model showed different predictions in erosion responses to the change of extreme rainfall regimes from the predictions made only by the changes of rainfall erosivities. The physically based GEOtopSed model successfully captured the impact of changes of the soil moisture on erosion while the rainfall erosivity method was only considering the energy change of the rainfall. The simulated erosion by GEOtopSed accounts for the soil moisture feedbacks, thus is not as large as the erosion predicted by rainfall erosivity method in general. The differences in erosion responses at areas with varied hydroclimatic conditions implied that the simple rainfall erosivity method may not be suitable for climate change impact analysis on erosion at areas where the hydrologic processes may have large influences on the processes of erosion generation. In general, we highlighted the impacts of hydrological processes on soil erosion

simulation. Methods such as erosivity were not able to capture the feedbacks from soil adjustments.

This study is based on the unit plot assumption from the USLE family model. The results represent the situation that erosion can be easily generated. No vegetation cover was considered. The results were at a plot-scale and the complexity of pathways in a watershed was not considered. For a comprehensive climate change impact analysis, more factors need to be accounted for along with the hydrologic feedbacks, such as temperature change, land use and land cover change, soil types, morphology, and etc.

5 Conclusions and Future Work

5.1 Conclusions

In this dissertation, we created a physically based model with comprehensive hydrological representations and tested it at both plot and watershed scales. Then we compared the newly developed erosion model with other erosion models with varied hydrological representations at different temporal scales. The spatial distributions of erosion and deposition were also compared among models. After we show the differences in simulation results from models with different levels of details for hydrological feedbacks, a multi-year ensemble simulation experiment with different extreme rainfall patterns was designed to show the potential impacts of different hydrological representations on applications of models.

In Chapter 2, we developed an open-source sediment erosion/deposition module for a 3D surface-subsurface hydrologic model, GEOtop, and evaluated its applicability at both plot and catchment scale. The model uses a physically-based representation of coupled surface-subsurface hydrologic processes and a comprehensive land-surface energy and water interaction scheme to simulate hydrologic response and consequent sediment dynamics. With the comprehensive representation of hydrological processes and land surface characteristics, the newly developed model showed reasonable timing and magnitude of stream flow and suspended sediment yield (SSY) from the plot scale to catchment scale. The biases in suspended sediment yield simulation were similar to

the biases in streamflow simulation. Daily precipitation magnitude can only explain limited observed SSY variation. Further examination of simulation results revealed that SSY per unit event magnitude varied proportionally with the prevailing soil moisture. All these findings indicate that the accuracy of flow simulations and spatial distribution of soil moisture critically influence the estimation accuracy of SSY. The modeling results also showed that the source (erosion) and sink (deposition) areas in a catchment were heterogeneous and dynamic, and could change from one event to the next, and the extent of source/sink areas were found to be influenced by prevailing moisture conditions, which in turn determined the quantity of runoff generation. Model results also suggest that long-term erosion rate from a location was not a simple function of slope-length. The spatio-temporal dynamics of erosion are shown to be influenced by hydrological processes such as evapo-transpiration, capillary rise and lateral groundwater flow and etc. The spatially-explicit simulations of coupled hydrologic processes for estimation of erosion/deposition distribution and sediment generation are crucial.

In Chapter 3, we compared erosion/sediment transport model with different hydrological processes representations, from simple to complex. The models with simple representations can have similar performances as models with comprehensive representations on SSY simulation for annual scale, yet varied a lot at short temporal scales. Model with hydrological input from complicate hydrological model, even though

has simplified sediment generate and transport processes, still can have similar performances on SSY with complicated erosion model across all selected temporal scales. This highlights the importance of hydrological processes in erosion and sediment transport simulations. The spatial distribution of erosion and deposition between different models were also compared. The results have good agreement for erosional area, but not for depositional area. For locations with small or large drainage area, different models have good agreement. Locations with moderate drainage area, LS factor and average soil moisture showed the largest discrepancies. The comparison of erosion on both temporal and spatial scales among different models clearly showed the limitations of models with simplified hydrological processes.

In Chapter 4, we showed the role of hydrologic processes on SSY responses to different hydroclimatic settings. Different predictions in SSY responses to the change of extreme rainfall regimes were showed between the modeling results and the results without soil moisture adjustment. The GEOtopSed model can capture the changes of the soil moisture as well as its impact on erosion simulation while the rainfall patterns changed. The differences in SSY responses at areas with varied hydroclimatic condition implied the importance of the hydrologic processes on erosion simulation. Without enough details about the hydrological processes in erosion model may result in quite different conclusions in climate change impact applications.

This work highlighted the differences in erosion simulation caused by varied hydrological process representations in models. Models with comprehensive hydrological process representations were able to capture both temporal and spatial variations of soil erosion due to hydrological processes, while other models with simplified representations cannot. The good agreement in SSY for long term simulation (annual scale) between models does not mean the simplified models have the good results by “right” simulation. The cancellation between positive and negative bias at shorter temporal scales results in a “better” performance at longer temporal scales for simplified models. Inter-comparison of models showed the more comprehensive hydrological process representations the model has, the larger capability of the model to capture the impacts from hydrological process on erosion simulations. Models with simplified hydrological process representations were not able to capture the hydrological feedbacks on erosion from soil adjustment in long term simulation applications, such as climate change application.

5.2 Suggestions for Future Work

Further confidence in the modeled estimates could be built by obtaining field estimates of states (e.g. ground water, residence time etc.) and related parameters (e.g. rill width, soil cohesion etc.), and by implementing the model in varied settings. The presented model version does not account for bank-erosion processes, which limits its applicability to watersheds with small bank erosion w.r.t. total hillslope losses. For using

the model as a predictive tool, vegetation dynamics in response to changes in meteorological forcings and hydrologic states need to be accounted for. Another important future direction is on the soil science itself. For a physically based soil erosion model, the mechanics of erosion process are dependent on a few soil parameters such as soil particle size, soil cohesion, and etc. For long term application, those soil parameters would not be constant. The erosion process would change soil texture, soil cohesion, and other soil parameters. Those processes should be considered in future erosion models. The chemical erosion was not considered in this work, which also can play an important role in erosion process at certain circumstances. In spite of aforementioned limitations, the open-source integrated modeling framework presented here offers the potential for its use both as an evaluation and retrospective-prediction tool, and as a virtual laboratory for understanding the role of hydrologic states and parameters on sediment dynamics.

References

- Aksoy H, Kavvas ML. 2005. A review of hillslope and watershed scale erosion and sediment transport models. *Catena*, **64**: 247-271. DOI: 10.1016/j.catena.2005.08.008.
- Albertson JD, Kiely G. 2001. On the structure of soil moisture time series in the context of land surface models. *Journal of Hydrology*, **243**: 101-119. DOI: 10.1016/S0022-1694(00)00405-4.
- Arnold JG, Fohrer N. 2005. SWAT2000: current capabilities and research opportunities in applied watershed modelling. *Hydrological Processes*, **19**: 563-572. DOI: 10.1002/hyp.5611.
- Arnold JG, Srinivasan R, Muttiah RS, Williams JR. 1998. Large area hydrologic modeling and assessment part i: Model development. *JAWRA Journal of the American Water Resources Association*, **34**: 73-89. DOI: 10.1111/j.1752-1688.1998.tb05961.x.
- Arnold JG, Williams J, Nicks A, Sammons N. 1990. SWRRB; a basin scale simulation model for soil and water resources management. Texas A & M University Press.
- Baartman JEM, Jetten VG, Ritsema CJ, de Vente J. 2012. Exploring effects of rainfall intensity and duration on soil erosion at the catchment scale using openLISEM: Prado catchment, SE Spain. *Hydrological Processes*, **26**: 1034-1049. DOI: 10.1002/hyp.8196.
- Bagnold R. 1966. An approach to the sediment transport problem from general physics. *US Geol. Surv. Prof. Paper*, **422**: 231-291.
- Bakker MM, Govers G, Kosmas C, Vanacker V, Oost Kv, Rounsevell M. 2005. Soil erosion as a driver of land-use change. *Agriculture, Ecosystems & Environment*, **105**: 467-481.
- Bakker MM, Govers G, Rounsevell MD. 2004. The crop productivity–erosion relationship: an analysis based on experimental work. *Catena*, **57**: 55-76.
- Beasley D, Huggins L, Monke E. 1980. Answers: a model for watershed planning. *Transactions of the ASAE-American Society of Agricultural Engineers*.

- Beasley DB, Huggins LF, Monke EJ. 1980. ANSWERS: A model for watershed planning. *Transactions of the ASAE*, **23**.
- Bertoldi G. 2004. The water and energy balance at basin scale: a distributed modeling approach. In: *Environmental Engineering*, University of Trento, pp: 202.
- Bertoldi G, Della Chiesa S, Notarnicola C, Pasolli L, Niedrist G, Tappeiner U. 2014. Estimation of soil moisture patterns in mountain grasslands by means of SAR RADARSAT2 images and hydrological modeling. *Journal of Hydrology*, **516**: 245-257. DOI: <http://dx.doi.org/10.1016/j.jhydrol.2014.02.018>.
- Boardman J. 2006. Soil erosion science: Reflections on the limitations of current approaches. *CATENA*, **68**: 73-86. DOI: <http://dx.doi.org/10.1016/j.catena.2006.03.007>.
- Bonumá NB, Rossi CG, Arnold JG, Reichert JM, Minella JP, Allen PM, Volk M. 2014. Simulating Landscape Sediment Transport Capacity by Using a Modified SWAT Model. *J. Environ. Qual.*, **43**: 55-66. DOI: 10.2134/jeq2012.0217.
- Bookhagen B, Strecker MR. 2012. Spatiotemporal trends in erosion rates across a pronounced rainfall gradient: Examples from the southern Central Andes. *Earth and Planetary Science Letters*, **327**: 97-110.
- Brandt J. 1988. The Transformation of Rainfall Energy by a Tropical Rain Forest Canopy in Relation to Soil Erosion. *Journal of Biogeography*, **15**: 41-48.
- Bullock MS, Kemper W, Nelson S. 1988. Soil cohesion as affected by freezing, water content, time and tillage. *Soil Science Society of America Journal*, **52**: 770-776.
- Cabral MC, Garrote L, Bras RL, Entekhabi D. 1992. A kinematic model of infiltration and runoff generation in layered and sloped soils. *Adv. Water Resour.*, **15**: 311-324. DOI: [http://dx.doi.org/10.1016/0309-1708\(92\)90017-V](http://dx.doi.org/10.1016/0309-1708(92)90017-V).
- Calder IR. 2001. Canopy processes: implications for transpiration, interception and splash induced erosion, ultimately for forest management and water resources. *Plant ecology*, **153**: 203-214.
- Cao Y, Ouyang ZY, Zheng H, Huang ZG, Wang XK, Miao H. 2008. Effects of forest plantations on rainfall redistribution and erosion in the red soil region of

- Southern China. *Land Degradation & Development*, **19**: 321-330. DOI: 10.1002/ldr.812.
- Capolongo D, Diodato N, Mannaerts CM, Piccarreta M, Strobl RO. 2008. Analyzing temporal changes in climate erosivity using a simplified rainfall erosivity model in Basilicata (southern Italy). *Journal of Hydrology*, **356**: 119-130. DOI: <http://dx.doi.org/10.1016/j.jhydrol.2008.04.002>.
- Chen X, Kumar M, McGlynn BL. 2014. Variations in Streamflow Response to Large Hurricane-Season Storms in a Southeastern U.S. Watershed. *Journal of Hydrometeorology*, **16**: 55-69. DOI: 10.1175/JHM-D-14-0044.1.
- Ciampalini R, Follain S, Le Bissonnais Y. 2012. LandSoil: A model for analysing the impact of erosion on agricultural landscape evolution. *Geomorphology*, **175-176**: 25-37. DOI: <http://dx.doi.org/10.1016/j.geomorph.2012.06.014>.
- Cohen J. 1960. A Coefficient of Agreement for Nominal Scales. *Educational and Psychological Measurement*, **20**: 37-46. DOI: 10.1177/001316446002000104.
- Cook HL. 1937. The Nature and Controlling Variables of the Water Erosion Process. *Soil Science Society of America Journal*, **1**. DOI: 10.2136/sssaj1937.03615995000100000085x.
- Croft AR, Monninger LV. 1953. Evapotranspiration and other water losses on some aspen forest types in relation to water available for stream flow. *Eos, Transactions American Geophysical Union*, **34**: 563-574. DOI: 10.1029/TR034i004p00563.
- Cronshey R. 1986. Urban hydrology for small watersheds. US Dept. of Agriculture, Soil Conservation Service, Engineering Division.
- de Vente J, Poesen J. 2005. Predicting soil erosion and sediment yield at the basin scale: Scale issues and semi-quantitative models. *Earth-Sci. Rev.*, **71**: 95-125. DOI: <http://dx.doi.org/10.1016/j.earscirev.2005.02.002>.
- de Vente J, Poesen J, Verstraeten G, Van Rompaey A, Govers G. 2008. Spatially distributed modelling of soil erosion and sediment yield at regional scales in Spain. *Global and Planetary Change*, **60**: 393-415. DOI: 10.1016/j.gloplacha.2007.05.002.

- Della Chiesa S, Bertoldi G, Niedrist G, Obojes N, Endrizzi S, Albertson JD, Wohlfahrt G, Hörtnagl L, Tappeiner U. 2014. Modelling changes in grassland hydrological cycling along an elevational gradient in the Alps. *Ecohydrology*, **7**: 1453-1473. DOI: 10.1002/eco.1471.
- DeRoo APJ, Offermans RJE, Cremers N. 1996. LISEM: A single-event, physically based hydrological and soil erosion model for drainage basins .2. Sensitivity analysis, validation and application. *Hydrological Processes*, **10**: 1119-1126.
- DeRoo APJ, Wesseling CG, Ritsema CJ. 1996. LISEM: A single-event physically based hydrological and soil erosion model for drainage basins .1. Theory, input and output. *Hydrological Processes*, **10**: 1107-1117.
- Diodato N, Bellocchi G. 2009. Assessing and modelling changes in rainfall erosivity at different climate scales. *Earth Surface Processes and Landforms*, **34**: 969-980. DOI: 10.1002/esp.1784.
- Donigian Jr A, Bicknell B, Imhoff J, Singh V. 1995. Hydrological Simulation Program-Fortran (HSPF). *Computer models of watershed hydrology.*: 395-442.
- Edlefsen NE, Anderson AB. 1943. *Thermodynamics of soil moisture*. University of California.
- Endrizzi S, Gruber S, Dall'Amico M, Rigon R. 2014. GEOtop 2.0: simulating the combined energy and water balance at and below the land surface accounting for soil freezing, snow cover and terrain effects. *Geosci. Model Dev.*, **7**: 2831-2857. DOI: 10.5194/gmd-7-2831-2014.
- Everaert W. 1991. EMPIRICAL RELATIONS FOR THE SEDIMENT TRANSPORT CAPACITY OF INTERRILL FLOW. *Earth Surface Processes and Landforms*, **16**: 513-532.
- Favis-Mortlock DT, Guerra AJT. 1999. The implications of general circulation model estimates of rainfall for future erosion: a case study from Brazil. *CATENA*, **37**: 329-354. DOI: [http://dx.doi.org/10.1016/S0341-8162\(99\)00025-9](http://dx.doi.org/10.1016/S0341-8162(99)00025-9).
- Fernandez GP, Chescheir GM, Skaggs RW, Amatya DM. 2005. Development and testing of watershed-scale models for poorly drained soils. *Transactions of the ASAE*, **48**: 639-652.

- Ferro V, Porto, P. 2000. Sediment Delivery Distributed (SEDD) Model. *Journal of Hydrologic Engineering*, **5**: 411-422. DOI: doi:10.1061/(ASCE)1084-0699(2000)5:4(411).
- Fisher RA. 1915. Frequency distribution of the values of the correlation coefficient in samples from an indefinitely large population. *Biometrika*: 507-521.
- Fitzjohn C, Ternan JL, Williams AG. 1998. Soil moisture variability in a semi-arid gully catchment: implications for runoff and erosion control. *CATENA*, **32**: 55-70. DOI: [http://dx.doi.org/10.1016/S0341-8162\(97\)00045-3](http://dx.doi.org/10.1016/S0341-8162(97)00045-3).
- Foster G, Yoder D, Weesies G, McCool D, McGregor K, Bingner R. 2005. Revised Universal Soil Loss Equation Version 2. Science Documentation.(Draft). USDA-ARS.
- Franks SW, Beven KJ, Quinn PF, Wright IR. 1997. On the sensitivity of soil-vegetation-atmosphere transfer (SVAT) schemes: equifinality and the problem of robust calibration. *Agricultural and Forest Meteorology*, **86**: 63-75. DOI: [http://dx.doi.org/10.1016/S0168-1923\(96\)02421-5](http://dx.doi.org/10.1016/S0168-1923(96)02421-5).
- Fu B. 1989. Soil erosion and its control in the loess plateau of China. *Soil Use Manage.*, **5**: 76-82. DOI: 10.1111/j.1475-2743.1989.tb00765.x.
- Garen DC, Moore DS. 2005. CURVE NUMBER HYDROLOGY IN WATER QUALITY MODELING: USES, ABUSES, AND FUTURE DIRECTIONS1. *JAWRA Journal of the American Water Resources Association*, **41**: 377-388. DOI: 10.1111/j.1752-1688.2005.tb03742.x.
- Ghimire CP, Bonell M, Bruijnzeel LA, Coles NA, Lubczynski MW. 2013. Reforesting severely degraded grassland in the Lesser Himalaya of Nepal: Effects on soil hydraulic conductivity and overland flow production. *Journal of Geophysical Research: Earth Surface*, **118**: 2528-2545. DOI: 10.1002/2013JF002888.
- Golubev GN. 1982. Soil erosion and agriculture in the world: an assessment and hydrological implications. *Hydrological Sciences Journal-Journal Des Sciences Hydrologiques*, **27**: 243-243.
- Goodrich DC, Unkrich CL, Smith RE, Woolhiser DA. 2002. KINEROS2-A distributed kinematic runoff and erosion model. In: *Hydrologic modeling for the 21st Century agenda: Second Federal Interagency Hydrologic Modeling Conference*,

July 28-August 1, 2002, Riviera Hotel, Las Vegas, Nevada, [Reston, Va.: United States Interagency Advisory Committee on Water Data] the Subcommittee on Hydrology, 2002.

Govers G. 1990. *Empirical Relationships for the Transport Capacity of Overland Flow*. In: *IAHS Publication, IAHS Press, Institute of Hydrology*, pp: p 45-63.

Gumiere SJ, Raclot D, Cheviron B, Davy G, Louchart X, Fabre JC, Moussa R, Le Bissonnais Y. 2011. MHYDAS-Erosion: a distributed single-storm water erosion model for agricultural catchments. *Hydrological Processes*, **25**: 1717-1728. DOI: 10.1002/hyp.7931.

Hagen L, Foster G. 1990. Soil erosion prediction technology. In: *Proceedings of Soil Erosion and Productivity Workshop*, pp: 117-135.

Hammad AHA, Børresen T, Haugen LE. 2006. Effects of rain characteristics and terracing on runoff and erosion under the Mediterranean. *Soil and Tillage Research*, **87**: 39-47. DOI: <http://dx.doi.org/10.1016/j.still.2005.02.037>.

Hao YL, Lal R, Izaurralde RC, Ritchie JC, Owens LB, Hothem DL. 2001. Historic assessment of agricultural impacts on soil and soil organic carbon erosion in an Ohio watershed. *Soil Sci.*, **166**: 116-126.

Haynes R, Swift R. 1990. Stability of soil aggregates in relation to organic constituents and soil water content. *Journal of soil science*, **41**: 73-83.

Henninger DL, Petersen GW, Engman ET. 1976. Surface Soil Moisture within a Watershed – Variations, Factors Influencing, and Relationship to Surface Runoff1. *Soil Science Society of America Journal*, **40**. DOI: 10.2136/sssaj1976.03615995004000050041x.

Heppner CS, Loague K, VanderKwaak JE. 2007. Long-term InHM simulations of hydrologic response and sediment transport for the R-5 catchment. *Earth Surface Processes and Landforms*, **32**: 1273-1292. DOI: 10.1002/esp.1474.

Heppner CS, Ran Q, VanderKwaak JE, Loague K. 2006. Adding sediment transport to the integrated hydrology model (InHM): Development and testing. *Adv. Water Resour.*, **29**: 930-943. DOI: <http://dx.doi.org/10.1016/j.advwatres.2005.08.003>.

- Hessel R, van den Bosch R, Vigiak O. 2006. Evaluation of the LISEM soil erosion model in two catchments in the East African Highlands. *Earth Surface Processes and Landforms*, **31**: 469-486. DOI: 10.1002/esp.1280.
- Hessell R. 2005. Effects of grid cell size and time step length on simulation results of the Limburg soil erosion model (LISEM). *Hydrological Processes*, **19**: 3037-3049. DOI: 10.1002/hyp.5815.
- Holden J, Burt TP. 2002. Infiltration, runoff and sediment production in blanket peat catchments: implications of field rainfall simulation experiments. *Hydrological Processes*, **16**: 2537-2557. DOI: 10.1002/hyp.1014.
- Hueso-González P, Ruiz-Sinoga J, Martínez-Murillo J, Lavee H. 2015. Overland flow generation mechanisms affected by topsoil treatment: Application to soil conservation. *Geomorphology*, **228**: 796-804.
- Idso S, Jackson R, Reginato R, Kimball B, Nakayama F. 1975. The dependence of bare soil albedo on soil water content. *Journal of Applied Meteorology*, **14**: 109-113.
- Ipcc. 2014. *Climate Change 2014: Impacts, Adaptation, and Vulnerability. Part A: Global and Sectoral Aspects. Contribution of Working Group II to the Fifth Assessment Report of the Intergovernmental Panel on Climate Change* [Field, C.B., V.R. Barros, D.J. Dokken, K.J. Mach, M.D. Mastrandrea, T.E. Bilir, M. Chatterjee, K.L. Ebi, Y.O. Estrada, R.C. Genova, B. Girma, E.S. Kissel, A.N. Levy, S. MacCracken, P.R. Mastrandrea, and L.L. White (eds.)]. Cambridge University Press.
- Ismail J, Ravichandran S. 2008. RUSLE2 Model Application for Soil Erosion Assessment Using Remote Sensing and GIS. *Water Resour. Manag.*, **22**: 83-102. DOI: 10.1007/s11269-006-9145-9.
- Ivanov VY, Vivoni ER, Bras RL, Entekhabi D. 2004. Catchment hydrologic response with a fully distributed triangulated irregular network model. *Water Resour. Res.*, **40**: n/a-n/a. DOI: 10.1029/2004WR003218.
- Jain M, Kothiyari U, Raju K. 2005. GIS Based Distributed Model for Soil Erosion and Rate of Sediment Outflow from Catchments. *Journal of Hydraulic Engineering*, **131**: 755-769. DOI: 10.1061/(ASCE)0733-9429(2005)131:9(755).

- Jetten V, de Roo A, Favis-Mortlock D. 1999. Evaluation of field-scale and catchment-scale soil erosion models. *CATENA*, **37**: 521-541. DOI: [http://dx.doi.org/10.1016/S0341-8162\(99\)00037-5](http://dx.doi.org/10.1016/S0341-8162(99)00037-5).
- Johnson BE, Julien PY, Molnar DK, Watson CC. 2000. The two-dimensional upland erosion model casc2d-sed1. *JAWRA Journal of the American Water Resources Association*, **36**: 31-42.
- Jordan P, Menary W, Daly K, Kiely G, Morgan G, Byrne P, Moles R. 2005. Patterns and processes of phosphorus transfer from Irish grassland soils to rivers—integration of laboratory and catchment studies. *Journal of Hydrology*, **304**: 20-34. DOI: <http://dx.doi.org/10.1016/j.jhydrol.2004.07.021>.
- Jost G, Schume H, Hager H, Markart G, Kohl B. 2012. A hillslope scale comparison of tree species influence on soil moisture dynamics and runoff processes during intense rainfall. *Journal of Hydrology*, **420**: 112-124.
- Julien P, Simons D. 1985. Sediment transport capacity of overland flow. *Transactions of the ASAE*, **28**: 755-762.
- Karl T, Koss WJ. 1984. Regional and national monthly, seasonal, and annual temperature weighted by area, 1895-1983. National Climatic Data Center.
- Kemper W, Rosenau R. 1984. Soil cohesion as affected by time and water content. *Soil Sci. Soc. Am. J.*, **48**: 1001-1005.
- Kim HS, Lee S. 2013. Assessment of a seasonal calibration technique using multiple objectives in rainfall-runoff analysis. *Hydrological Processes*: n/a-n/a. DOI: 10.1002/hyp.9785.
- Kim J, Ivanov VY, Katopodes ND. 2013. Modeling erosion and sedimentation coupled with hydrological and overland flow processes at the watershed scale. *Water Resour. Res.*, **49**: 5134-5154. DOI: 10.1002/wrcr.20373.
- Kinnell PIA. 2005. Raindrop-impact-induced erosion processes and prediction: a review. *Hydrological Processes*, **19**: 2815-2844. DOI: 10.1002/hyp.5788.
- Kinnell PIA. 2010. Event soil loss, runoff and the Universal Soil Loss Equation family of models: A review. **385**: 384–397. DOI: 10.1016/j.jhydrol.2010.01.024.

- Knapp AK, Beier C, Briske DD, Classen AT, Luo Y, Reichstein M, Smith MD, Smith SD, Bell JE, Fay PA. 2008. Consequences of more extreme precipitation regimes for terrestrial ecosystems. *Bioscience*, **58**: 811-821.
- Knisel WG. 1980. CREAMS : a field scale model for chemicals, runoff and erosion from agricultural management systems. U.S.D.A.
- Knisel WG. 1980. CREAMS: A field-scale model for chemicals, runoff and erosion from agricultural management systems. USDA Conservation Research Report.
- Krause P, Boyle D, Båse F. 2005. Comparison of different efficiency criteria for hydrological model assessment. *Advances in Geosciences*, **5**: 89-97.
- Kumar M, Duffy CJ, Salvage KM. 2009. A Second-Order Accurate, Finite Volume–Based, Integrated Hydrologic Modeling (FIHM) Framework for Simulation of Surface and Subsurface Flow. *Vadose Zone Journal*, **8**: 873-890. DOI: 10.2136/vzj2009.0014.
- Laflen JM, Lane LJ, Foster GR. 1991. WEPP: A new generation of erosion prediction technology. *J. Soil Water Conserv.*, **46**: 34-38.
- Legates DR, Mahmood R, Levia DF, DeLiberty TL, Quiring SM, Houser C, Nelson FE. 2011. Soil moisture: A central and unifying theme in physical geography. *Progress in Physical Geography*, **35**: 65-86.
- Lewis C. 2003. Phosphorus, Nitrogen and Suspended Sediment Loss from Soil to Water from Agricultural Grassland. In: Department of Civil and Environmental Engineering, University College Cork.
- Lewis C. 2011. Measurement and modelling of soil hydrological properties for use in the distributed rainfall runoff model - GEOtop. In: Department of Civil and Environmental Engineering, University College Cork.
- Lewis C, Albertson J, Xu X, Kiely G. 2012. Spatial variability of hydraulic conductivity and bulk density along a blanket peatland hillslope. *Hydrological Processes*, **26**: 1527-1537. DOI: 10.1002/hyp.8252.
- Lewis C, Albertson J, Zi T, Xu X, Kiely G. 2013. How does afforestation affect the hydrology of a blanket peatland? A modelling study. *Hydrological Processes*, **27**: 3577-3588.

- Licciardello F, Zema, D.A. , Zimbone, S.M. , Bingner, R.L. 2007. Runoff and Soil Erosion Evaluation by the AnnAGNPS Model in a Small Mediterranean Watershed. Transactions of the ASABE 2007 Sept-Oct, v. 50, no. 5.
- Littleboy M, Silburn D, Freebairn D, Woodruff D, Hammer G, Leslie J. 1992. Impact of soil erosion on production in cropping systems .I. Development and validation of a simulation model. Soil Research, **30**: 757-774. DOI: <http://dx.doi.org/10.1071/SR9920757>.
- Liu S, Namkhai A. 2000. Temporal and spatial scales of observed soil moisture variations in the extratropics. J Geophys Res, **105**: 1186511877Fraedrich.
- Luk S-h. 1985. Effect of antecedent soil moisture content on rainwash erosion. CATENA, **12**: 129-139. DOI: [http://dx.doi.org/10.1016/S0341-8162\(85\)80012-6](http://dx.doi.org/10.1016/S0341-8162(85)80012-6).
- Ma Y, Huang HQ, Xu J, Brierley GJ, Yao Z. 2010. Variability of effective discharge for suspended sediment transport in a large semi-arid river basin. Journal of Hydrology, **388**: 357-369. DOI: <http://dx.doi.org/10.1016/j.jhydrol.2010.05.014>.
- Madsen T, Figdor E. 2007. When it rains, it pours: global warming and the rising frequency of extreme precipitation in the United States. Environment Texas Research & Policy Center.
- Mati BM, Morgan RPC, Quinton JN. 2006. Soil erosion modelling with EUROSEM at Embori and Mukogodo catchments, Kenya. Earth Surface Processes and Landforms, **31**: 579-588. DOI: 10.1002/esp.1347.
- Medeiros PH, Güntner A, Francke T, Mamede GL, Carlos de Araújo J. 2010. Modelling spatio-temporal patterns of sediment yield and connectivity in a semi-arid catchment with the WASA-SED model. Hydrological Sciences Journal–Journal des Sciences Hydrologiques, **55**: 636-648.
- Merritt WS, Letcher RA, Jakeman AJ. 2003. A review of erosion and sediment transport models. Environmental Modelling & Software, **18**: 761-799. DOI: 10.1016/s1364-8152(03)00078-1.
- Meyles E, Williams A, Ternan L, Dowd J. 2003. Runoff generation in relation to soil moisture patterns in a small Dartmoor catchment, Southwest England. Hydrological Processes, **17**: 251-264.

- Miguez-Macho G, Fan Y. 2012. The role of groundwater in the Amazon water cycle: 1. Influence on seasonal streamflow, flooding and wetlands. *Journal of Geophysical Research: Atmospheres* (1984–2012), **117**.
- Miller WP, Baharuddin MK. 1986. Relationship of soil dispersibility to infiltration and erosion of southeastern soils. *Soil Sci.*, **142**: 235-240.
- Millward AA, Mersey JE. 1999. Adapting the RUSLE to model soil erosion potential in a mountainous tropical watershed. *Catena*, **38**: 109-129.
- Montaldo N, Toninelli V, Albertson JD, Mancini M, Troch PA. 2003. The effect of background hydrometeorological conditions on the sensitivity of evapotranspiration to model parameters: analysis with measurements from an Italian alpine catchment. *Hydrol. Earth Syst. Sci.*, **7**: 848-861. DOI: 10.5194/hess-7-848-2003.
- Morgan RPC, Quinton JN, Smith RE, Govers G, Poesen JWA, Auerswald K, Chisci G, Torri D, Styczen ME. 1999. The European soil erosion model (EUROSEM): A dynamic approach for predicting sediment transport from fields and small catchments - Reply. *Earth Surface Processes and Landforms*, **24**: 567-568.
- Morgan RPC, Quinton JN, Smith RE, Govers G, Poesen JWA, Auerswald K, Chisci G, Torri D, Styczen ME. 1998. The European Soil Erosion Model (EUROSEM): A dynamic approach for predicting sediment transport from fields and small catchments. *Earth Surface Processes and Landforms*, **23**: 527-544.
- Moriasi D, Arnold J, Van Liew M, Bingner R, Harmel R, Veith T. 2007. Model evaluation guidelines for systematic quantification of accuracy in watershed simulations. *Trans. ASABE*, **50**: 885-900.
- Musgrave G. 1947. The quantitative evaluation of factors in water erosion, a first approximation. *J. Soil Water Conserv.*, **2**: 133-138.
- Nash JE, Sutcliffe JV. 1970. River flow forecasting through conceptual models part I — A discussion of principles. *Journal of Hydrology*, **10**: 282-290. DOI: 10.1016/0022-1694(70)90255-6.
- Nasr A, Bruen M, Jordan P, Moles R, Kiely G, Byrne P. 2007. A comparison of SWAT, HSPF and SHETRAN/GOPC for modelling phosphorus export from three

- catchments in Ireland. *Water Research*, **41**: 1065-1073. DOI: <http://dx.doi.org/10.1016/j.watres.2006.11.026>.
- Nearing MA. 2001. Potential changes in rainfall erosivity in the U.S. with climate change during the 21st century. *J. Soil Water Conserv.*, **56**: 229-232.
- Nearing MA, Jetten V, Baffaut C, Cerdan O, Couturier A, Hernandez M, Le Bissonnais Y, Nichols MH, Nunes JP, Renschler CS, Souchère V, van Oost K. 2005. Modeling response of soil erosion and runoff to changes in precipitation and cover. *CATENA*, **61**: 131-154. DOI: <http://dx.doi.org/10.1016/j.catena.2005.03.007>.
- Niu G-Y, Pasetto D, Scudeler C, Paniconi C, Putti M, Troch P, DeLong S, Dontsova K, Pangle L, Breshears D. 2014. Incipient subsurface heterogeneity and its effect on overland flow generation—insight from a modeling study of the first experiment at the Biosphere 2 Landscape Evolution Observatory. *Hydrology and Earth System Sciences*, **18**: 1873-1883.
- Noble CA, Morgan RPC. 1983. Rainfall interception and splash detachment with a Brussels sprouts plant: A laboratory simulation. *Earth Surface Processes and Landforms*, **8**: 569-577. DOI: 10.1002/esp.3290080608.
- NRCS. 2010. 2007 NRI Soil Erosion. In: 2007 National Resources Inventory.
- O'Neal MR, Nearing MA, Vining RC, Southworth J, Pfeifer RA. 2005. Climate change impacts on soil erosion in Midwest United States with changes in crop management. *CATENA*, **61**: 165-184. DOI: <http://dx.doi.org/10.1016/j.catena.2005.03.003>.
- Orchard CM, Lorentz SA, Jewitt GPW, Chaplot VAM. 2013. Spatial and temporal variations of overland flow during rainfall events and in relation to catchment conditions. *Hydrological Processes*, **27**: 2325-2338. DOI: 10.1002/hyp.9217.
- Owoputi L, Stolte W. 1995. Soil detachment in the physically based soil erosion process: a review. *Transactions of the ASAE*, **38**: 1099-1110.
- Palecki MA, Angel JR, Hollinger SE. 2005. Storm Precipitation in the United States. Part I: Meteorological Characteristics. *Journal of Applied Meteorology*, **44**: 933-946. DOI: 10.1175/JAM2243.1.

- Penna D, Tromp-van Meerveld H, Gobbi A, Borga M, Dalla Fontana G. 2011. The influence of soil moisture on threshold runoff generation processes in an alpine headwater catchment. *Hydrology and Earth System Sciences*, **15**: 689-702.
- Penna D, Tromp-van Meerveld HJ, Gobbi A, Borga M, Dalla Fontana G. 2011. The influence of soil moisture on threshold runoff generation processes in an alpine headwater catchment. *Hydrol. Earth Syst. Sci.*, **15**: 689-702. DOI: 10.5194/hess-15-689-2011.
- Philip JR. 1957. The theory of infiltration: 4. Sorptivity and algebraic infiltration equations. *Soil Sci.*, **84**: 257-264.
- Pieri L, Bittelli M, Wu JQ, Dun S, Flanagan DC, Pisa PR, Ventura F, Salvatorelli F. 2007. Using the Water Erosion Prediction Project (WEPP) model to simulate field-observed runoff and erosion in the Apennines mountain range, Italy. **336**: 84-97. DOI: 10.1016/j.jhydrol.2006.12.014.
- Podmanicky L, Balazs K, Belenyasi M, Centeri C, Kristof D, Kohlheb N. 2011. Modelling soil quality changes in Europe. An impact assessment of land use change on soil quality in Europe. *Ecological Indicators*, **11**: 4-15. DOI: 10.1016/j.ecolind.2009.08.002.
- Poesen J, De Luna E, Franca A, Nachtergaele J, Govers G. 1999. Concentrated flow erosion rates as affected by rock fragment cover and initial soil moisture content. *CATENA*, **36**: 315-329. DOI: [http://dx.doi.org/10.1016/S0341-8162\(99\)00044-2](http://dx.doi.org/10.1016/S0341-8162(99)00044-2).
- Porporato A, Daly E, Rodriguez, x, Iturbe I, Associate Editor: William FF. 2004. Soil Water Balance and Ecosystem Response to Climate Change. *The American Naturalist*, **164**: 625-632. DOI: 10.1086/424970.
- Pruski FF, Nearing MA. 2002. Climate-induced changes in erosion during the 21st century for eight U.S. locations. *Water Resour. Res.*, **38**: 34-31-34-11. DOI: 10.1029/2001WR000493.
- Pruski FF, Nearing MA. 2002. Runoff and soil-loss responses to changes in precipitation: A computer simulation study. *J. Soil Water Conserv.*, **57**: 7-16.
- Ramsankaran R, Kothiyari UC, Ghosh SK, Malcherek A, Murugesan K. 2013. Physically-based distributed soil erosion and sediment yield model (DREAM) for

- simulating individual storm events. *Hydrological Sciences Journal*, **58**: 872-891. DOI: 10.1080/02626667.2013.781606.
- Ran Q, Heppner CS, VanderKwaak JE, Loague K. 2007. Further testing of the integrated hydrology model (InHM): multiple-species sediment transport. *Hydrological Processes*, **21**: 1522-1531. DOI: 10.1002/hyp.6642.
- Ran Q, Su D, Li P, He Z. 2012. Experimental study of the impact of rainfall characteristics on runoff generation and soil erosion. *Journal of Hydrology*, **424**: 99-111.
- Reich P, Eswaran H, Beinroth F. 1999. Global dimensions of vulnerability to wind and water erosion. In: *Sustaining the global farm. Selected papers from the 10th International Soil Conservation Organization Meeting*, pp: 24-29.
- Renard KG, Foster GR, Weesies GA, Porter JP. 1991. RUSLE: Revised universal soil loss equation. *J. Soil Water Conserv.*, **46**: 30-33.
- Renard KG, Yoder DC, Lightle DT, Dabney SM. 2010. Universal Soil Loss Equation and Revised Universal Soil Loss Equation. In: *Handbook of Erosion Modelling*, John Wiley & Sons, Ltd, pp: 135-167.
- Rigon R, Bertoldi G, Over TM. 2006. GEOtop: A distributed hydrological model with coupled water and energy budgets. *Journal of Hydrometeorology*, **7**: 371-388.
- Rockwell DL. 2002. The influence of groundwater on surface flow erosion processes during a rainstorm. *Earth Surface Processes and Landforms*, **27**: 495-514. DOI: 10.1002/esp.323.
- Rose C, Coughlan K, Fentie B. 1998. Griffith University Erosion System Template (GUEST). In: *Modelling Soil Erosion by Water*, Boardman J, Favis-Mortlock D (eds.) Springer Berlin Heidelberg, pp: 399-412.
- Rosenberg E, Clark E, Steinemann A, Lettenmaier D. 2013. On the contribution of groundwater storage to interannual streamflow anomalies in the Colorado River basin. *Hydrology and Earth System Sciences*, **17**: 1475-1491.
- Safeeq M, Mauger GS, Grant GE, Arismendi I, Hamlet AF, Lee S-Y. 2014. Comparing Large-Scale Hydrological Model Predictions with Observed Streamflow in the

- Pacific Northwest: Effects of Climate and Groundwater*. *Journal of Hydrometeorology*, **15**: 2501-2521.
- Sahu RK, Mishra SK, Eldho TI. 2010. An improved AMC-coupled runoff curve number model. *Hydrological Processes*, **24**: 2834-2839. DOI: 10.1002/hyp.7695.
- Schmidt J. 1991. A mathematical model to simulate rainfall erosion. *Catena Suppl*, **19**: 101-109.
- SCS. 1972. SCS national engineering handbook, section 4: hydrology. The Service.
- Shen ZY, Gong YW, Li YH, Hong Q, Xu L, Liu RM. 2009. A comparison of WEPP and SWAT for modeling soil erosion of the Zhangjiachong Watershed in the Three Gorges Reservoir Area. *Agricultural Water Management*, **96**: 1435-1442. DOI: <http://dx.doi.org/10.1016/j.agwat.2009.04.017>.
- Simoni S, Zanotti F, Bertoldi G, Rigon R. 2008. Modelling the probability of occurrence of shallow landslides and channelized debris flows using GEOTOP-FS. *Hydrological Processes*, **22**: 532-545. DOI: 10.1002/hyp.6886.
- Singh J, Knapp HV, Arnold J, Demissie M. 2005. Hydrological modeling of the Iroquois River watershed using HSPF and SWAT. *J. Am. Water Resour. Assoc.*, **41**: 343-360.
- Singh V. 1997. Effect of spatial and temporal variability in rainfall and watershed characteristics on stream flow hydrograph. *Hydrological Processes*, **11**: 1649-1669.
- Smith D, Whitt D. 1948. Estimating soil losses from field areas of claypan soil. *Soil Science Society of America Journal*, **12**: 485-490.
- Smith RE, Goodrich DC, Quinton JN. 1995a. Dynamic, distributed simulation of watershed erosion: the KINEROS2 and EUROSEM models. *J. Soil Water Conserv.*, **50**: 517-520.
- Smith RE, Goodrich DC, Woolhiser DA, Unkrich CL, Singh VP. 1995. KINEROS-A kinematic runoff and erosion model. *Computer models of watershed hydrology.*: 697-732.
- Sun G, McNulty SG, Moore J, Bunch C, Ni J. 2002. Potential impacts of climate change on rainfall erosivity and water availability in China in the next 100 years.

- Tao J, Barros AP. 2014. Coupled prediction of flood response and debris flow initiation during warm- and cold-season events in the Southern Appalachians, USA. *Hydrol. Earth Syst. Sci.*, **18**: 367-388. DOI: 10.5194/hess-18-367-2014.
- Tenberg A, Da Veiga M, Dechen S, Stocking M. 1998. Modelling the impact of erosion on soil productivity: A comparative evaluation of approaches on data from southern Brazil. *Experimental Agriculture*, **34**: 55-71.
- Terranova O, Antronico L, Coscarelli R, Iaquina P. 2009. Soil erosion risk scenarios in the Mediterranean environment using RUSLE and GIS: An application model for Calabria (southern Italy). **112**: 228–245. DOI: 10.1016/j.geomorph.2009.06.009.
- Tsara M, Kosmas C, Kirkby MJ, Kosma D, Yassoglou N. 2005. An evaluation of the pesera soil erosion model and its application to a case study in Zakynthos, Greece. *Soil Use Manage.*, **21**: 377-385. DOI: 10.1079/SUM2005322.
- Turnbull L, Wainwright J, Brazier RE. 2010. Changes in hydrology and erosion over a transition from grassland to shrubland. *Hydrological Processes*, **24**: 393-414. DOI: 10.1002/hyp.7491.
- van Dijk AIJM, Bruijnzeel LA, Rosewell CJ. 2002. Rainfall intensity–kinetic energy relationships: a critical literature appraisal. *Journal of Hydrology*, **261**: 1-23. DOI: [http://dx.doi.org/10.1016/S0022-1694\(02\)00020-3](http://dx.doi.org/10.1016/S0022-1694(02)00020-3).
- Van Oost K, Govers G, Desmet P. 2000. Evaluating the effects of changes in landscape structure on soil erosion by water and tillage. *Landscape Ecology*, **15**: 577-589. DOI: 10.1023/A:1008198215674.
- Van Rompaey A, Verstraeten G, Van Oost K, Govers G, Poesen J. 2001. Modelling mean annual sediment yield using a distributed approach. *Earth Surface Processes and Landforms*, **26**: 1221-1236.
- Van Rompaey AJ, Verstraeten G, Van Oost K, Govers G, Poesen J. 2001. Modelling mean annual sediment yield using a distributed approach. *Earth Surface Processes and Landforms*, **26**: 1221-1236.
- VanderKwaak JE, Loague K. 2001. Hydrologic-Response simulations for the R-5 catchment with a comprehensive physics-based model. *Water Resour. Res.*, **37**: 999-1013. DOI: 10.1029/2000WR900272.

- Verstraeten G, Prosser IP, Fogarty P. 2007. Predicting the spatial patterns of hillslope sediment delivery to river channels in the Murrumbidgee catchment, Australia. *Journal of Hydrology*, **334**: 440-454.
- Vieira JHD. 1983. Conditions governing the use of approximations for the Saint-Venant equations for shallow surface water flow. *Journal of Hydrology*, **60**: 43-58. DOI: [http://dx.doi.org/10.1016/0022-1694\(83\)90013-6](http://dx.doi.org/10.1016/0022-1694(83)90013-6).
- Viney NR, Sivapalan M. 1999. A conceptual model of sediment transport: application to the Avon River Basin in Western Australia. *Hydrological Processes*, **13**: 727-743. DOI: 10.1002/(SICI)1099-1085(19990415)13:5<727::AID-HYP776>3.0.CO;2-D.
- Vis M. 1986. Interception, drop size distributions and rainfall kinetic energy in four Colombian forest ecosystems. *Earth Surface Processes and Landforms*, **11**: 591-603.
- von Freyberg J, Rao PSC, Radny D, Schirmer M. 2015. The impact of hillslope groundwater dynamics and landscape functioning in event-flow generation: a field study in the Rietholzbach catchment, Switzerland. *Hydrogeology Journal*: 1-14.
- Vorst HAvd. 1992. BI-CGSTAB: a fast and smoothly converging variant of BI-CG for the solution of nonsymmetric linear systems. *SIAM J. Sci. Stat. Comput.*, **13**: 631-644. DOI: 10.1137/0913035.
- Walling D. 1983. The sediment delivery problem. *Journal of Hydrology*, **65**: 209-237.
- Warner S, Kiely G, Morgan G, O'Halloran J. 2009. Does quantifying antecedent flow conditions improve stream phosphorus export estimation? *Journal of Hydrology*, **378**: 97-104. DOI: <http://dx.doi.org/10.1016/j.jhydrol.2009.09.009>.
- Wei L, Zhang B, Wang M. 2007. Effects of antecedent soil moisture on runoff and soil erosion in alley cropping systems. *Agricultural Water Management*, **94**: 54-62. DOI: <http://dx.doi.org/10.1016/j.agwat.2007.08.007>.
- Wicks JM, Bathurst JC. 1996. SHESED: a physically based, distributed erosion and sediment yield component for the SHE hydrological modelling system. *Journal of Hydrology*, **175**: 213-238. DOI: [http://dx.doi.org/10.1016/S0022-1694\(96\)80012-6](http://dx.doi.org/10.1016/S0022-1694(96)80012-6).

- Wicks JM, Bathurst JC. 1996. SHESED: a physically based, distributed erosion and sediment yield component for the SHE hydrological modelling system. *Journal of Hydrology*, **175**: 213-238. DOI: 10.1016/s0022-1694(96)80012-6.
- Williams J. 1977. Sediment delivery ratios determined with sediment and runoff models. *IAHS Publ*, **122**: 168-179.
- Williams J, Nearing M, Nicks A, Skidmore E, Valentin C, King K, Savabi R. 1996. Using soil erosion models for global change studies. *J. Soil Water Conserv.*, **51**: 381-385.
- Williams JR. 1975. Sediment-yield prediction with universal equation using runoff energy factor. Present and prospective technology for predicting sediment yields and sources, **40**: 244-252.
- Williams JR. 1975. Sediment-yield prediction with Universal Equation using runoff energy factor. In: Present and Prospective Technology for Predicting Sediment Yield and Sources, U.S. Dept. Agric., pp: 244-252.
- Willmott CJ. 1981. On the validation of models. *Physical Geography*, **2**: 184-194
- Wischmeier WH. 1959. A Rainfall Erosion Index for a Universal Soil-Loss Equation¹. *Soil Science Society of America Journal*, **23**. DOI: 10.2136/sssaj1959.03615995002300030027x.
- Wischmeier WH, Smith DD. 1958. Rainfall energy and its relationship to soil loss. *Eos, Transactions American Geophysical Union*, **39**: 285-291. DOI: 10.1029/TR039i002p00285.
- Wischmeier WH, Smith DD. 1960. A universal soil-loss equation to guide conservation farm planning. *Transactions 7th int. Congr. Soil Sci.*, **1**: 418-425.
- Wischmeier WH, Smith DD. 1978. Predicting rainfall erosion losses: a guide to conservation planning. Dept. of Agriculture, Science and Education Administration: for sale by the Supt. of Docs., US Govt. Print. Off.
- Wu TH, McKinnell Iii WP, Swanston DN. 1979. Strength of tree roots and landslides on Prince of Wales Island, Alaska. *Canadian Geotechnical Journal*, **16**: 19-33. DOI: 10.1139/t79-003.

- Yang CT. 1972. Unit stream power and sediment transport. *Journal of the Hydraulics Division*, **98**: 1805-1826.
- Yang D, Kanae S, Oki T, Koike T, Musiak K. 2003. Global potential soil erosion with reference to land use and climate changes. *Hydrological Processes*, **17**: 2913-2928. DOI: 10.1002/hyp.1441.
- Ye S, Covino TP, Sivapalan M, Basu NB, Li H-Y, Wang S-W. 2012. Dissolved nutrient retention dynamics in river networks: A modeling investigation of transient flows and scale effects. *Water Resour. Res.*, **48**: n/a-n/a. DOI: 10.1029/2011WR010508.
- Young RA, Onstad CA, Bosch DD, Anderson WP. 1989. AGNPS: A nonpoint-source pollution model for evaluating agricultural watersheds. *J. Soil Water Conserv.*, **44**: 168-173.
- Zhang Y, Hernandez M, Anson E, Nearing MA, Wei H, Stone JJ, Heilman P. 2012. Modeling climate change effects on runoff and soil erosion in southeastern Arizona rangelands and implications for mitigation with conservation practices. *J. Soil Water Conserv.*, **67**: 390-405. DOI: 10.2489/jswc.67.5.390.
- Zi T, Kumar M, Kiely G, Lewis C, Albertson J. 2016. Simulating the spatio-temporal dynamics of soil erosion, deposition, and yield using a coupled sediment dynamics and 3D distributed hydrologic model. *Environmental Modelling & Software*, **in review**.
- Ziadat FM, Taimeh AY. 2013. EFFECT OF RAINFALL INTENSITY, SLOPE, LAND USE AND ANTECEDENT SOIL MOISTURE ON SOIL EROSION IN AN ARID ENVIRONMENT. *Land Degradation & Development*, **24**: 582-590. DOI: 10.1002/ldr.2239.
- Zimmermann A, Schinn DS, Francke T, Elsenbeer H, Zimmermann B. 2013. Uncovering patterns of near-surface saturated hydraulic conductivity in an overland flow-controlled landscape. *Geoderma*, **195–196**: 1-11. DOI: <http://dx.doi.org/10.1016/j.geoderma.2012.11.002>.

Biography

Tan Zi was born in Sichuan, China. After spending 18 years there with panda bears, he went to Beijing for his bachelor's degree at China Agricultural University. He majored in applied meteorology. He continued his graduate study in meteorology at China Agricultural University after he got his bachelor's degree. In 2006, he got his master's degree in meteorology by conducting research project related to evapotranspiration at the transition zone of agriculture and pasture in Inner Mongolia with the companion of sheep. Then he spent three years working at China Meteorological Administration. During the three years, he got chances to travel to many meteorological stations all over China for inspection and investigation. He also collaborated with scientists and engineers on the development of air quality observation network. He enrolled in the Ph.D. program at Duke in 2009. His research interest changed to fluids which have much smaller Reynolds number than air since then. In 2014, he became a water resource engineer at Tetra Tech, Inc. After his Ph.D., he will continue his career as an engineer at consulting company.